Cape Peninsula University of Technology

# Synthesis and characterization of bimetallic silver and platinum nanoparticles as electrochemical sensor for nevirapine, an anti-HIV drug

**by**

**OKUMU FREDRICK OLUOCH**

B. Sc. (University of Nairobi), M. Tech. (Cape Peninsula University of Technology)

**Thesis submitted in fulfilment of the requirements for the degree**

**Doctor of Philosophy: (Chemistry)**

**In the Faculty of Applied Sciences**

**At the Cape Peninsula University of Technology**

**Supervisor:** Prof. M. C. Matoetoe

**Co-supervisor:** Prof. O. S. Fatoki

**Cape Town**

April 2016

## DECLARATION

I, **Okumu Fredrick Oluoch**, declare that the contents of this thesis represent my own unaided work, and that this thesis has not previously been submitted for academic examination towards any qualification. Furthermore, it represents my own opinions and not necessarily those of the Cape Peninsula University of Technology.

**Signed.....Date.....**

## ABSTRACT

Bimetallic silver-platinum (Ag-Pt) nanoparticles (NPs) were synthesized via simultaneous reduction of varying mole fractions of metal precursors $H_2PtCl_6.6H_2O$ and $AgNO_3$ by sodium citrate. Kinetics rates of were as follows; Ag NPs (0.079 $s^{-1}$), Ag-Pt NPs 1:1 (0.082 $s^{-1}$) and Pt NPs (0.006 $s^{-1}$). The UV visible spectrum of Ag NPs exhibited a characteristic absorption band while Pt NPs and Ag-Pt bimetallic NPs exhibited no absorption peaks. Successful formation of both monometallic and bimetallic NPs was confirmed via transmission electron microscopy (TEM); selected area electron diffraction (SAED) and energy dispersive X-ray (EDX) analysis. TEM images depicted core-shell arrangement in the bimetallic (BM) NP ratios (1:1, 1:3 and 3:1) with an average particle size of 21 nm. The particle size trend where monometallic Ag NPs (60 nm) > Pt NPs (2.5 nm) while in the BM ratios Ag-Pt NPs 1:1 (25 nm) > Ag-Pt NPs 1:3 (20.7 nm). X-ray diffraction (XRD) patterns depicted crystallinity in all the synthesized NPs with confirmation of the face centred cubic structure formation. Transducers were fabricated by drop casting the nanoparticless on the glassy carbon electrode (GCE) and their electrochemical properties studied via cyclic voltammetry (CV). High diffusion coefficient (D) and surface coverage reported were Ag NPs (6.70 $cm^2$ $s^{-1}$, 54.49 mol $cm^{-2}$ ) and Ag-Pt NPs 1:1 (0.62 $cm^2$ $s^{-1}$1.85 mol $cm^{-2}$). Electrochemical band gaps ranged from 1.45 to 1.70 eV while the Tauc's model band gaps of nanoparticles were found in the range of 2.48 to 3.84 eV. These band gaps were found to be inversely proportional to particle size, which was attributed to the quantum confinement effect. Both optical and electrochemical band gap portrayed similar trend as well as an increase in the BM NP relative to monometallics. These nanoparticles band gaps are within semiconductor range for most materials. The electrochemical behaviour and surface characteristics were studied using 0.1 M PBS solution by scan rates variations for the diffusion coefficient determination of modified electrodes which ranged from 0.62 to 6.10 x $10^{-5}$ $cm^2$ $s^{-1}$. Laviron's approach for parameters such as apparent charge transfer rate constant, $k_s$, and charge transfer coefficient, α, for electron transfer between NPs and GCE were investigated using CV. The values of electron-transfer coefficients ranged from 0.1 to 0.7 while the charge transfer rate constant values ranged from 0.74 to 31.13 $s^{-1}$.

Various detection platforms were investigated in the electrooxidation of NVP by CV and DPV. BM Ag-Pt 3:1 NPs was found to be the best modifier, with low background current. However, its use as NVP sensor was hampered by signal instability. The introduction of MWCNT to the BM resulted in well resolved, good signal stability DPV voltamograms with MWCNT/Ag-Pt NPs 3:1 film on GCE surface. The sensor was optimised for method parameter and supporting electrolyte concentration. MWCNT/Ag-Pt NPs 3:1/GCE showed excellent

electrocatalytic activity for the oxidation of NVP under optimal experimental conditions of a 0.01 mol $L^{-1}$ NaOH solution of (supporting electrolyte), pulse amplitude of 25 mV, initial potential of 0.20 V, and a scan rate of 20 mV $s^{-1}$. Cyclic voltammetry was used to investigate the redox properties of MWCNT/Ag-Pt NPs 3:1/GC electrode at various scan rates based on Laviron's equation. The apparent charge transfer rate constant ($k_s$) and electron transfer coefficient (α) between NVP and MWCNT/Ag-Pt NPs 3:1/GC electrode were calculated to be 0.8835 $s^{-1}$ and 0.31 respectively with the diffusion coefficient of 5.2048 x $10^{-10}$ $cm^2$ $s^{-1}$ reported in the electrocatalytic oxidation of NVP. The mechanism of the NVP electrooxidation process was investigated by CV and found to undergo a 2-electron transfer process. The oxidation peak current of NVP had a linear range of 7.6 × $10^{-7}$ to 4.6 × $10^{-6}$ mol $L^{-1}$ with a correlation coefficient of 0.9980. Lower detection limit of 0.021 µM coupled with 86 % reproducibility showed that the repetitive usability exhibited by the proposed modified electrode are good enough to make it a suitable sensor for the determination of NVP in real samples with complex matrices such as milk and human urine. The application of the developed sensor for the determination of NVP in pharmaceutical tablets using standard addition method showed good recovery of 98 % average. This proposed method was sensitive and simple.

## ACKNOWLEDGEMENTS

First and foremost, I dearly thank the Almighty God for His grace in the period over which I carried out this study.

To my supervisor and academic advisor Prof. M.C. Matoetoe, thank you so much for the progressive evaluation of this work and for giving me the opportunity to work with this project. It is an honour for me to work with you, and to learn from your work ethics. This thesis would not have been possible without your guidance, and your encouragement. I also want to thank you for being very patient with me and assisting me until the very end. My co-supervisor Prof. O.S. Fatoki, thank you so much for the facilitation that ensured successful completion. Kindly feel highly appreciated.

To the electrochemistry lab colleagues (Malefetsane Khesoue and Audry Bovingou) and all my friends including Rob Walker (Student-Y), Erick Jondiko and Alvin Ouko, your support and motivation are highly appreciated.

To the German Academic Exchange Service (DAAD) thank you for the financial assistance and Cape Peninsula University of Technology (CPUT) your support towards this research is hereby acknowledged.

Much appreciation to my family for their love and care during the period of study. Maureen Ahawo Oluoch (my wife), my sister and brothers: Pauline Akinyi Okumu, Michael Onyango Okumu (the late), Gregory Ochieng Okumu, each time you assured me of your moral support while studying, I felt highly encouraged and loved. Thank you so much.

Lastly, to my parents Mrs. Monica A. Okumu and Mr. Benedict M. Okumu, this is for you. Thank you very much for your love, care, education and upbringing.

## DEDICATION

This is dedicated to me, my wife Maureen Ahawo Oluoch and the entire Okumu family. I would not have done it without their love and support.

- I thank God Almighty for all the blessings and for keeping up with me through all the hard times.

- To Prof. Beatrice Anyango, your tremendous effort is gracefully appreciated thank you so much and may God bless you abundantly.

- To my late brother Michael Onyango Okumu, thank you very much for the support and the hard times we shared.

# PREFACE

## Objective and Overview of Thesis

This thesis is focusing on the synthesis of novel Ag-Pt bimetallic-based nanoparticles, the study of their electrocatalytic properties and application in detection of an anti-HIV drug, nevirapine. The main objective is to obtain an efficient detection platform, which can be explored in part by improving its electroactivity, sensitivity, efficiency and reliability. Here are the outlines of the remaining chapters in this thesis.

- **Chapter one** of the thesis provides the background of this research work and explains more on the statement of the problem coupled with objectives of interest.

- **Chapter two** of the thesis gives the literature review by introducing theoretical background of anti-HIV drugs including nevirapine, different ways of detecting ARVs and their fate in the environment. A closer look into the various detection tools for ARVs such as sensors together with nanoparticles applications is highlighted.

- **Chapter three** deals with synthesis, kinetics and particle characterization of bimetallic silver-platinum nanoparticles. It concentrates on the general experimental procedures for the chemical synthesis of bimetallic Ag-Pt NPs, their kinetics of formation and characterization using UV-visible spectroscopy, transmission electron microscopy (TEM), selected area electron diffraction (SAED), energy dispersive X-ray (EDX) analysis and X-ray diffraction (XRD).

- **Chapter four** of this thesis concentrates on the electrochemical characterization of the synthesized nanoparticles. The electrochemical behaviour and properties of the synthesized NPs is investigated, reported and discussed. Furthermore, the electrochemical band gap study was done and compared to the optical band gap results.

- **Chapter five** examines the application of the modified GC electrode with nanocomposite film (MWCNT/Ag-Pt 3:1 NPs) for the detection of nevirapine. Various optimization studies on the electrooxidation of NVP were done together with recovery studies.

- **Chapter six** summarizes the main conclusions and recommendation of this work.

## RESEARCH OUTPUTS

### 1. Publications

(i) Sneha Mohan, **Fredrick Okumu**, Oluwatobi Oluwafemi, Mangaka Matoetoe and Omotayo Arotiba. 2016. Electrochemical behaviour of silver nanoparticle-MWCNTs hybrid nanostructures synthesized via a simple method. *International Journal of Electrochemical Science,* 11: 745-753.

(ii) **Fredrick Okumu,** Mangaka Matoetoe. Kinetics and morphological analysis of silver platinum bimetallic nanoparticles. 2016. *Acta Mettallurgica Sinica (English Letters),* 29(4): 320-325.

(iii) **Fredrick Okumu,** Mangaka Matoetoe. Electrochemical characterization of silver-platinum core-shell nanoparticles. *Journal of Nano Research*, xx-yy. (**Paper accepted**).

(iv) Khesoue Malefestasane, Mangaka Matoetoe, **Fredrick Okumu**. Potential of silver nanoparticles functionalised polyaniline as an electrochemical transducer. *Journal of Nano Research*, xx-yy. (**Paper accepted**).

### 2. Conference presentations

(i) Annual Postgraduate Conference 2013 Cape Peninsula University of Technology, Cape Town, South Africa. 11th November, 2013. (Oral)

**F.O. Okumu**, M. C. Matoetoe. Title: Synthesis and characterization of bimetallic silver and platinum alloy nanoparticles for development of amperometric sensor.

(ii) 3rd International Symposium on Electrochemistry, “Materials, Analytical and Physical Electrochemistry Today” (MAPET’15)”. ElectrochemSA, SACI Bellville, South Africa. 26-28 May 2015. (Oral)

**F. Okumu**, M. C. Matoetoe. Title: Electrochemical characterization of Silver-Platinum Bimetallic Nanoparticles.

(iii) The 2nd International Conference on Sensors, Materials and Manufacturing (ICSMM 2016) Nha Trang, Vietnam. February 26-28, 2016. (Oral)

**F. Okumu**, M. C. Matoetoe. Title: Optical and Electrochemical Band gaps of varying ratios of Ag-Pt bimetallic nanoparticles.

### 3. Seminar presentations

(i) Nanotechnology Research Seminar. Faculty of Engineering, Cape Peninsula University of Technology, Cape Town, South Africa. 11th April, 2014. (Oral)

**F.O. Okumu,** M.C. Matoetoe. Synthesis and characterization of bimetallic silver and platinum alloy nanoparticles for development of amperometric sensor.

## TABLE OF CONTENTS

## LIST OF FIGURES

## LIST OF TABLES

## LIST OF SCHEMES

## APPENDICES

## GLOSSARY

| Terms/Acronyms/Abbreviations | Definition/Explanation |
|---|---|
| ARV | Antiretroviral |
| TEM | Transmission electron microscopy |
| EIS | Electrochemical impedance spectroscopy |
| CV | Cyclic voltammetry |
| HPLC | High performance liquid chromatography |
| HIV | Human Immune Deficiency Virus |
| AIDS | Acquired Immune Deficiency Syndrome |
| LC/MS | Liquid Chromatography / Mass Spectrometry |
| UV | Ultraviolet |
| PPCPs | Pharmaceutical and Personal Care Products |
| STPs | Sewage Treatment Plants |
| NPs | Nanoparticles |
| XRD | X-ray diffraction |
| RNA | Ribonucleic Acid |
| DNA | Deoxyribonucleic Acid |
| FDA | Food and Drug Administration |
| MALDI | Matrix-Assisted Laser Desorption Ionization |
| TOF | Time of Flight |
| MEKC | Micellar Electrokinetic Chromatographic |
| HPTLC | High Performance Thin Layer Chromatography |
| IgG | Immunoglobulin G |
| HBV | Hepatitis B virus |
| HCV | Hepatitis C virus |
| CMV | Cytomegalovirus |
| CMEs | Chemically Modified Electrodes |
| ART | Antiretroviral Therapy |
| TB | Tuberculosis |
| LSV | Linear Sweep Voltammetry |
| DPV | Differential Pulse Voltammetry |
| SWV | Square Wave Voltammetry |
| QSE | Quantum Size Effect |
| LUMO | Lowest Unoccupied Molecular Orbital |

| | |
|---|---|
| HOMO | Highest Occupied Molecular Orbital |
| PBS | Phosphate Buffer Solution |
| CNTs | Carbon Nanotubes |
| MWCNT | Multi-Walled Carbon Nanotubes |
| BR | Britton-Robbinson |
| AdSV | Adsorptive Stripping Voltammetry |
| EDX | Electron Diffraction |
| LOD | Limit of Detection |
| LOQ | Limit of Quantification |
| SAED | Selected Area Electron Diffraction |
| RSD | Relative Standard Deviation |
| WHO | World Health Organization |
| SOD | Superoxide Dismutase |
| CD4 | Cluster of Differentiation 4 |
| TDM | Therapeutic Drug Monitoring |
| NVP | Nevirapine |
| GCE | Glassy Carbon Electrode |
| PDMS | Poly-Di-Methyl-Siloxane |
| BM | Bimetallic |
| MSA | Mass Specific Activity |
| CCS | Controlled Colloidal Synthesis |
| AFM | Atomic Force Microscopy |
| SEM | Scanning Electron Microscopy |
| NRTI | Nucleoside Reverse Transcriptase Inhibitor |
| NNRTI | Non-Nucleoside Reverse Transcriptase Inhibitor |

# CHAPTER ONE
# INTRODUCTION

## 1.1 Background

Antiretroviral drugs are used in the treatment of infections by retroviruses, primarily human immunodeficiency viruses (HIV) that can lead to acquired immunodeficiency syndrome (AIDS) (Teradal *et al.,* 2012). The scale-up of antiretroviral treatment (ART) in resource-poor countries has been impressive, both in its scope and in its impact. Treatment of common infections occurring with HIV is also increasing, as most HIV-infected persons live in areas where infectious diseases such as tuberculosis (TB) and malaria are prevalent. The use of over-the-counter and natural health products is also pervasive (WHO, 2005).

Anti-HIV drugs are widely popular with the treatment and management of HIV AIDS in the health sector of our African society, thus there is a great need to improve on their reported analytical work in the literature. The growing demand for these drugs stimulates a search for new and even more effective drugs monitoring techniques, but also calls for higher level of quality control of these therapeutic substances and preparations. Therefore, it seems appropriate to develop new and or improve on the existing analytical methods regarding their qualitative and quantitative analysis. Lately, different analytical methods have been used to monitor anti-HIV drugs. However, one that has been gaining more and more applications is the electroanalytical methods.

Amongst the current challenges facing the medical fraternity, environment in general and researchers in particular is the antiviral drugs. The information on their presence in various matrices such as human serum, urine and breast milk remains a key, as these helps to promote safety and efficacy upon drug administration to patients who depend on these drugs for life support. Due to the widespread usage of ARVs, common challenges like improper administration of these drugs has resulted to drug resistance and poor treatment in some cases. The ARVs dose abuse continue to pose challenges in the antiretroviral therapy (ART) for HIV patients and raised questions on the best monitoring practices available. Therefore, drug monitoring information would help in the management of ART by minimizing cases of drug resistance, drug-food interaction and drug-drug interaction for patients taking combinational therapy, which is widely administered currently. In addition, the knowledge helps researchers evaluate the extent of drug efficacy thereby reducing the occurrences of drug resistance among various HIV patients.

Electroanalytical methods are widely used in scientific studies, monitoring of industrial materials, pharmaceutical, biological and environmental chemicals. Amperometric techniques are the most widespread electroanalytical methods. For electroanalytical determinations, cyclic voltammetry (CV), linear sweep voltammetry (LSV), differential pulse voltammetry (DPV), square wave voltammetry (SWV), and polarography have been used (Bozal *et al.,* 2011). These methods permit the screening and determination of most organic compounds especially pharmaceutical substances with a detection limit of $10^{-7}$ M (Bozal *et al.,* 2011). Electrochemical techniques are also effective in deciphering redox mechanism of drug compounds and provide important information about DNA-drug interaction (Dogan-Topal *et al.,* 2009). Voltammetric and polarographic analysis of drugs in pharmaceutical preparations by far is the most common use of electrochemistry for analytical-pharmaceutical problems. As a rule, many of active compounds of the formulations can be readily oxidized or reduced. Analysis of drugs in various matrices such as; raw material, pharmaceutical dosage forms even those involving a complex matrix such as syrups, tablets, creams, suppositories, ointments, as well as in biological fluids had been reported (Teradal *et al.,* 2012; Zhang *et al.,* 2013; Shahrokhian *et al.,* 2015). The principal advantage of the modern electroanalytical methods is that the excipients do not interfere and generally, the separation and extraction is not necessary. Thus, sample preparation usually consists of dissolving out the active substance from the pharmaceutical dosage form with a suitable solvent and performing direct analysis on an aliquot portion of this solution (Ozkan *et al.,* 2003). Electrochemical data are often correlated to the molecular structure and the pharmacological activity. Therefore, electrochemical techniques are most suitable for the investigation of the redox properties of a new drug (like new anti-HIV agents); thus gaining insights into its metabolic fate, drugs interactions with metal ions or proteins as well as degradation mechanisms processes triggered by photo- or pH changes (Smith and Vos, 1992; Ozkan *et al.,* 2003; Uslu and Ozkan, 2007a).

In its broad sense, electrochemistry involves a chemical phenomenon associated with charge separation at an electrode surface. As voltammetric methods continue to develop, the range of working electrode materials continues to expand. Both the geometry and composition of the working electrode material must be considered since they will influence the performance of the voltammetric method. In addition, the physical form of the working electrode may influence the diffusion process and the electron transfer processes involved in the detection of the analyte (Wang, 1988; Hart, 1990; Smith and Vos, 1992; Gosser, 1993; Kissinger and Heineman, 1996; Wang, 2000; Kellner *et al.,* 2004; Uslu and Ozkan, 2007b).

The current trend in pharmaceutical electroanalytical chemistry is the fabrication of metal nanoparticles as transducers and sensors using various electrochemical methods for the electrode modification process in electroanalytical chemistry. This research is aimed at developing an efficient and effective electroanalytical detection platform that can be applied in the detection of nevirapine in formulations and biological samples. This will also involve understanding of the interaction between ARV drugs and metal NPs. The search for highly effective electrocatalysts and detailed mechanistic understanding has spanned to the exploration of nanometer-size catalysts. To address these issues, we have synthesized bimetallic silver and platinum nanoparticles, characterized and interrogated them as possible probes for the detection of nevirapine.

## 1.2 Research problem

Many antiretroviral (ARVs) drugs were discovered quite earlier, but their application as antiviral drugs is relatively recent. Their usage in HIV/AIDs treatment is widely appreciated more so in Africa. Access to antiretroviral therapy (ART) is improving in the developing countries, which experience the greatest disease burden arising from HIV infection. The successful roll-out of ART was achieved by adopting a public health approach to HIV care and treatment involving cost minimization, delegation of tasks from highly skilled to less skilled health workers and simplification of the routine laboratory tests that are used to monitor ongoing efficacy of ART (WHO, 2003; WHO, 2010). Due to cost constraints, laboratory monitoring of ART efficacy is often limited to the CD4 cell count - a test that has low accuracy for identifying patients experiencing treatment failure to ART (Bangsberg *et al.,* 2006; Nachega *et al.,* 2006; Reynolds *et al.,* 2009). The gold standard for treatment failure, viral load testing, is largely unavailable in developing countries because of its complexity and costs. Low-cost laboratory tests are needed to optimize ART monitoring in developing countries such as sub-Saharan Africa. Adherence to ART is critical for treatment success, but routine clinical measures of adherence (e.g. patient self-report) are subjective and can be prone to social desirability bias such as traditional cultures.

The confirmation of treatment failure is limited by the high cost of definitive diagnostics (e.g. HIV viral load and resistance testing). Consequently, in resource-limited settings, it is often difficult to distinguish patients who are non-adherent from patients with treatment failure arising from the emergence of drug-resistant virus. International guidelines recommend that patients with suspected treatment failure to nevirapine-based ART be switched to second-line regimens being significantly more expensive than first-line regimens (WHO, 2010; Sempa *et al.,* 2012). Thus, therapeutic drug monitoring (TDM) can be used to identify non-adherent patients and thereby prevent unnecessary switching to more expensive ART

regimens (Hugen *et al.,* 2002). Dosing of antiretroviral agents can be complex, due to significant drug interaction potential, adverse effect profiles, and adherence challenges (Moyer *et al.*, 1999; Plipat *et al.*, 2004). Therefore, the TDM of ARVs such as nevirapine may therefore be helpful in individual treatment decisions by assessing the actual nevirapine body level. The efficient TDM strategies require elaborate analytical methods for the quantification of drug concentrations, which will assist in maximizing the efficacy and safety of these regimens and further trace disposal routes. However, TDM can only be recommended if such methods are accurate, robust, available and affordable in developing countries. To this end, few studies in sub-Saharan Africa have provided such platforms.

Past studies on quantitative detection of nevirapine are predominantly chromatography and its spectroscopic hyphens, with mass spectrometer detectors (Ahmed *et al.,* 2011; Zanolli Filho *et al.,* 2011). The success of the above-mentioned methods, require long analysis times, elaborate extraction and purification steps, or on-line sample extraction, and are relatively costly therefore limiting their applications in routine laboratories. Hence, there is an urgent need to investigate new alternative methods such as the use of nanoparticle platforms, which provide a more user-friendly option with high sensitivity. Research has confirmed that nanoparticle based platforms are effective for the identification of chemical and biological agents, hence, offer substantial benefits to biomedical and environmental science. These platforms benefit from the availability of a wide variety of core materials as well as the unique physical and chemical properties of these nanoscale materials (Agasti *et al.,* 2010).

This study involves nevirapine, which is one of the most commonly prescribed antiretroviral drugs due to its wide usage as a component of first-line antiretroviral therapy (ART), low cost, good long-term tolerability, and high efficacy (Havlir *et al.,* 1995; WHO, 2006). These advantages add to its preference for wide use in reduction of vertical transmission (Parienti and Peytavin, 2011) and prevention of mother to child transmission (PMCT) in sub-Saharan Africa. Nevirapine-based regimens are preferred in resource-limited settings because of the lower cost in comparison with Efavirenz (Lamorde *et al.,* 2014). Due to its low genetic barrier, resistance occurs rapidly if sub-therapeutic drug levels occur (Gonzalez de Requena, 2005). Moreover, drug-to-drug interactions may lead to unexpected high or low nevirapine drug levels (Boffito *et al.,* 2005). Nevirapine concentrations are widely measured in various biological samples including human serum (Zhang *et al.,* 2013), urine (Teradal *et al.,* 2012) and saliva (Rakhmanina *et al.,* 2007). These matrices are the most common point source of anti-HIV drugs that would help monitor their intake and efficacy. In light of numerous use of nevirapine in HIV-infected patients, a need to pursue this drug in terms of its detection was of great concern in this study.

The need to develop sensitive and efficient detection methods for antiretroviral drugs monitoring especially for the NVP, which is widely used in treatment of HIV type 1 is eminent. This is important, especially in African countries where the majority of antiretroviral treated adults are women and pregnancy rates in this population are high (Wester *et al.,* 2005). This challenge has motivated the integration of chemical sensors and natural resources in designing monitoring techniques. In this regard, an alternative low cost technique based on electrochemical sensing is proposed and developed. This method will have a potential application in a wide matrix including biological samples such as human serum, urine and in recovery studies. Previously, the research work on detection of ARV drugs has been scarcely reported due to lack of knowledge for efficient detection techniques.

## 1.3 Research questions

i. What is the structural comparison in the synthesised nanoparticles and their properties?

ii. What are the appropriate nanoparticles to employ in the detection of nevirapine?

iii. Are the present methods of determination of nevirapine suitable for application in various sample matrices?

iv. How best can the current modified electrode be utilised in the detection of Nevirapine?

v. Are there variations in the methodology between the developed electroanalytical method of nevirapine analysis and the recovery studies?

## 1.4 Objectives of the research

The aim of this study was to develop a better ARVs detection platform using bimetallic nanoparticles as significant friendly sensing materials modified on an electrode surface using electroanalytical methods, which are suitable for sensitive and selective ARV drug detection. With the elaboration of the new electrode modification and voltammetric measurement method, this study aimed at improving the main analytical performance parameters such as detection limit and sensitivity compared to the other voltammetric techniques performed with similar chemically modified electrodes in ARV drug detection.

The specific objectives of the study are:

1) To synthesize chemically silver-platinum bimetallic nanoparticles in various precursor ratios.

2) To characterize the synthesized Ag-Pt bimetallic nanoparticles by UV-Visible spectroscopy, cyclic voltammetry (CV), transmission electron microscopy (TEM) and X-ray diffraction (XRD).

3) To fabricate transducers by modification of the glassy carbon electrode (GCE) surface with silver-platinum bimetallic nanoparticles and to study their electroactivity properties.

4) Apply the fabricated Ag-Pt bimetallic nanoparticles/GCE as sensor platforms in the detection of selected ARV drug; nevirapine and further compare the various platforms developed to obtain the best results.

5) To analyze real samples and validate the developed method.

## 1.5 References

Agasti, S.S., Rana, S., Park, M.H., Kim, C.K., You, C.C., Rotello, V.M. 2010. Nanoparticles for detection and diagnosis. *Adv. Drug Deliv. Rev.,* 62: 316-328.

Ahmed, M.S.M., Reddy, J.S., Chakravarth, I.E., Prabhavathi, K. 2011. A simple spectrophotometric determination of nevirapine in pharmaceutical dosage form. *J. Chem. Pharm. Res.*, 3(4): 172-176.

Bangsberg, D.R., Acosta, E.P., Gupta, R., Guzman, D., Riley, E.D., Harrigan, P.R., Parkin, N., Deeks, S.G. 2006. Adherence-resistance relationships for protease and non-nucleoside reverse transcriptase inhibitors explained by virological fitness. *AIDS*, 20: 223-231.

Boffito, M., Acosta, E., Burger, D., Fletcher, C.V., Flexner, C., Garaffo, R., Gatti, G., Kurowski, M., Perno, C.F., Peytavin, G., Regazzi, M. and Back. D. 2005. Therapeutic drug monitoring and drug-drug interactions involving antiretroviral drugs. *Antivir. Ther.,* (10): 469-477.

Bozal, B., Uslu, B. and Ozkan, S.A. 2011. A review of electroanalytical techniques for determination of anti-HIV drugs. *Int. J. Electrochem*., 1-17.

Dogan-Topal, B., Uslu, B. and Ozkan, S.A. 2009. Voltammetric studies on the HIV-1 inhibitory drug Efavirenz: the interaction between dsDNA and drug using electrochemical DNA biosensor and adsorptive stripping voltammetric determination on disposable pencil graphite electrode. *Biosens. Bioelectron*., 24(8): 2358-2364.

Gonzalez de Requena, D., Bonora, S., Garazzino, S., Sciandra, M., D'Avolio, A., Raiteri, R., Marrone, R., Boffito, M., De Rosa, F.G., Sinicco, A. and Di Perri. G. 2005. Nevirapine plasma exposure affects both durability of viral suppression and selection of nevirapine primary resistance mutations in a clinical setting. *Antimicrob. Agents Chemother.,* (49): 3966-3969.

Gosser, Jr. D.K. 1993. Ed. *Cyclic voltammetry: simulation and analysis of reaction mechanism*. Wiley-VCH, New York, NY, USA.

Hart, J.P. 1990. Ed., *Electroanalysis of biologically important compounds*, Ellis Harwood, New York, NY, USA.

Havlir, D., Cheeseman, S.H., McLaughlin, M., Murphy, R., Erice, A., Spector, S.A., Greenough, T.C., Sullivan, J.L., Hall, D., Myers, M. 1995. High-dose nevirapine: safety, pharmacokinetics, and antiviral effect in patients with human immunodeficiency virus infection. *J. Infect. Dis*., 171: 537-545.

Hugen, P.W., Burger, D.M., Aarnoutse, R.E., Baede, P.A., Nieuwkerk, P.T., Koopmans, P.P., Hekster, Y.A. 2002. Therapeutic drug monitoring of HIV-protease inhibitors to assess noncompliance. *Ther. Drug Monit.,* 24: 579-587.

Kellner, R., Mermet, J.M., Otto, M., Valcarcel, M. and Widmer, H.M. 2004. Eds., *Analytical chemistry: a modern approach to analytical science*. Wiley-VCH, Weinheim, Germany, 2nd edition.

Kissinger, P.T. and Heineman, W.R. Eds. 1996. *Laboratory techniques in electroanalytical chemistry*. Marcel Dekker, New York, NY, USA, 2nd edition.

Lamorde, M., Fillekes, Q., Sigaloff, K., Kityo, C., Buzibye, A., Kayiwa, J., Merry, C., Nakatudde-Katumba, L., Burger, D. and Rinke de Wit, T.F. 2014. Therapeutic drug monitoring of nevirapine in saliva in Uganda using high performance liquid chromatography and a low cost thin-layer chromatography technique. *BMC Infectious Diseases*, 14: 473.

Moyer, T.P., Temesgen, Z., Enger, R., Estes, L., Charson, J., Oliver, L. and Wright, A. 1999. Drug monitoring of antiretroviral therapy for HIV-1 infection: method validation and results of a pilot study*. Clin. Chem.,* 45: 1465-1476*.*

Nachega, J.B., Hislop, M., Dowdy, D.W., Lo, M., Omer, S.B., Regensberg, L., Chaisson, R.E., Maartens, G. 2006. Adherence to highly active antiretroviral therapy assessed by pharmacy claims predicts survival in HIV-infected South African adults. *J. Acquir. Immune Defic. Syndr.,* 43: 78-84.

Ozkan, S.A., Uslu, B. and Aboul-Enein, H.Y. 2003. Analysis of pharmaceuticals and biological fluids using modern electroanalytical techniques. *Crit. Rev. Anal. Chem.,* 33(3): 155-181.

Parienti, J.J., Peytavin, G. 2011. Nevirapine once daily: pharmacology, metabolic profile and efficacy data of the new extended-release formulation. *Expert Opin. Drug Metab. Toxicol*., 7(4): 495-503.

Plipat, N., Ruan, P.K., Fenton, T. and Yogev, R. 2004. Rapid human immunodeficiency virus decay in highly active antiretroviral therapy (HAART)-experienced children after starting mega-HAART. *J. Virol.,* 72: 11272-11275.

Rakhmanina, N.Y., Capparelli, E.V., Van Den Anker, J.N., Williams, K., Sever, J.l., Spiegel, H.M. and Soldin, S.J. 2007. Nevirapine concentration in non-stimulated saliva: an alternative to plasma sampling in children with human immunodeficiency virus infection. *Ther. Drug Monit.,* 29: 110-117.

Reynolds, S.J., Nakigozi, G., Newell, K., Ndyanabo, A., Galiwongo, R., Boaz, I., Quinn, T.C., Gray, R., Wawer, M., Serwadda, D. 2009. Failure of immunologic criteria to appropriately identify antiretroviral treatment failure in Uganda. *AIDS*, 23: 697-700.

Sempa, J., Ssennono, M., Kuznik, A., Lamorde, M., Sowinski, S., Semeere, A., Hermans, S., Castelnuovo, B., Manabe, Y.C. 2012. Cost-effectiveness of early initiation of first-line combination antiretroviral therapy in Uganda. *BMC Public Health*, 12: 736.

Shahrokhian, S., Kohansal, R., Ghalkhani, M. and Amini, M.K. 2015. Electrodeposition of copper oxide nanoparticles on precasted carbon nanoparticles film for electrochemical investigation of anti-HIV drug nevirapine. *Electroanalysis*, 27: 1-10.

Smith, M.R. and Vos, J.G. 1992. *Analytical Voltammetry*, vol. XXVII, Elsevier Science, Amsterdam, the Netherlands.

Teradal, N.L., Prashanth, S.N., Seetharamappa, J. 2012. Electrochemical studies of nevirapine, an anti-HIV drug, and its assay in tablets and biological samples. *J. Electrochem. Sci. Eng.,* 2: 67-75.

Uslu, B. and Ozkan, S.A. 2007a. Electroanalytical application of carbon based electrodes to the pharmaceuticals. *Anal. Lett.,* 40(5): 817-853.

Uslu, B. and Ozkan, S.A. 2007b. Solid electrodes in electroanalytical chemistry: present applications and prospects for high throughput screening of drug compounds. *Com. Chem. High. T. Scr.,* 10(7): 495-513.

Wang, J. Ed. 1988. *Electroanalytical techniques in clinical chemistry and laboratory medicine*, Wiley-VCH, New York, NY, USA.

Wang, J. 2000. *Analytical Electrochemistry*, Wiley-VCH, New York, NY, USA. 2000.

Wester, C.W., Kim, S., Bussmann, H., Avalos, A., Ndwapi, N., Peter, T.F., Gaolathe, T., Mujugira, A., Busang, L., Vanderwarker, C., Cardiello, P., Johnson, O., Thior, I., Mazonde, P., Moffat, H., Essex, M., Marlink, R. 2005. Initial response to highly active antiretroviral therapy in HIV-1C-infected adults in a public sector treatment program in Botswana. *J. Acquir. Immune Defic. Syndr.,* 40: 336-343.

World Health Organization (WHO). 2003. A public health approach to antiretroviral treatment: overcoming constraints. Geneva, Switzerland: World Health Organization.

World Health Organization (WHO). 2005. Malaria and HIV interactions and their implications for public health policy: report of a technical consultation. Geneva, Switzerland: World Health Organization.

World Health Organization (WHO). 2006. Antiretroviral therapy for HIV infection adults and adolescents in resource limited settings: towards universal access. Geneva: World Health Organization.

World Health Organization (WHO). 2010. Antiretroviral therapy for HIV infection in adults and adolescents. Recommendations for a public health approach (2010 version). Geneva, Switzerland: World Health Organization.

Zanolli Filho, L.A., Galdez, C.R., Silva, C.A., Tavares, M.F.M., Costa, D.M., Prado, M.S.A. 2011. Development and validation of a simple and rapid capillary zone electrophoresis method for determination of NNRTI nevirapine in pharmaceutical formulations. *J. Braz. Chem. Soc.*, 22(10): 2005-2012.

Zhang, F., Li, L., Luo, L., Ding, Y., Liu, X. 2013. Electrochemical oxidation and determination of antiretroviral drug nevirapine based on uracil-modified carbon paste electrode. *J. Appl. Electrochem*., 43: 263-269.

# CHAPTER TWO
# LITERATURE REVIEW

## 2.1 Antiretroviral drugs (ARVs)

This chapter presents a review of relevant literature related to antiretroviral drugs and the various methods used in their monitoring and detection. The various materials potential as detection probes for ARVs in pharmaceutical samples is equally highlighted. Different methods are mentioned especially the application of sensors in the detection of analytes such as drugs and other biological samples. The development of sensitive and effective detection platforms based on rapid and robust chemical sensors is of great importance in the search for better ways of improving the monitoring techniques available for pharmaceuticals.

In the half decade since the first large-scale antiretroviral treatment (ART) program for HIV/AIDS was launched in sub-Saharan Africa, much attention has focused on patients' day-to-day adherence to antiretroviral (ARV) medications (Gill *et al.,* 2005; Mills *et al.,* 2006). The most significant advancement in the medical management of HIV-1 infection has been the treatment of patients with antiviral drugs i.e., medicines that stop or slow virus actions (Stiver, 2003) by suppressing HIV-1 replication to undetectable levels. Viruses are obligate intracellular parasites, wholly dependent on a living host cell for the replication (Lees, 2000). The conventional approach to the control of viral diseases is to develop effective vaccines, but this is not always feasible. Because of their mode of replication, viruses present a larger therapeutic challenge than bacteria (Fraser *et al.,* 1991). Because of the genetic flexibility of viruses, new strains constantly emerge, the most well-known example being human immunodeficiency virus (HIV), the causative agent of AIDS (Anderson *et al.,* 2009). As of today, there are no approved vaccines to treat HIV viruses. The use of antiviral medicines is one of several strategies for encountering an antiviral pandemic, which may extend for many months. Over 30 years since the discovery of HIV, more than 25 anti-HIV drugs have been approved for the treatment of AIDS according to different categories. The chronic treatment of individuals infected with the HIV type 1 remains a vital need in the near future, since both eradication of the virus and an ending to new infections are unlikely scenarios.

## 2.2 Classification of Antiviral Drugs

Antiviral drugs are classified into two main groups namely antiretroviral (ARVs) drugs and general antiviral drugs (Non-antiretroviral drugs) (Tyring, 2004). Currently, one-half of all antiviral agents are antiretrovirals. Presently, four classes of antiretroviral drugs are available

namely (i) nucleoside/tide reverse transcriptase (NRTI) inhibitors, (ii) non-nucleoside (NNRTI) inhibitors, (iii) protease (PI) inhibitors and (iv) fusion inhibitors (Rao and Shinde, 2009). More than 20 US food and drug administration (FDA) approved antiretroviral drugs are available and many more are in clinical trials. Among protease inhibitors approved in US and Canada are saquinavir (Invirase), indinavir (Crixivan) and ritonavir (Norvir) (Kumar *et al.,* 1996; Chiba *et al.,* 1997). Other classes of the antiviral drugs available for commercial use are as shown in Table 2.1. The (non-antiretroviral) drugs include nucleoside analogs like acyclovir, famciclovir, valacyclovir, ganciclovir, penciclovir, valganciclovir and ribavirin. These are important antivirals in the treatment of herpes virus infections (Tyring, 2004).

**Table 2.1: Antiviral Drugs in Clinical Use or in Progressive Stages of Development (Anderson *et al.,* 2009)**

| **Targets / Strategies** | **Enzymes / Mechanisms** | **Antiviral Drugs** | **Viruses** |
|---|---|---|---|
| Viral enzymes | Polymerase | Acyclovir, Ganciclovir, Penciclovir, Lamivudine, Adefovir, Entecavir, *Valopicitabine* | Herpes viruses HBV *HCV* |
| | Protease | Amprenavir, Atazanavir, Ritonavir, Tipranavir *VX950* | HIV *HCV* |
| | Neuraminidase | Oseltamivir, Zanamivir | Influenza virus |
| Cellular targets | Receptors or coreceptors | Maraviroc, *Vicriviroc, TNX355, Pro140* | HIV |
| | Capping enzyme | Ribavirin | HCV |
| | Immune response | Interferons | HBV, HCV |
| | | *Actilon* | *HCV* |
| Other viral targets | *Attachment Proteins* | *BMS488043* | *HIV* |
| | Fusion proteins | Enfuvirtide | *HIV* |
| | Disassembly/Uncoating | Amantadine, Rimantadine *Pleconaril* | Influenza virus, *Picornaviruses* |
| | *Virion maturation* | *Bevirimat UK201844* | HIV |
| Novel strategies | Antisense RNA *Ribozymes* | Fomivirsen | CMV retinitis |

*(see Glossary for abbreviations)

## 2.3 Occurrence and fate of antiviral drugs in environment

Antiviral drugs occur in the environment through various aqueous systems such as raw wastewater, wastewater treatment plant (WWTP) effluents, surface water, ground water and even drinking water (Ternes *et al.,* 2002; Buchberger, 2007; Kummerer, 2009). Other ways

include domestic and sewage wastes such as septic tanks, leaking underground sewage lines, and surface water run-off or indirectly excreted as faeces or urine of unmetabolised parent compounds. The level to which a compound is transformed in the body depends on its mechanism of action and structure. The rest may be hydroxylated or conjugated and excreted in the faeces (Bound and Voulvoulis, 2005). Some antiviral agents, when consumed are excreted largely unchanged (e.g. acyclovir) whereas others go through extensive biotransformation prior to removal from the body (Galasso *et al.,* 2002). Some antiviral drugs have been predicted as toxic towards daphnids, fish and algae (Sanderson *et al.,* 2004). Some of these drugs or their metabolites are nonbiodegradable (Mascolo *et al.,* 2010). In addition, disposal of out-of-date or unwanted medicines, which may occur via the sink/toilet or in household waste then taken to landfill sites and leach to groundwater. Entry into the environment by this way is dependent on the efficiency of prescription practices leading to some unfinished prescriptions and the habits of the patient faeces (Bound and Voulvoulis, 2005). The unmetabolised antiviral drugs are excreted via faeces and urine and thus are present in the wastewater (Accinelli *et al.,* 2007; Prasse *et al.,* 2010). However, most drugs are partially removed during wastewater treatment (Prasse *et al.,* 2010) and they find their way to surface and ground water. Usually presence of small concentration of antiviral drugs in drinking water may cause resistance towards these drugs, ultimately harming animals and human beings.

Antiviral compounds vary widely in their structure (De Clercq, 2004) and therefore they are expected to vary in their recalcitrance to wastewater treatment and environmental behaviour. For example, a number of antiviral medicines were detected in rivers in Germany, sources being sewage outflows and manufacturing facilities (Prasse *et al.,* 2010). Comparisons of treated and raw wastewater indicated that the drugs lamivudine, acyclovir and abacavir were amenable to removal during sewage treatment, whereas nevirapine, zidovudine and oseltamivir were not (Prasse *et al.,* 2010). These highlights indicate the coverage and fate of antivirals in the wider environment besides human body. Due to their continuous usage amongst the HIV infected persons, these drugs have found their way into the environment because of poor disposal and dose abuse.

## 2.4 Analysis of Antiviral Drugs

Detection of chemical and biological agents plays a pivotal role in medical, forensic, agricultural, and environmental sciences (Diamond, 1998). Sensitive methods that allow identification of drugs provide the prospect of better health and more effective drug monitoring studies. Technological platforms that provide sensors of high sensitivity, selectivity and stability are therefore in high demand. Various methods available for the

determination of antiviral drugs include HPLC, capillary electrophoresis, mass spectrometry, liquid chromatography tandem mass spectrometry and spectrophotometric methods. However, most antiviral drugs can be analysed using hyphenated chromatographic techniques (Swati *et al.,* 2011). Spectrophotometric methods suffer from low sensitivity, high detection limits, tedious experimental conditions and complex procedures for the preparation of samples or standard solutions. In general, HPLC and LC/MS/MS based techniques are expensive and a high degree of resolution has made them choice of the researchers.

## 2.5 Nevirapine

Currently, nevirapine (NVP) is one of the most prescribed antiretroviral drugs in the developing world, both as a single drug to prevent mother-to-child HIV transmission and as a component of currently recommended combined antiretroviral therapy (CART) (Marseille *et al.,* 1999; Jackson *et al.,* 2003; Lallemant *et al.,* 2004; Lockman *et al.,* 2007). The high efficacy levels of the drug, favourable lipid profile, and suitability for use during pregnancy have since granted NVP-based regimens a significant role in HIV-1 treatment strategies (Thompson *et al.,* 2010). Nevirapine is recommended for treating HIV infections in combination with other reverse transcriptase inhibitors such as stavudine and lamivudine (Gulick *et al.,* 1997; Rey *et al.,* 2004).

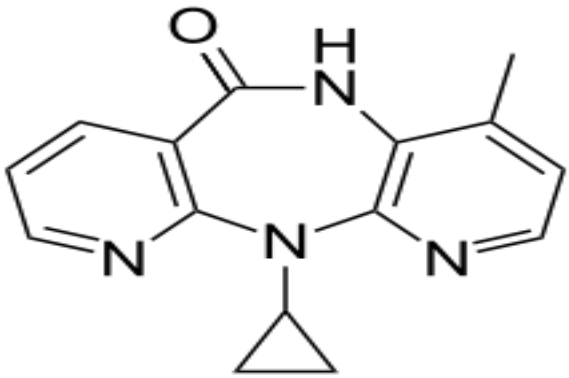


**Figure 2.1. Structure of Nevirapine.**

Nevirapine, 11-cyclopropyl-5, 11-dihydro-4-methyl-6H-dipyrido [3, 2-b: 20, 30-e] [1, 4] diazepin-6-one (Figure 2.1) is the first member of the non-nucleoside reverse transcriptase inhibitors (Hollanders *et al.,* 2000). It displays a butterfly-like conformation (Scheme 2.1), which is verified from the crystalline structure of the pure compound (Mui *et al.,* 1992) and some complexes with the HIV-1 reverse transcriptase (Stammers *et al.,* 1994; Ren *et al.,* 2000; Ren *et al.,* 2004). Several researchers suggested that this conformation is related to

the degree of affinity of the drug and to the probability of appearance of viral resistance (Mager, 1997; Parreira *et al.,* 2001). Based on its widespread usage and availability in HIV treatment as highlighted in past literature, NVP drug was selected for this study.

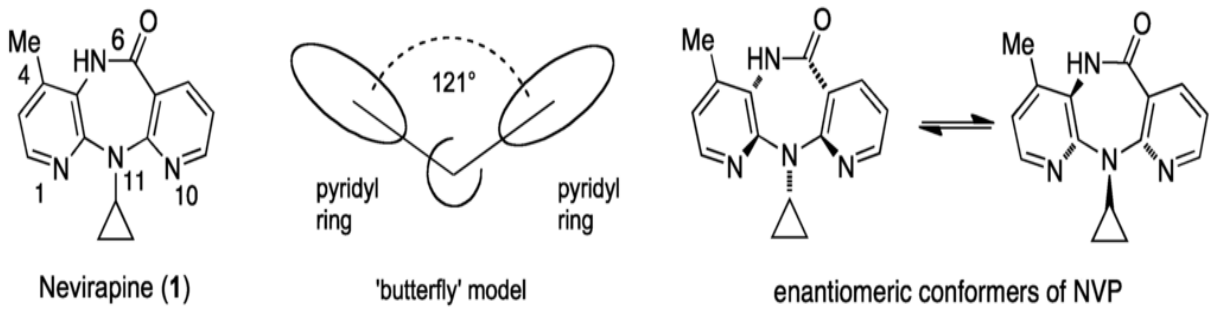


**Scheme 2.1 Butterfly model and enantiomeric conformers of nevirapine (Famiglini and SIlvestri, 2016).**

Nevirapine is synthesized in four steps, starting from 2-chloro-4-methyl-3-nitropyridine. This is reduced to 3-amino-2-chloro-4methlypyridine, which is then condensed with 2-chloronicotinic acid chloride to the amide (Ren *et al.,* 2004). Reaction with cyclopropylamine, followed by cyclization, results in the chemical structure for nevirapine represented in Figure 2.1. Nevirapine is weakly basic (pKa= 2.8) and exhibits pH dependent solubility (Sarkar, 2008). At pH values less than the pKa, it is highly soluble in aqueous buffer. In comparison to other drugs, nevirapine is a poorly soluble hydrophobic molecule (Sarkar, 2008).

### 2.5.1 Mechanism of action

Nevirapine is a dipyridodiazepinone inhibitor of the HIV-1 reverse transcriptase polymerase and is remarkably specific for the HIV-1 reverse transcriptase enzyme (RT). It binds directly to allosteric site on reverse transcriptase and inhibits both the ribonucleic acid (RNA) and deoxyribonucleic acid (DNA) dependant polymerase activities. At high concentrations, nevirapine fails to inhibit the RT of HIV-2, simian immunodeficiency virus, or feline immunodeficiency virus, nor does it inhibit human DNA polymerase-α, -β, δ, or –γ (Merluzzi *et al.,* 1990). As a prototypic member of the NNRTI class of antiretroviral agents, nevirapine demonstrates non-competitive inhibition with respect to deoxyguanosine triphosphate either through allosteric binding to the binary (RT: template-primer) or ternary (RT: template-primer: deoxyguanosine triphosphate) enzyme complex (Koup *et al.,* 1991), and does not cause chain termination (Gu *et al.,* 1995).

It exhibits a 50 % inhibitory concentration ($IC_{50}$) of 0.084 µM (0.023 µg $mL^{-1}$) in enzyme assays, and an $IC_{50}$ of 0.040 µM (0.011 µg $mL^{-1}$) against wild-type HIV-1 replication in cell culture, where one molecule of inhibitor is sufficient to inactivate one molecule of the RT enzyme, binding at the tyrosine 181 and tyrosine 188 sites of the enzyme (Grob *et al.,* 1992). These conserved tyrosine residues of the HIV-RT subunit lie in a pocket that is defined by two β-sheets of amino acid residues 100 to 110 and 180 to 190 (Shih *et al.,* 1991; Wu *et al.,* 1991). By binding to this hydrophobic pocket close to the polymerase catalytic site of RT, nevirapine slows the rate of polymerization catalysed by the enzyme (Spence *et al.,* 1995): this binding also predicts where RT mutations leading to resistance, would occur.

### 2.5.2 Detection methods for Nevirapine

Some of the common ARVs detected in past studies include tenofovir, which has been analysed using high performance liquid chromatography (HPLC) (Jullien *et al.,* 2003), reversed phase liquid chromatography (Sentenac *et al.,* 2003; Kandagal *et al.,* 2008), Liquid chromatography-tandem mass spectrometry (King *et al.,* 2006; Gomes *et al.,* 2008), and UV Spectrophotometry (Shirkhedkar *et al.,* 2009). Indinavir has been detected using Ion-pair reversed-phase high performance liquid chromatography (Li *et al.,* 1999), solid phase extraction and LC/MS (Rose *et al.,* 2000), high performance liquid chromatography (Remmel *et al.,* 2000), LC/MS (Jayewardene *et al.,* 2001), capillary electrophoresis (Prado *et al.,* 2004), UV Spectrophotometry (Sarma and Sastri, 2002; Erk, 2004).

However, for the detection of nevirapine some of the methods that have been reported for its analysis are shown in Table 2.2. Electrochemical methods have proven to be sensitive and reliable for the determination of numerous electroactive compounds (Uslu and Ozkan, 2007a; Gupta *et al.,* 2011). Under some circumstances, electrochemical methods can offer optimal solutions for drug analysis. Simplicity, low cost and relatively short analysis times make electrochemical techniques more useful for routine analytical applications thus provides best alternative approach in this case.

Lately applications of modified electrodes for the determinations of drug molecules has attracted more attention because the modifiers could greatly enhance/increase the responds and selectivity for analytes (Hammam, 2004; Radi, 2005; Mashhadizadeh and Akbarian, 2009; Ma *et al.,* 2012). Organic small molecules, polymer, metal nanoparticles, carbon nanotubes, and graphene have been used as modifiers to fabricate the modified electrodes (Hammam, 2004; Goyal *et al.,* 2005; Ma *et al.,* 2012). Among them, organic small molecules grafted electrodes showed super stability, quick response and high sensitivity as potential

sensors. Based on these concerns, there is a need for improvement on the available detection methods for monitoring NVP.

**Table 2.2: Various detection methods for Nevirapine**

| Technique | Detection method | Matrix | LODs | References |
|---|---|---|---|---|
| Electrochemical | AdSV | NVP tablet | 0.003 µM | Castro *et al.,* 2011 |
| | DPV | Human serum | 0.05 µM | Zhang *et al.,* 2013 |
| | DPV | NVP formulation | 1.026 µM | Teradal *et al.,* 2012 |
| Chromatographic | HPLC | Human plasma | 0.2 µM | Van Heeswijk *et al.,* 1998 |
| | MALDI-TOF/TOF MS | Human plasma | 0.04 µM | Notari *et al.,* 2008 |
| | LC-MS/MS | Human plasma | 3.7 µM | Chi *et al.,* 2003 |
| | MEKC | NVP formulation | 6.0 µM | Sekar and Azhaguvel, 2008 |
| | Capillary electrophoresis | Nevirapine formulation | - | Chen *et al.,* 2010 |
| | HPTLC | Tablet, NVP formulation | 10 ng per spot | Kaul *et al.,* 2004 |
| | HPLC-UV | Human plasma, serum, milk and cerebrospinal fluid | 8 ng $mL^{-1}$ | Pav *et al.,* 1999 |
| Others | Radio-immunoassay | Human plasma, urine | 2-5 ng $mL^{-1}$ | Kaul *et al.,* 1996 |

*(see Glossary for abbreviations)

Nanoparticles (NPs) possess several distinctive physical and chemical attributes that make them promising synthetic scaffold for the creation of novel chemical and biological detection systems (Rosi and Mirkin, 2005). Indeed, in the last few years nanostructured materials, such as noble metal nanoparticles, quantum dots, and magnetic nanoparticles, have been employed in a broad spectrum of highly innovative approaches for assays of metal ions, small molecules, protein and nucleic acid biomarkers (West and Halas, 2000; Niemeyer, 2001; Parak *et al.,* 2003; Alivisatos, 2004). In this study, an electrochemical sensor was constructed using bimetallic nanoparticles.

## 2.6 Sensors

A sensor is a device, which detects a variable quantity usually electronically, and converts the measurement into signals for recording. They are composed of active sensing surface, which is connected to a signal transducer (Scheme 2.2). The role of these two important components in sensors is to transmit the signal from a selective compound or from a change

in a reaction. These devices produce signals such as electrical, thermal or optical output signals, which are converted into digital signals for further processing. The most important aspects of investigation of sensors are sensitivity, selectivity, and stability.

Sensors can be classified, according to the type of energy transfer, as thermal, electromagnetic, mechanical, and electrochemical (Ahammad *et al.,* 2009). One of the ways of classifying sensors is based on these output signals. However, from past literature, sensors have been classified according to multiple criteria (Rodgriguez *et al.,* 2004). The most common way to group sensors considers either the transducing mechanism (electrical, optical, mass, thermal, piezoelectric, etc.), the recognition principle (enzymatic, DNA, molecular recognition, etc.) or the applications (environmental, food, medical diagnosis, etc.). The general characteristics of chemical sensors include; ability to transform chemical quantities into electrical signals, responds rapidly, maintain their activity over a long time period, be small, cheap and specific to a particular analyte (Grundler, 2007).

The classifications following signal transduction include; optical sensors, which relies on absorbance, reflectance, luminescence, fluorescence, refractive index and light scattering. Electrochemical sensors among them voltammetric and potentiometric devices that are based on chemically sensitized field effect transistor and potentiometric solid electrolyte gas sensors. Electrical sensors include those with metal oxide and organic semiconductors as well as electrolytic conductivity sensors. Mass sensitive sensors include piezoelectric devices and those based on surface coustic waves. Magnetic sensors mainly based on paramagnetic gas properties. Thermometric sensors based on the measurement of the heat effect of a specific chemical reaction or adsorption involving the analyte. Other sensors are based on emission or absorption of radiation (Grundler, 2007).

On the other hand, sensors can be broadly classified into two categories as chemical sensors and biosensors. The biosensors can be defined in terms of sensing aspects, where these sensors can sense biochemical compounds such as biological proteins, nucleotides and even tissues (Wilson and Gifford, 2005; Chen and Chzo, 2006; Sakaguchi *et al.,* 2007). Biosensors are chemical sensors whereby the recognition system is based on the biochemical or biological mechanisms. Within these sensors, the active sensing material on the electrode should act as a catalyst and catalyze the reaction of the biochemical chemical compounds to obtain the output signals (Simoyi *et al.,* 2003; Vasantha and Chen, 2006). The combination of these two different ways of classifications has given rise to a new type of sensors, which are called electrochemical biosensors, where the electrochemical methods are applied for the construction and working of a biosensor (Zhang *et al.,* 2005; Balasubramanian and Burghard, 2006).

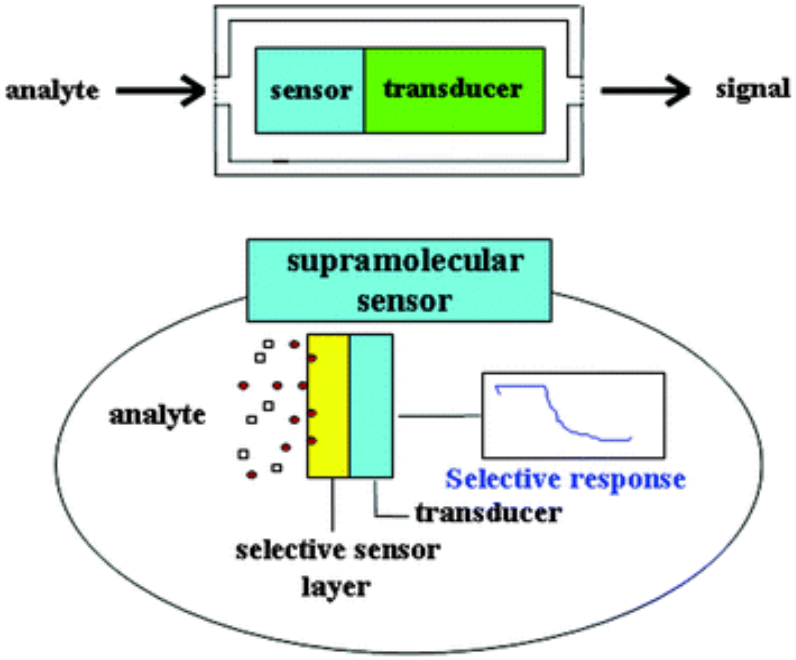


**Scheme 2.2. Series of recognition process typical in sensors (Pirondini and Dalcanale, 2007).**

Electrochemical sensors have advantage over other sensors because they can sense the materials, which are present within the host without doing any damage to the host system. They have high degree of selectivity and sensitivity. They are frequently used in clinical diagnostics, occupational safety, medical engineering, process measuring engineering, and environmental analysis (Ahammad *et al.,* 2009). They are widely used in the determination of concentrations of various analytes in samples such as fluids and dissolved solid materials.

### 2.6.1 Sensor signal transduction

Generally, a chemical sensor performs mainly two functions; recognition (sensing) and transduction. The analyte interacts in a more or less selective way with the recognition or sensing element, which shows affinity for the analyte. The sensing element may be composed of distinct molecular units called recognition receptors. The recognition element can be a material that includes in its composition certain recognition sites or a material with no distinct recognition sites but capable of interacting with the analyte. In a chemical sensor, the recognition and transduction function are integrated in the same device. An analytical device with no recognition function included is not a chemical sensor but a concentration transducer (Banica, 2012).

As a result of analyte interaction with the sensing element, certain physical or chemical properties of the sensing element vary as a function of the analyte concentration. A chemical

sensor converts this change into a measureable physical quantity. This process is called signal transduction and is reversible. In most chemical sensors, the sensing element is composed of selective layer (active materials) to improve the sensing ability as shown in Scheme 2.2. The selection and development of an active material is a challenge. The active sensing materials maybe of any kind as whichever acts as a catalyst for sensing a particular analyte or a set of analytes (Yogeswaran and Chen, 2008).

The recent development in the nanotechnology has paved the way for large number of new materials and devices of desirable properties, which have useful functions for numerous electrochemical sensor and biosensor applications (Hubalek *et al.,* 2007). New generations of low power, low cost and portable sensing devices are needed for monitoring in agriculture, chemistry, physics, medical and manufacturing areas. With the recent developments in nanoscience and nanotechnology, there is a pressing need for flexible, robust and environmentally stable sensors. The use of nanostructures including nanotubes and nanoparticles continues to be a major focus of electrochemical sensor fabrication due to their unique chemical and physical properties, such as high surface to volume ratio.

### 2.6.2 Sensors based on nanoparticles

Some of the emerging approaches for robust applications of sensors rely on nanoparticles (NPs) with diameters that range from 10 to 100 nm (Xiao *et al.,* 2011). Among the numerous reasons why exploiting NPs for sensors is promising, is the presumed ability to synthesize, if not at will, then with much control, nearly any type of NP. Several studies have shown the ability to control the NPs type (Masala and Seshadri, 2004), starting with cores made of pure metal (e.g., Au, Ag, Ni, Co, Pt, Pd, Cu, Al), metal alloys (e.g., Au/Ag, Au/Cu, Au/Ag/Cu, Au/Pt, Au/Pd, and Au/Ag/ Cu/Pd, PtRh, NiCo, PtNiFe) (Cushing *et al.,* 2004), metal oxides, semiconducting materials (e.g., Si, Ge) (Murphy, 2002), and more (Yin *et al.,* 2011; Millyard *et al.,* 2012). Secondly, the ability to cap the NPs with wide variety of molecular ligands, including alkylthiols, alkanethiolates, arenethiolate, alkyl-trimethyloxysilane, dialkyl disulfides, xanthates, oligonucleotides, DNA, proteins, sugars, phospholipids, enzymes, and more (Yonezawa *et al.,* 2001; Bhattacharya and Srivastava, 2003).

For sensing applications, this ability implies that one can obtain NPs with a hybrid combination of chemical and physical functions, which would have a great effect on the sensitivity and selectivity of the sensors. Thirdly, the ability to vary the nanoparticles size (1-100 nm) and shape (sphere-, rectangle-, hexagon-, cube-, triangle-, and star-, and branchlike outlines) and, consequently, the surface-to-volume ratio (Qian and Park, 2010; Yin *et al.,* 2011). For sensing applications, these features would allow deliberate control over the

surface properties and the related interaction “quality” with the physical parameters such as pressure, temperature, plasmon resonance, and more (Shipway *et al.,* 2000; Zamborini *et al.,* 2011). The fourth reason is attributed to the ability to prepare films of NPs with controllable porous properties. This allows control over interparticle distance as well as controllable signal and noise levels, which eventually dominates the device sensitivity on exposure to either physical or chemical parameters (Krasteva *et al.,* 2002; Haick, 2007). In addition, the presumed ability of NPs allows easier, faster, more cost-effective fabrication of flexible sensors compared to those currently in use, which mostly rely on complicated, multistep processes (Maheshwari and Saraf, 2006; Rogers and Huang, 2009; Takei *et al.,* 2010).

### 2.6.3 Fabrication of nanoparticle based sensors

Nanoparticles can either be deposited on substrates at low temperatures as sensing cap-layers or they can be integrated into the composite of a material. The common procedure for producing such NPs requires a (metal) salt as precursor, from which NPs are formed by elevating the temperature, leading to thermolysis of the pressures (Aiken and Finke, 1999; Liz-Marzán, 2004). The distance between the encapsulated NPs are controlled by choosing the encapsulating molecules or the assembly/deposition procedure. The application of the NPs on a substrate is achieved by a number of techniques such as layer by layer (LbL) (Olichwer *et al.,* 2012), coating from suspension (Xu and Wang, 2009) stamping methods (Wang *et al.,* 2009), drop casting (Segev-Bar *et al.,* 2013), inkjet printing (Herrmann *et al.,* 2007), stop and- go convective self-assembly (CSA), (Farcau *et al.,* 2011, Sangeetha *et al.,* 2012; Moreira *et al.,* 2013) and electrodeposition (Sun and Wang, 2007). Other production routes include deposition of NPs in a vacuum for strain and gas sensing, using a technique based on sputtering and condensation of atoms from a metallic target (Tanner *et al.,* 2012; Skotadis *et al.,* 2013). Additional fabrication methods that do not involve metal salts as precursors are also reported. For example, carbon NPs are fabricated by a simple flame synthesis process and then integrated into a poly-di-methyl-siloxane (PDMS) substrate, providing a durable infrared sensor that also exhibited self-cleaning properties (Yuan *et al.,* 2011).

For fabrication of sensors, it is important to pay special attention to the way the NPs are incorporated onto the substrates. Several studies have shown that variation in thickness, morphology (Segev-Bar *et al.,* 2012) and density (Tang *et al.,* 2012) of the NP films affects the sensitivity, selectivity and the overall functionality of the NP-based sensors. These variations might raise concerns regarding the reproducibility of the fabricated sensors. Nevertheless, recent advances in the fabrication of NP films e.g., layer-by-layer (Olichwer *et*

*al.,* 2012) and stop-and-go convective self assembly (Farcau *et al.,* 2011) raise expectations that NP-based sensors are likely to become a technological reality in the near future. In general, different substrates have different adhesion properties relative to the NP films. Additionally, the substrate's mechanical and geometrical properties affect the sensing signal (Segev-Bar *et al.,* 2013) as well as the sensor's lifetime.

### 2.6.4 Nanoparticles

Nanoparticles are defined as particulate dispersions or solid particles with a size in the range of 10-1000 nm (Mohanraj and Chen, 2006). In recent years, noble metal nanoparticles have been the subject of research due to their unique electronic, optical, mechanical, magnetic and chemical properties that are significantly different from those of bulk materials (Mazur, 2004). These special and unique properties could be attributed to their small sizes and large specific surface area. Monometallic and bimetallic nanoparticles (NPs) are key components in many catalytic, optical, and magnetic devices. The ability to control the composition, shape (Xiong *et al.,* 2005; Bratlie *et al.,* 2007) and architecture (Park *et al.,* 2004; Zhou *et al.,* 2005; Alayoglu *et al.,* 2008) of multi-component NP systems is of increasing importance in tailoring the resulting properties.

Synthetic approaches to NP synthesis have been evolving over the last 100 years, but most structural/ compositional information is gleaned from TEM and XRD analysis (Chou and Schaak, 2007; Fan *et al.,* 2008). These methods are quite satisfactory for large NPs (~10 nm), but obtaining similar information for smaller, catalytically relevant particles of less than 5 nm is more challenging (Nashner *et al.,* 1998; Siepen *et al.,* 2000; Garcia-Gutierrez *et al.,* 2004; Liu *et al.,* 2005; Chen *et al.,* 2008). The vast majority of bimetallic NP catalysts are prepared by impregnation/ deposition methods that often give well-dispersed, highly active systems, but the details of structure and local composition are difficult to ascertain and often remain ill-defined (Nashner *et al.,* 1997; Hills *et al.,* 1999).

Nanoalloys are bi- or multi-component metallic particles in the size range between 1-100 nm (Ferrando *et al.,* 2008). These nanoparticles are of great interest for both basic science and technological applications to magnetism, catalysis and optics. This wealth of possible applications stems from the very high degree of tunability of the physical and chemical properties of these systems, which is a direct consequence of the great variety of morphologies that nanoalloys can assume. Nanoalloys can present a variety of geometric shapes, ranging from crystalline structures, i.e. fragments of bulk crystals, to non-crystalline structures, the most common being icosahedra, decahedra and polyicosahedra (Rossi *et al.,*

2004). However, variety is not limited to the geometric shape, since the atomic arrangement in nanoalloys can form qualitatively different chemical ordering patterns.

### 2.6.5 Bimetallic nanoparticles

Bimetallic nanoparticles consist of two metal nanoparticles and have been reported to have higher catalytic properties compared to their corresponding monometallic nanoparticles due to their increased surface area (Zhou *et al.,* 2006). There are two types of bimetallic nanoparticles namely alloy nanoparticles and core-shell nanoparticles. The difference between the two arises from their method of preparation where bimetallic alloy nanoparticles are as a result of simultaneous reduction of the metal salts to nanoparticles while core-shell nanoparticles result from successive reduction of the more noble metal salt followed by the reduction of the less noble metal salt. The alloy nanoparticles are homogeneously distributed over the whole volume on an atomic scale; however, the core-shell metal nanoparticles constitute the core of the structure and the other NP as an external shell.

Bimetallic nanoparticles are of considerable interest since they posses interesting size depended electrical, chemical and optical properties (Devarajan *et al.,* 2004). They are of special importance in the field of catalyst, since they often exhibit better catalytic properties than their monometallic counterparts (Zhou *et al.,* 2006). The structure, composition, and architecture of bimetallic nanoparticles are defined by many parameters. For example, the nanoparticle shape (e.g., cuboctahedral *versus* truncated octahedral) is a distinct structural characteristic, in addition to the crystal structure (i.e., fcc vs. hcp) (Martin *et al.,* 1991; Schmid, 1995; Aiken and Finke, 1999). Bimetallic nanoparticles with the same composition, shape, and crystal structure can have different architectures (i.e., spherical fcc Pt-Rh alloys and core shell NPs) (Alayoglu and Eichhorn, 2008). They are widely used in the development of electrochemical sensors and biosensors. Recent studies have shown that shape, structure, composition (Park *et al.,* 2008) and architecture (Zhou *et al*., 2005; Alayoglu *et al.,* 2008) are extremely important parameters affecting catalytic activities of bimetallic nanostructured materials, and, as such, knowledge of these parameters is critical in understanding the underlying surface science and catalytic chemistry.

### 2.6.6 Synthesis of Nanoparticles

The synthesis of nanoparticles is a complex process and hence there is a wide range of techniques available for producing different kinds of nanoparticles. The result is that it is impossible to generalize all the synthesis techniques currently available. However, broadly these techniques essentially fall into three categories: (i) condensation from vapor, (ii)

synthesis by chemical reaction, and (iii) solid-state processes such as milling (Ghosh and Paria, 2012). By using the above-mentioned techniques, not only pure nanoparticles but also hybrid or coated nanoparticles (with hydrophilic or hydrophobic materials depending on the suitability of the applications) can be synthesized (Ghosh and Paria, 2012). Initially researchers studied single nanoparticles because such particles have much better properties than the bulk materials. Later, in the late 1980s, researchers found that heterogeneous, composite or sandwich colloidal particles have better efficiency than their corresponding single particles; in some cases, they even develop some new properties (Spanhel *et al.,* 1987; Youn *et al.,* 1988; Henglein, 1989). More recently, there has been a gradual increase in research activity because of the tremendous need for advanced nanomaterials fuelled by the demands of modern technology.

Approaches for nanomaterial synthesis can be broadly divided into two categories: "top-down" and "bottom-up". The "top-down" approach often uses traditional workshop or microfabrication methods where externally controlled tools are used to cut, mill, and shape materials into the desired shape and order. For example, the most common techniques are lithographic techniques (e.g., UV, electron or ion beam, scanning probe, optical near field) (Subramanian *et al.,* 1998) laser-beam processing (Hong *et al.,* 1997), and mechanical techniques (e.g., machining, grinding, and polishing) (Dodd, 2009). "Bottom-up" approaches, on the other hand, exploit the chemical properties of the molecules to cause them to self-assemble into some useful conformation. The most common bottom-up approaches are chemical synthesis, chemical vapor deposition, laser-induced assembly (i.e., laser tapping), self-assembly, colloidal aggregation, film deposition and growth (Sneh *et al.,* 2002; Yoo *et al.,* 2009), etc. Currently neither the top-down nor bottom-up approach is superior; each has its advantages and disadvantages. However, the bottom-up approach can produce much smaller sized particles and has the potential to be more cost-effective in the future because of the advantages of absolute precision, complete control over the process, and minimum energy loss compared with that of a top-down approach.

In order to obtain nanoparticles efficiently and effectively, several physical and chemical methods have been used for synthesizing and stabilizing nanoparticles (Senapati, 2005). However, the most popular chemical approaches, include chemical reduction using a variety of organic and inorganic reducing agents, electrochemical techniques, physicochemical reduction, and radiolysis. Solution-phase reduction method (Pillai and Kamat, 2004) appears to be of particular interest since they offer the potential of simple operation, controlling the size of the synthesized nanoparticles easily. The nanoparticle synthesis usually makes use of a soluble metal salt, a reducing agent, and a stabilizing agent. The stabilizing agent caps the particle and prevents further growth or aggregation. Reducing agents such as citrate

(Pillai and Kamat, 2004) and sodium borohydride (Turkevich *et al.,* 1951; Yee *et al.,* 1999) are commonly used for the preparation of metal nanoparticles. Since one can control the growth process by the choice of the stabilizer, it is possible to manipulate the shape and size of the metal nanoparticles (Pillai and Kamat, 2004).

Various forms of nanostructures such as nanoparticles, nanospheres or nanocapsules can be obtained depending upon the method of preparation. Metal nanostructures have been synthesized in many forms, such as nanorods, nanowires, nanotubes, and shape-controlled nanocrystals (Ahmadi *et al.,* 1996; Fu *et al.,* 2002; Melosh *et al.,* 2003, Zhao *et al.,* 2004). The development of new nanostructured materials with optimal physicochemical characteristics for specific scientific and technological applications has necessarily promoted the use of chemical methods, which can obtain materials with controlled particle size and distribution (Morales *et al.,* 2010).

### 2.6.7 Properties of nanoparticles

There are numerous properties of nanoparticles, among many others, on a nanoscale are the small size, which leads to an increased surface area to volume ratio and to an increase in the dominance of the surface atoms of the nanoparticle over those in its interior (Ghosh and Paria, 2012) and as a result the domain where quantum effects predominate is entered. The unique optical properties associated with nanoparticles and their composite materials include a high- or low-refractive index, high transparency, novel photoluminescence properties, photonic crystal, and plasmon resonance (Jain *et al.,* 2007). The properties of nanoparticles are not only size dependent but are also linked to the actual shape. Other nanoparticle physical and chemical properties such as catalytic activity and selectivity (Wang *et al.,* 1997; Lee *et al.,* 2006), electrical (Lieber, 1998) and optical properties (Stuart *et al.,* 2005; Millstone *et al.,* 2009) and melting point (Gupta *et al.,* 2008) are also all highly shape-dependent. Nanoparticles are very different from their bulk materials in their electronic, optical and catalytic properties originated from their quantum-scale dimensions (Alivisatos, 1996; Israel *et al.,* 2001). These properties make most nanoparticles ideal for variety of applications such as sensors and catalysts.

## 2.7 Nanoparticles as sensors

The unique physical and chemical properties of nanostructured materials provide excellent prospects for interfacing chemical recognition events with electronic signal transduction and for designing a new generation of sensing probes with novel functions and improved sensing devices, especially electrochemical sensors and biosensors. Nanoparticles of monometallic,

bimetallic, metal oxide and semi-conductors have been used for constructing electrochemical sensors, for example, the use of gold nanoparticles modified glassy carbon electrode (Liu *et al.,* 2008) as an electrochemical sensor for the determination of trace Cr (VI) has been developed.

Metal nanoparticles provide three important functions for electroanalysis namely improved mass transport, high effective surface area and catalytic properties (Luo *et al.,* 2006). Several monometallic and bimetallic nanoparticles have been used as catalysts and electrocatalyst due to the unique catalytic properties caused by their high surface area. For example, Tianyan *et al*., 2003, prepared a highly sensitive $H_2O_2$ sensor based on the modification of carbon film electrode with Pt nanoparticles. In other applications, an electrochemical nitrate sensor was developed by the modification of glassy carbon electrode with Au-Fe (III) nanoparticles (Liu *et al.,* 2009). Silver-gold bimetallic nanoparticles immobilized on the surface of glassy carbon electrode was used in the electrocatalytic oxidation of glucose (electrochemical glucose sensor) (Tominaga *et al.,* 2008). Both bimetallic Pt-based alloy nanoparticles and core-shell nanoparticles have been used as more effective heterogeneous catalysts in the development of an efficient energy technology (Long *et al.,* 2011).

Nanoparticles have excellent conductivity and catalytic properties, which make them act as “electronic wires” to enhance the electron transfer between redox centers in proteins and electrode surfaces, and as catalysts to increase electrochemical reactions. Oxide nanoparticles are often used as labels or tracers for electrochemical analysis. Gold nanoparticles have been used to immobilize proteins through the covalent bonds formed between the gold atoms and amide groups and cysteine residues of proteins (Gole *et al.,* 2002). Other nanoparticles such as Pt, Ag, $TiO_2$, $ZrO_2$ and bimetallic nanoparticles such as Ag-Au and Au-Pt alloy nanoparticles have also been applied in the immobilization of enzymes. Electrochemical immunosensors based on the immobilization of antigen or antibody with nanoparticles have also been applied extensively. For example, Zhuo *et al*., 2005 developed a reagent less amperometric immunosensor based on the immobilization of ά-1-fetoprotein antibody onto gold nanoparticles and the immunosensor exhibited good long-term stability.

The introduction of nanoparticles with catalytic effects into electrochemical sensors and biosensors can decrease overpotentials of many analytically important electrochemical reactions and even realize the reversibility of some redox reactions, which are irreversible at common unmodified electrode. For example, Ohsaka and Coworkers, Raj *et al.,* 2003 developed an electrochemical sensor for selective detection of dopamine in the presence of

ascorbic acid based on the catalytic effect of gold nanoparticles on the ascorbic acid oxidation. This resulted in the decrease of the oxidation overpotential of ascorbic acid and the effective separation of the oxidation potentials of ascorbic and dopamine, thus allowing the selective electrochemical detection.

In addition, nanoparticles have been used to fabricate biosensors whereby certain enzymes have been attached on nanoparticles-modified electrodes. According to Luo *et al*., (2006) both monometallic and bimetallic nanoparticles have several functions in electrochemical sensors and biosensors. For example, an electrochemical biosensor was developed by the immobilization of superoxide dismutase (SOD) on gold nanoparticles modified indium /tin oxide film coated glass (Wang *et al.,* 2008). Moreover, Kang and others developed a novel glucose biosensor based on immobilization of glucose oxidase in chitosan on GCE modified with gold-platinum alloy nanoparticles (Kang *et al.,* 2007).

However, enzymes usually lack direct electrochemical communication with electrodes since the active centers are surrounded by considerably thick insulating protein shells, hence blocking the electron transfer between electrodes and the active centers. Conductivity properties of nanoparticles, mostly metal nanoparticles at nanoscale dimensions makes them suitable for enhancing the electron transfer between the active centers of enzymes and the electrodes. They act as electron transfer “mediators” or “electrical wires” e.g. Ag and Au nanoparticles, which have good conductivity and have been used to enhance electron transfer between proteins and electrodes (Liu *et al.,* 2003).

The labelling of biomolecules, such as antigen, antibody and DNA with nanoparticles plays an increasingly important role in developing sensitive electrochemical biosensors. Biomolecules labelled with nanoparticles can retain their bioactivity and interact with their counterparts. Based on the electrochemical detection of those label nanoparticles, the amount or concentration of analytes can be determined. Metal nanoparticles labels can be used in both immunosensors and DNA sensors. Gold nanoparticles are the most frequently used among all the metal nanoparticles labels available. For example, Limoges’s group (Dequaire *et al.,* 2000) has reported a sensitive electrochemical immunosensor for goat immunoglobulin G (IgG) based on a gold nanoparticles label.

Nanoparticles are chemically more active than the related bulk materials due to their high surface energy. For example, $MnO_2$ is known to catalyze the decomposition of $H_2O_2$, while $MnO_2$ nanoparticles can react with $H_2O_2$ directly (Xu *et al.,* 2005). However, the application of the special reactivity of electrochemical sensors and biosensors has not been extensively studied. Reviewing the literature revealed a need to develop effective detection platforms for

the monitoring of various pharmaceuticals such as antiretrovirals. This is further necessitated by the scourge in AIDS pandemic, which has a global effect on human lives. Until recently, few studies have reported voltammetric techniques for such applications with the incorporation of bimetallic nanoparticles as detection probes for pharmaceuticals.

## 2.8 References


Accinelli, C., Caracciolo, A.B. and Grenni, P. 2007. Degradation of the antiviral drug oseltamivir carboxylate in surface water samples. *Int. J. Environ. Anal. Chem.,* 87(8): 579-587.

Ahammad, A.J.S., Lee, J.J. and Rahman, Md. A. 2009. Review. Electrochemical sensors based on carbon nanotubes. *Sensors*, 9: 2289-2319.

Ahmadi, T.S., Wang, Z.L., Green, T.C., Henglein, A., El-Sayed, M.A. 1996. Shape controlled synthesis of colloidal platinum nanoparticles. *Science*, 272: 1924-1926.

Aiken, J.D., Finke, R.G. 1999. Review of modern transition- metal nanoclusters: their synthesis, characterization and applications in catalysis. *J. Mol. Catal. A: Chem.*, 145: 1-44.

Alayoglu, S., Eichhorn, B. 2008. Rh-Pt bimetallic catalysts: synthesis, characterization, and catalysis of core-shell, alloy, and monometallic nanoparticles. *J. Am. Chem. Soc.,* 130: 17479-17486.

Alayoglu, S., Nilekar, A.U., Mavrikakis, M., Eichhorn, B. 2008. Ru-Pt core-shell nanoparticles for preferential oxidation of carbon monoxide in hydrogen. *Nat. Mater.,* 7: 333-338.

Alivisatos, A.P. 1996. Semiconductor clusters, nanocrystals and quantum dots. *Science*, 271: 933.

Alivisatos, P. 2004. The use of nanocrystals in biological detection. *Nat. Biotechnol.,* 22: 47-52.

Anderson, J., Kräusslich, H.G. and Bartenschlager, R. (Ed.) 2009. *Handbook of Experimental Pharmacology, 189: Antiviral strategies.* Springer Verlag, Berlin Heidelberg.

Balasubramanian, K., Burghard, M. 2006. Biosensors based on carbon nanotubes. *Anal. Bioanal. Chem.,* 385: 452-468.

Banica, F.G. 2012. *Chemical Sensors and Biosensors*: *Fundamentals and Applications*. Chichester, UK: John Wiley & Sons, Science. p. 576.

Bhattacharya, S., Srivastava, A. 2003. Synthesis and characterization of novel cationic lipid and cholesterol-coated gold nanoparticles and their interactions with dipalmitoylphosphatidylcholine membranes. *Langmuir,* 19: 4439-4447.

Bound, J.P. and Voulvoulis, N. 2005. Household disposal of pharmaceuticals as a pathway for aquatic contamination in the United Kingdom. *Environ. Health Perspect.,* 113(12): 1705-1711.

Bratlie, K.M., Lee, H., Komvopoulos, K., Yang, P.D., Somorjai, G.A. 2007. Platinum nanoparticle shape effects on benzene hydrogenation selectivity. *Nano Letters,* 7: 3097-3101.

Buchberger, W.W. 2007. Novel analytical procedures for screening of drug residues in water, waste water, sediment and sludge. *Anal. Chim. Acta*, 593(2): 129-139.

Castro, A.A., Aucelio, R.Q., Rey, N.A., Miguel, E.M., Farias, P.A. 2011. Determination of the antiretroviral drug nevirapine in diluted alkaline electrolyte by adsorptive stripping voltammetry at the mercury film electrode. *Comb. Chem. High Throughput Screening*, 14: 22-27.

Chen, S.M., Chzo, W.Y. 2006. Simultaneous voltammetric detection of dopamine and ascorbic acid using didodecyldimethylammonium bromide (DDAB) film-modified electrodes. *J. Electroanal. Chem.,* 587: 226-234.

Chen, W., Li, W., Ling, X., Wang, X., Liu, J. 2010. Study on the interaction between HIV reverse transcriptase and its non-nucleoside inhibitor nevirapine by capillary electrophoresis. *J. Chromatogr. B*, 878: 1714-1717.

Chen, Y.M., Yang, F., Dai, Y., Wang, W.Q., Chen, S.L. 2008. Ni-Pt core-shell nanoparticles: synthesis, structural and electrochemical properties. *J. Phys. Chem. C,* 112: 1645-1649.

Chi, J., Jayewardene, A.L., Stone, J.A., Aweeka, F.T. 2003. An LC-MS-MS method for the determination of nevirapine, a non-nucleoside reverse transcriptase inhibitor, in human plasma. *J. Pharm. Biomed. Anal.,* 31: 953-959.

Chiba, M., Hensleigh, M. and Lin, J.H. 1997. Hepatic and intestinal metabolism of indinavir, an HIV protease inhibitor, in rat and human microsomes. *Biochem. Pharmacol.,* 53: 1187-1195.

Chou, N.H., Schaak, R.E. 2007. Shape-controlled conversion of -Sn nanocrystals into intermetallic M-Sn (M=Fe, Co, Ni, Pd) nanocrystals. *J. Am. Chem. Soc.*, 129: 7339-7345.

Cushing, B.L., Kolesnichenko, V.L., O'Connor, C.J. 2004. Recent advances in the liquid-phase syntheses of inorganic nanoparticles. *Chem. Rev.,* 104: 3893-3946.

De Clercq, E. 2004. Antivirals and antiviral strategies. *Nat. Rev. Microbiol.,* 2: 704-720.

Dequaire, M., Degrand, C. and Limoges, B. 2000. An electrochemical metalloimmunoassay based on a colloidal gold label. *J. Anal. Chem.,* 72(22): 5521-5528.

Devarajan, S., Vimalan, B., Sampath, S. 2004. Phase transfer of Au-Ag alloy nanoparticles from aqueous medium to an organic solvent: effect of aging of surfactant on the formation of Ag-rich alloy compositions. *J. Colloid Interface Sci.,* 278: 126-132.

Diamond, D. 1998. *Principles of chemical and biological sensors*. John Wiley & Sons, Inc.; New York, NY. pp. 1-18.

Dodd, A.C. 2009. A comparison of mechanochemical methods for the synthesis of nanoparticulate nickel oxide. *Powder Technol.,* 196(1): 30-35.

Erk, N. 2004. Spectrophotometric determination of indinavir in bulk and pharmaceutical formulations using bromocresol purple and bromothymol blue. *Pharmazie*, 59(3): 183-186.

Famiglini, V. and Silvestri, R. 2016. Review Focus on Chirality of HIV-1 Non-Nucleoside Reverse Transcriptase Inhibitors. *Molecules,* 21: 221.

Fan, F.R., Liu, D.Y., Wu, Y.F., Duan, S., Xie, Z.X., Jiang, Z.Y., Tian, Z.Q. 2008. Epitaxial growth of heterogeneous metal nanocrystals: from gold nano-octahedra to palladium and silver nanocubes. *J. Am. Chem. Soc.*, 130(22): 6949-6951.

Farcau, C., Sangeetha, N.M., Moreira, H., Viallet, B., Grisolia, J., Ciuculescu-Pradines, D., Ressier, L. 2011. High-sensitivity strain gauge based on a single wire of gold nanoparticles fabricated by stop-and-go convective self-assembly. *ACS Nano.,* 5: 7137-7143.

Ferrando, R., Jellinek, J. and Johnston, R.L. 2008. Nanoalloys: from theory to applications of alloy clusters and nanoparticles. *Chem. Rev*., 108(3): 845-910.

Fraser, C.M., Bergeron, J.A., Mays, A. and Aiello, S.E. 1991. *The Merck Veterinary Manual*, Merck Sharp and Dohme, NJ.

Fu, X., Wang, Y., Wu, N., Gui, L., Tang, Y. 2002. Shape-selective preparation and properties of oxalate-stabilized Pt colloid. *Langmuir*, 18: 4619-4624.

Galasso, G.J., Boucher, C.A.B., Cooper, D.A. and Katzenstein, D.A. 2002. *Practical guidelines in antiviral therapy*. 1st Edition, Elsevier B.V., Amsterdam.

Garcia-Gutierrez, D., Gutierrez-Wing, C., Miki-Yoshida, M., Jose-Yacaman, M. 2004. HAADF study of Au-Pt core-shell bimetallic nanoparticles. *Appl. Phys. A,* 79: 481-487.

Ghosh, C.R. and Paria, S. 2012. Core/shell nanoparticles: classes, properties, synthesis mechanisms, characterization and applications. *Chem. Rev.,* 112: 2373-2433.

Gill, C.J., Hamer, D., Simon, J.L., Thea, D.M., Sabin, L. 2005. No room for complacency about adherence to antiretroviral therapy in sub-Saharan Africa. *AIDS*, 19: 1243-1249.

Gole, A., Vyas, S., Phadtare, S., Lachke, A., Sastry, M. 2002. Studies on the formation of bioconjugates of endoglucanase with colloidal gold. *Colloids Surf. B,* 25(2): 129-138.

Gomes, N.A., Vaidya, V.V., Pudage, A., Joshi, S.S. and Parekh, S.A. 2008. Liquid chromatography tandem mass spectrometry (LCMS/MS) method for simultaneous determination of tenofovir and emtricitabine in human plasma and its application to a bioequivalence study. *J. Pharm. Biomed. Anal.,* 48(3): 918-926.

Goyal, R.N., Gupta, V.K., Oyama, M., Bachheti, N. 2005. Differential pulse voltammetric determination of paracetamol at nanogold modified indium tin oxide electrode. *Electrochem. Commun.,* 7: 803-807.

Grob, P.M., Wu, J.C., Cohen, K.A., Ingraham, R.H., Shih, C.K., Hargrave, K.D., McTague, T.L., Merluzzi, V.J. 1992. Non-nucleoside inhibitors of HIV-1 reverse transcriptase: nevirapine as a prototype drug. AIDS Res. *Hum. Retroviruses*. 8(2): 145-152.

Grundler, P. 2007. *Chemical Sensors: An introduction for scientists and engineers*. Springer, Berlin Heidelberd New York. p. 274.

Gu, Z., Quan, Y., Li, Z., Arts, E.J., Wainberg, M.A. 1995. Effects of non-nucleoside inhibitors of human immunodeficiency virus type 1 in cell-free recombinant reverse transcriptase assays. *J. Boil. Chem.,* 270(52): 31046-31051.

Gulick, R.M., Mellors, J.W., Havlir, D., Eron, J.J., Gonzalez, C., McMahon, D., Richman, D.D., Valentine, F.T., Jonas, L., Meibohm, A., Emini, E.A. and Chodakewitz, J.A. 1997. Treatment with indinavir, zidovudine and lamivudine in adults with human immunodeficiency virus infection and prior antiretroviral therapy. *N. Engl. J. Med.,* 337: 734-739.

Gupta, S.K., Talati, M., Jha, P.K. 2008. Shape and size dependent melting point temperature of nanoparticles. *Mater. Sci. Forum,* 570: 132-137.

Gupta, V.K., Jain, R., Radhapyari, K., Jadon, N., Agarwal, S. 2011. Voltammetric techniques for the assay of pharmaceuticals-a review. *Anal. Biochem.,* 408: 179-196.

Haick, H. 2007. Chemical sensors based on molecularly modified metallic nanoparticles. *J. Phys. D: Appl. Phys.,* 40(23): 7173-7186.

Hammam, E. 2004. Behaviour and quantification studies of amiloride drug using cyclic and square-wave adsorptive stripping voltammetry at a mercury electrode. *J. Pharm. Biomed. Anal.,* 34: 1109-1116.

Henglein, A. 1989. Small-particle research: physicochemical properties of extremely small colloidal metal and semiconductor particles. *Chem. Rev.,* 89(8): 1861-1863.

Herrmann, J., Muller, K.H., Reda, T., Baxter, G.R., Raguse, B., De Groot, G.J.J.B., Chai, R., Roberts, M., Wieczorek, L. 2007. Nanoparticle films as sensitive strain gauges. *Appl. Phys. Lett.*, 91: 183105.

Hills, C.W., Nashner, M.S., Frenkel, A.I., Shapley, J.R., Nuzzo, R.G. 1999. Carbon support effects on bimetallic Pt-Ru nanoparticles formed from molecular precursors. *Langmuir*, 15: 690-700.

Hollanders, R.M.F., van Ewijk-Beneken Kolmer, E.W.J., Burger, D.M., Wuis, E.W., Koopmans, P.P., Hekster, Y.A. 2000. Determination of nevirapine, an HIV-1 non-nucleoside

reverse transcriptase inhibitor, in human plasma by reversed-phase high-performance liquid chromatography. *J. Chromatogr. B,* 744: 65-71.

Hong, L.I., Vilar, R.M., Youming, W. 1997. Laser beam processing of a SiC particulate reinforced 6061 aluminium metal matrix composite. *J. Mater. Sci.,* 32: 5545-5550.

Hubalek, J., Hradecky, J., Adam, V., Krystofova, O., Huska, D., Masarik, M., Trnkova, L., Horna, A., Klosova, K., Adamek, M., Zehnalek, J., Kizek, R. 2007. Spectrometric and voltammetric analysis of urease-nickel nanoelectrode as an electrochemical sensor. *Sensors,* 7: 1238-1255.

Israel, L.B., Kariuki, N.N., Li, H., Maye, M.M., Luo, J., Zhong, C.J. 2001. Electroactivity of $Cu^{2+}$ at a thin film assembly of gold nanoparticles linked by 11-mercaptoudecanoic acid. *J. Electroanal. Chem.,* 517(1-2): 69-71.

Jackson, J.B., Musoke, P., Fleming, T., Guay, L.A., Bagenda, D., Allen, M., Nakabiito, C., Sherman, J., Bakaki, P., Owor, M., Ducar, C., Deseyve, M., Mwatha, A., Emel, L., Duefield, C., Mirochnick, M., Fowler, M.G., Mofenson, L., Miotti, P., Gigliotti, M., Bray, D. and Mmiro, F. 2003. Intrapartum and neonatal single-dose nevirapine compared with zidovudine for prevention of mother-to-child transmission of HIV-1 in Kampala, Uganda: 18-month follow-up of the HIVNET 012 randomised trial. *Lancet*, 362(9387): 859-868.

Jain, P.K., Huang, X., El-Sayed, I.H., El-Sayed, M.A. 2007. Review of some interesting surface plasmon resonance-enhanced properties of noble metal nanoparticles and their applications to biosystems. *Plasmonics,* 2: 107-118.

Jayewardene, A.L., Kearney, B., Stone, J.A., Gambertoglio, J.G. and Aweeka, F.T. 2001. An LCMSMS method for the determination of indinavir, an HIV 1 protease inhibitor, in human plasma. *J. Pharm. Biomed. Anal.,* 25(2): 309-317.

Jullien, V., Tréluyer, J.M., Pons, G. and Rey, E. 2003. Determination of tenofovir in human plasma by high performance liquid chromatography with spectrofluorimetric detection. *J. Chromatogr. B*, 785(2): 377-381.

Kandagal, P.B., Manjunatha, D.H., Seetharamappa, J. and Kalanur, S.S. 2008. RPHPLC method for the determination of tenofovir in pharmaceutical formulations and spiked human plasma. *Anal. Lett.,* 41(4): 561-570.

Kang, X., Mai, Z., Zou, X., Cia, P., Mo, D.J. 2007. A novel glucose biosensor based on immobilization of glucose oxidase in Chitosan on a glassy carbon electrode modified with gold-platinum alloy nanoparticles/multiwall carbon nanotubes. *Anal. Biochem.,* 369: 71-79.

Kaul, N., Agrawal, H., Paradkar, A.R., Mahadik, K.R. 2004. HPTLC method for determination of nevirapine in pharmaceutical dosage form. *Talanta*, 62: 843-852.

Kaul, S., Stouffer, B., Mummaneni, V., Turabi, N., Mantha, S., Jayatilak, P., Barbhaiya, R. 1996. Specific radioimmunoassays for the measurement of stavudine in human plasma and urine. *J. Pharm. Biomed. Anal.,* 15: 165-174.

King, T., Bushman, L., Kiser, J., Anderson, P.L., Ray, M., Delahunty, T. and Fletcher, C.V. 2006. Liquid chromatography tandem mass spectrometric determination of tenofovirdiphosphate in human peripheral blood mononuclear cells. *J. Chromatogr. B,* 843(2): 147-156.

Koup, R.A., Merluzzi, V.J., Hargrave, K.D., Adams, J., Grozinger, K., Eckner, R.J. and Sullivan, J.L. 1991. Inhibition of Human immunodeficiency virus type 1 (HIV-1) replication by the dipyridodiazepinone BI-RG-587. *J. infect. Dis.,* 163(5): 966-970.

Krasteva, N., Besnard, I., Guse, B., Bauer, R.E., Müllen, K., Yasuda, A., Vossmeyer, T. 2002. Self-assembled gold nanoparticle/ dendrimer composite films for vapor sensing applications. *Nano Lett.,* 2: 551-555.

Kumar, G.N., Rodrigues, A.D., Buko, A.M. and Denissen, J.F. 1996. Cytochrome P450-mediated metabolism of the HIV-1 protease inhibitor ritonavir (ABT-538) in human liver microsomes. *J. Pharmacol. Exp. Ther.,* 277: 423-431.

Kummerer, K. 2009. The presence of pharmaceuticals in the environment due to human use-present knowledge and future challenges. *J. Environ. Manag.,* 90(8): 2354-2366.

Lallemant, M., Jourdain, G., Le Coeur, S., Mary, J.Y., Ngo-Giang-Huong, N., Koetsawang, S., Kanshana, S., McInstosh, K. and Thaineua, V., Perinatal HIV Prevention Trial (Thailand) Investigators. 2004. Single-dose perinatal nevirapine plus standard zidovudine to prevent mother-to-child transmission of HIV-1 in Thailand. *N. Engl. J. Med.*, 351(3): 217-228.

Lee, H., Habas, S.E., Kweskin, S., Butcher, D., Somorjai, A., Yang, P. 2006. Morphological control of catalytically active platinum nanocrystals. *Angew. Chem. Int. Ed.,* 45: 7824-7828.

Lees, D. 2000. Viruses and bivalve shellfish. *Int. J. Food Microbiol.*, 59: 81-116.

Li, W., Coombs, R.W., Collier, A.C. and Raisys, V.A. 1999. Determination of indinavir, a HIV-1 protease inhibitor, in human plasma using ion pair reversed phase high performance liquid chromatography. *Ther. Drug Monit.,* 21(3): 360-366.

Lieber, C.M. 1998. One-dimensional nanostructures: Chemistry, physics and applications. *Solid State Commun.,* 107(11): 607-616.

Liu, B., Lu, L., Wang, M. and Yanqin, Z. 2008. A study of nanostructured gold modified glassy carbon electrode for the determination of trace Cr (VI). *J. Chem. Sci.*, 5: 493-498.

Liu, H.B., Pal, U., Medina, A., Maldonado, C., Ascencio, J.A. 2005. Structural incoherency and structure reversal in bimetallic Au-Pd nanoclusters. *Phys. Rev. B*, 71: 075403.

Liu, T., Gan, X., Fan, C., Li, G. and Matsuda, N. 2003. Wiring electrons of cytochrome C with silver nanoparticles in layered films. *ChemPhysChem*, 4: 1364-1366.

Liu, T., Kang, T., Lu, L., Zhang, Y., Cheng, S. 2009. Au-Fe(III) nanoparticle modified glassy carbon electrode for electrochemical nitrite sensor. *J. Electroanal. Chem.,* 632(1-2): 197-200.

Liz-Marzán, L.M. 2004. Nanometals: Formation and color. *Mater. Today*, 17: 26-31.

Lockman, S., Shapiro, R.L., Smeaton, L.M., Wester, C., Thior, I., Stevens, L., Chand, F., Makhema, J., Moffat, C., Asmelash, A., Ndase, P., Arimi, P., Van Widenfelt, E., Mazhani, L., Novitsky, V., Lagakos, S. and Essex, M. 2007. Response to antiretroviral therapy after a single, peripartum dose of nevirapine. *N. Engl. J. Med.*, 356(2): 135-147.

Long, N.V., Hien, T.D., Asaka, T., Ohtaki, M., Nogami, M. 2011. Synthesis and characterization of Pt-Pd alloy and core-shell bimetallic nanoparticles for direct methanol fuel cells (DMFCs): Enhanced electrocatalytic properties of well-shape core-shell morphologies and nanostructures. *Int. J. Hydrog. Energy*, 36: 8478-8491.

Luo, X., Morrin, A., Killard, A.J., Smyth, M.R. 2006. Application of nanoparticles in electrochemical sensors and biosensors*. Electroanalysis*, 18(4): 319-326.

Ma, J.Y., Zhang, Y.S., Zhang, X.H., Zhu, G.B., Liu, B., Chen, J.H. 2012. Sensitive electrochemical detection of nitrobenzene based on macro-/meso-porous carbon materials modified glassy carbon electrode. *Talanta*, 88: 696-700.

Mager, P.P. 1997. ChemInform abstract: a check on rational drug design: molecular simulation of the allosteric inhibition of HIV-1 reverse transcriptase. *Med. Res. Rev.,* 17: 235-276.

Maheshwari, V., Saraf, R.F. 2006. High-resolution thin-film device to sense texture by touch. *Science,* 312: 1501-1504.

Marseille, E., Kahn, J.G., Mmiro, F., Guay, L., Musoke, P., Fowler, M.G. and Jackson, J.B. 1999. Cost effectiveness of single-dose nevirapine regimen for mothers and babies to decrease vertical HIV-1 transmission in sub-Saharan Africa. *Lancet*, 354(9181): 803-809.

Martin, T.P., Bergmann, T., Gohlich, H., Lange, T. 1991. Shell structure of clusters. *J. Phys. Chem.,* 95: 6421-6429.

Masala, O., Seshadri, R. 2004. Synthesis routes for large volumes of nanoparticles. *Annu. Rev. Mater. Res.,* 34: 41-81.

Mascolo, G., Balest, L., Cassano, D., Laera, G., Lopez, A., Pollice, A. and Salerno, C. 2010. Biodegradability of pharmaceutical industrial wastewater and formation of recalcitrant organic compounds during aerobic biological treatment. *Bioresour. Technol.,* 101(8): 2585-2591.

Mashhadizadeh, M.H., Akbarian, M. 2009. Voltammetric determination of some anti-malarial drugs using a carbon paste electrode modified with $Cu(OH)_2$ nano-wire. *Talanta,* 78: 1440-1445.

Mazur, M. 2004. Electrochemically prepared silver nanoflakes and nanowires. *Electrochem. Commun.,* 6(4): 400-403.

Melosh, N.A., Doukai, A., Diana, F., Gerardot, B., Badolato, A., Petroff, P.M., Heath, J.R. 2003. Ultra high-density nanowire lattices and circuits. *Science*, 300: 112-115.

Merluzzi, V.J., Hargrave, K.D., Labadia, M., Grozinger, K., Skoog, M., Wu, J.C., Shih, C.K., Eckner, K., Hattox, S., Adams, J., Rosenthal, A.S., Faanes, R., Ecker, R.J., Koup, R.A.,

Sullivian, J.L. 1990. Inhibition of HIV-1 replication by a non-nucleoside reverse transcriptase inhibitor. *Science*, 250(4986): 1411-1413.

Mills, E.J., Nachega, J.B., Buchan, I., Orbinski, J., Attaran, A., Singh, S., Rachlis, B., Wu, P., Cooper, C., Thabane, L., Wilson, K., Guyatt, G.H., Bangsberg, D.R. 2006. Adherence to antiretroviral therapy in sub-Saharan Africa and North America: a meta-analysis. *J. Am. Med. Assoc.,* 296(6): 679-690.

Millstone, J.E., Hurst, S.J., Metraux, G.S., Cutler, J.I., Mirkin, C.A. 2009. Colloidal gold and silver triangular nanoprisms. *Small,* 5: 646-664.

Millyard, M.G., Min Huang, F., White, R., Spigone, E., Kivioja, J., Baumberg, J.J. 2012. Stretch-induced plasmonic anisotropy of self-assembled gold nanoparticle. *Mats. Appl. Phys. Lett.,* 100: 073101.

Mohanraj, V.J. and Chen, Y. 2006. Nanoparticles-A Review. *Trop. J. Pharm. Res.,* 5(1): 561-573.

Morales, B.E., Gamboa, S.A., Pal, U., Guardian, R., Acosta, D., Magan, C., Mathew, X. 2010. Synthesis and characterization of colloidal platinum nanoparticles for electrochemical applications*. Int. J. Hydrogen Energy,* 35: 4215-4221.

Moreira, H., Grisolia, J., Sangeetha, N.M., Decorde, N., Farcau, C., Viallet, B., Chen, K., Viau, G., Ressier, L. 2013. Electron transport in gold colloidal nanoparticle-based strain gauges. *Nanotechnology*, 24: 095701.

Mui, P.W., Jacober, S.P., Hargrave, K.D., Adams, J. 1992. Crystal structure of nevirapine, a non-nucleoside inhibitor of HIV-1 reverse transcriptase, and computational alignment with a structurally diverse inhibitor. *J. Med. Chem.,* 35: 201-202.

Murphy, C.J. 2002. Optical sensing with quantum dots. *Anal. Chem.*, 74: 520A-526A.

Nashner, M.S., Frenkel, A.I., Adler, D.L., Shapley, J.R., Nuzzo, R.G. 1997. Structural characterization of carbon-supported platinum-ruthenium nanoparticles from the molecular cluster precursor $PtRu_5C(CO)_{16}$. *J. Am. Chem. Soc.,* 119: 7760-7771.

Nashner, M.S., Frenkel, A.I., Somerville, D., Hills, C.W., Shapley, J.R., Nuzzo, R.G. 1998. Core shell inversion during nucleation and growth of bimetallic Pt/Ru nanoparticles. *J. Am. Chem. Soc.,* 120: 8093-8101.

Niemeyer, C.M. 2001. Nanoparticles, proteins, and nucleic acids: Biotechnology meets materials science. *Angew. Chem. Int. Ed.,* 40: 4128-4158.

Notari, S., Mancone, C., Alonzi, T., Tripodi, M., Narciso, P., Ascenzi, P. 2008. Determination of abacavir, amprenavir, didanosine, efavirenz, nevirapine, and stavudine concentration in human plasma by MALDI-TOF/TOF. *J. Chromatogr. B,* 863: 249-257.

Olichwer, N., Leib, E.W., Halfar, A.H., Petrov, A., Vossmeyer, T. 2012. Cross-linked gold nanoparticles on polyethylene: resistive responses to rensile strain and vapors. *ACS Appl. Mater. Interfaces*, 4: 6151-6161.

Parak, W.J., Gerion, D., Pellegrino, T., Zanchet, D., Micheel, C., Williams, S.C., Boudreau, R., Le Gros, M.A., Larabell, C.A., Alivisatos, A.P. 2003. Biological applications of colloidal nanocrystals. *Nanotechnology,* 14: R15-R27.

Park, J.I., Kim, M.G., Jun, Y.W., Lee, J.S., Lee, W.R., Cheon, J. 2004. Characterization of superparamagnetic “core-shell” nanoparticles and monitoring their anisotropic phase transition to ferromagnetic “solid solution” nanoalloys. *J. Am. Chem. Soc.*, 126: 9072-9078.

Park, J.Y., Zhang, Y., Grass, M., Zhang, T., Somorjai, G.A. 2008. Tuning of catalytic co oxidation by changing composition of Rh-Pt bimetallic nanoparticles. *Nano Lett.*, 8: 673-677.

Parreira, R.L.T., Abrahao, O., Galembeck, S.E. 2001. Conformational preferences of non-nucleoside HIV-1 reverse transcriptase inhibitors. *Tetrahedron*, 57: 3243-3253.

Pav, J.W., Rowland, L.S., Korpalski, D.J. 1999. HPLC-UV method for the quantitation of nevirapine in biological matrices following solid phase extraction. *J. Pharm. Biomed. Anal.,* 20: 91-98.

Pillai, Z.S. and Kamat, P.V. 2004. What factors control the size and shape of silver nanoparticles in the citrate ion reduction method? *J. Phys. Chem. B,* 108(3): 945-951.

Pirondini, L. and Dalcanale, E. 2007. Molecular recognition at the gas-solid interface: a powerful tool for chemical sensing. *Chem. Soc. Rev.,* 36(5): 695-706.

Prado, A., María, S., Kedor Hackmann, E.R.M., Santoro, M., Pinto, T.J.A. and Tavares, M.F.M. 2004. Capillary electrophoretic method for determination of protease inhibitor indinavir sulfate used in human immunodeficiency virus therapy. *J. Pharm. Biomed. Anal.,* 34(2): 441-450.

Prasse, C., Schlusener, M.P., Schulz, R. and Ternes, T.A. 2010. Antiviral drugs in wastewater and surface waters: a new pharmaceutical class of environmental relevance? *Environ. Sci. Technol.,* 44(5): 1728-1735.

Qian, X., Park, H.S. 2010. Strain effects on the SERS enhancements for spherical silver nanoparticles. *Nanotechnology*, 21: 365704.

Radi, A. 2005. Accumulation and trace measurement of chloroquine drug at DNA-modified carbon paste electrode. *Talanta*, 65: 271-275.

Raj, C.R., Okajima, T., Ohsaka, T. 2003. Gold nanoparticle arrays for the voltammetric sensing of dopamine. *J. Electroanal. Chem.,* 543: 127-133.

Rao, R.N., Shinde, D.D. 2009. Two-dimensional LC-MS/MS determination of antiretroviral drugs in rat serum and urine. *J. Pharm. Biomed. Anal.,* 50(5): 994-999.

Remmel, R.P., Kawle, S.P., Weller, D. and Fletcher, C.V. 2000. Simultaneous HPLC assay for quantification of indinavir, nelfinavir, ritonavir, and saquinavir in human plasma. *Clin. Chem.*, 46(1): 73-81.

Ren, J., Milton, J., Weaver, K.L., Short, S.A., Stuart, D.I., Stammers, D.K. 2000. Structural basis for the resilience of efavirenz (DMP-266) to drug resistance mutations in HIV-1 reverse transcriptase. *Structure*, 8(10): 1089-1094.

Ren, J., Nichols, C.E., Chamberlain, P.P., Weaver, K.L., Short, S.A., Stammers, D.K. 2004. Crystal structures of HIV-1 reverse transcriptases mutated at codons 100, 106 and 108 and mechanisms of resistance to non-nucleoside inhibitors. *J. Mol. Biol.,* 336: 569-578.

Rey, D., Partisani, M., Hess-Kempf, G., Krantz, V., Priester, M., Cheneau, C., Bernard-Henry, C., De Mautort, E., Decroix, L., Lang, J.M. 2004. Tolerance of a short course of nevirapine, associated with 2 nucleoside analogues, in post exposure prophylaxis of HIV. *J. Acquir. Immune Defic. Syndr.,* 37: 1454-1456.

Rodrıguez-Mozaz, S., Marco, M.P., Lopez de Alda, M.J., Barcelo, D. 2004. Biosensors for environmental applications: Future development trends. *Pure Appl. Chem.,* 76(4): 723-752.

Rogers, J.A., Huang, Y. 2009. A curvy, stretchy future for electronics. *Proc. Natl. Acad. Sci.* U.S.A., 106: 10875-10876.

Rose, M.J., Merschman, S.A., Eisenhandler, R., Woolf, E.J., Yeh, K.C., Lin, L., Fang, W., Hsieh, J., Braun, M.P. and Gatto, G.J. 2000. High throughput simultaneous determination of the HIV protease inhibitors indinavir and L756423 in human plasma using semi automated 96-well solid phase extraction and LCMS/MS. *J. Pharm. Biomed. Anal.,* 24(2): 291-305.

Rosi, N., Mirkin, C.A. 2005. Nanostructures in Biodiagnostics. *Chem. Rev.,* 105: 1547-1562.

Rossi, G., Rapallo, A., Mottet, C., Fortunelli, A., Baletto, F. and Ferrando, R. 2004. Magic polyicosahedral core-shell clusters. *Phys. Rev. Lett*., 93: 105503.

Sakaguchi, T., Morioka, Y., Yamasaki, M., Iwanaga, J., Beppu, K., Maeda, H., Morita, Y., Tamiya, E. 2007. Rapid and onsite BOD sensing system using luminous bacterial cells-immobilized chip. *Biosens. Bioelectron.,* 22: 1345-1350.

Sanderson, H., Johnson, D.J., Reitsma, T., Brain, R.A., Wilson, C.J. and Solomon, K.R. 2004. Ranking and prioritization of environmental risks of pharmaceuticals in surface waters. *Regul. Toxicol. Pharm.,* 39(2): 158-183.

Sangeetha, N.M., Decorde, N., Viallet, B., Viau, G., Ressier, L. 2012. Nanoparticle based strain gauges fabricated by convective self-assembly: strain sensitivity and hysteresis with respect to nanoparticle sizes. *J. Phys. Chem. C,* 117: 1935-1940.

Sarkar, M., Perumal, O.P., Panchagnula, R. 2008. Solid-state characterization of nevirapine. *Indian J. Pharm. Sci*., 70(5): 619-630.

Sarma, C.S.N. and Sastri, K. 2002. Spectrophotometric determination of indinavir sulphate with precipitation reagents. *Indian J. Pharm. Sci.,* 64(6): 581-583.

Schmid, G. 1995. Chemical synthesis of large metal clusters and their properties. *Nanostruct. Mater.,* 6: 15-24.

Segev-Bar, M., Lendman, A., Nir-Shapira, M., Shuster, G., Hossam, H.A. 2013. Tunable touch sensor and combined sensing platform: towards nanoparticle-based electronic skin. *ACS Appl. Mater. Interfaces*, 5: 5531-5541.

Segev-Bar, M., Shuster, G., Haick, H. 2012. Effect of perforation on the sensing properties of monolayer-capped metallic nanoparticle films. *J. Phys. Chem. C,* 116: 15361-15368.

Sekar, R., Azhaguvel, S. 2008. MEKC determination of antiretroviral reverse transcriptase inhibitors lamivudine, stavudine, and nevirapine in pharmaceutical formulations. *Chromatographia*, 67: 389-398.

Senapati, S. 2005. Biosynthesis and immobilization of nanoparticles and their applications. University of Pune, India.

Sentenac, S., Fernandez, C., Thuillier, A., Lechat, P. and Aymard, G. 2003. Sensitive determination of tenofovir in human plasma samples using reversed phase liquid chromatography. *J. Chromatogr. B*, 793(2): 317-324.

Shih, C.K., Rose, J.M., Hansen, G.L., Wu, J.C., Bacolla, A., Griffin, J.A. 1991. Chimeric human immunodeficiency virus type1/type 2 reverse transcriptase display reversed sensitivity to nonnucleoside analog inhibitors. *Proc. Natl. Acad. Sci. USA*. 88(21): 9878-9882.

Shipway, A.N., Katz, E., Willner, I. 2000. Nanoparticle arrays on surfaces for electronic, optical, and sensor applications. *ChemPhysChem.,* 1: 18-52.

Shirkhedkar, A., Bhirud, H. and Surana, J. 2009. Application of UV spectrophotometric methods for the estimation of tenofovir disoproxil fumarate in tablets. *J. Pharm. Sci.,* 22(1): 27-29.

Siepen, K., Bonnemann, H., Brijoux, W., Rothe, J., Hormes, J. 2000. EXAFS/XANES, chemisorption and IR investigations of colloidal Pt/Rh bimetallic catalysts. *Appl. Organomet. Chem.,* 14: 549-556.

Simoyi, M.F., Falkenstein, E., Dyke, K.V., Blemings, K.P., Klandorf, H. 2003. Allantoin the oxidation product of uric acid is present in chicken and turkey plasma. *Comp. Biochem. Physiol. Part B*, 135: 325-335.

Skotadis, E., Mousadakos, D., Katsabrokou, K., Stathopoulos, S., Tsoukalas, D. 2013. Flexible polyimide chemical sensors using platinum nanoparticles. *Sensors Actuat. B*, 189: 106-122.

Sneh, O., Clark-Phelps, R.B., Londergan, A.R., Winkler, J., Seidel, T.E. 2002. Thin film atomic layer deposition equipment for semiconductor processing. *Thin Solid Films*, 402(1): 248-261.

Spanhel, L., Weller, H., Henglein, A. 1987. Photochemistry of semiconductor colloids. 22. electron injection from illuminated CdS into attached $TiO_2$ and ZnO particles. *J. Am. Chem. Soc.,* 109: 6632-6635.

Spence, R.A., Kati, W.M., Anderson, K.S., Johnson, K.A. 1995. Mechanism of inhibition of HIV-1 reverse transcriptase by nonnucleoside inhibitors. *Science,* 267(5200): 988-993.

Stammers, D.K., Somers, D.O., Ross, C.K., Kirby, I., Ray, P.H., Wilson, J.E., Norman, M., Ren, J.S., Esnouf, R.M., Garman, E.F. 1994. Crystals of HIV-1 reverse transcriptase diffracting to 2.2 A resolution. *J. Mol. Biol.,* 242: 586-588.

Stiver, G. 2003. The treatment of influenza with antiviral drugs. *Can. Med. Assoc. J.,* 168(1): 49-57.

Stuart, D.A., Haes, A.J., Yonzon, C.R., Hicks, E.M., Duyne, R.P. 2005. Biological applications of localised surface plasmonic phenomenae. *IEEE Proc. Nanobiotechnol.,* 152: 13-32.

Subramanian, R., Denney, P.E., Singh, J., Otooni, M. 1998. A novel technique for synthesis of silver nanoparticles by laser-liquid interaction. *J. Mater. Sci.,* 33(13): 3471-3477.

Sun, Y., Wang, H.H. 2007. Electrodeposition of Pd nanoparticles on single-walled carbon nanotubes for flexible hydrogen sensors. *Appl. Phys. Lett.,* 90: 213107.

Swati, J., Raj, K.V., Prabhat, P., Sangeeta, V. 2011. A review on fate of antiviral drugs in environment and detection techniques. *Int. J. Environ. Sci.,* 1(7): 1526-1541.

Takei, K., Takahashi, T., Ho, J.C., Ko, H., Gillies, A.G., Leu, P.W., Fearing, R.S., Javey, A. 2010. Nanowire active-matrix circuitry for low-voltage macroscale artificial skin. *Nat. Mater.*, 9: 821-826.

Tang, J., Skotadis, E., Stathopoulos, S., Roussi, V., Tsouti, V., Tsoukalas, D. 2012. PHEMA functionalization of gold nanoparticles for vapor sensing: chemi-resistance, chemi-capacitance and chemi-impedance. *Sensors Actuat. B*, 170: 129-136.

Tanner, J.L., Mousadakos, D., Giannakopoulos, K., Skotadis, E., Tsoukalas, D. 2012. High strain sensitivity controlled by the surface density of platinum nanoparticles. *Nanotechnology,* 23: 285501.

Teradal, N.L., Prashanth, S.N., Seetharamappa, J. 2012. Electrochemical studies of nevirapine, an anti-HIV drug, and its assay in tablets and biological samples. *J. Electrochem. Sci. Eng.,* 2(2): 67-75.

Ternes, T.A., Meisenheimer, M., McDowell, D., Sacher, F., Brauch, H.J., HaistGulde, B., Preuss, G., Wilme, U. and ZuleiSeiberts, N. 2002. Removal of pharmaceuticals during drinking water treatment. *Environ. Sci. Technol.,* 36(17): 3855-3863.

Thompson, M.A., Aberg, J.A., Cahn, P., Montaner, J.S.G., Rizzardini, G., Telenti, A., Gatell, J.M., Gunthard, H.F., Hammer, S.M., Hirsch, M.S., Jacobsen, D.M., Reiss, P., Richman, D.D., Volberding, P.A., Yeni, P. and Schooley, R.T. 2010. Antiretroviral treatment of adult HIV infection: 2010 recommendations of the International AIDS Society-USA panel. *J. Am. Med. Assoc.,* 304(3): 321-333.

Tianyan, O.N., Masato, T. and Shigeru, H. 2003. Characterization of platinum nanoparticle-embedded carbon film electrode and its detection of hydrogen peroxide*. Anal. Chem.,* 75(9): 2080-2085.

Tominaga, M., Shimazoe, T., Makoto, N., Isao, T. 2008. Composition-activity relationships of carbon electrodes-supported bimetallic gold-silver nanoparticles in electrocatalytic oxidation of glucose. *J. Electroanal. Chem.,* 615: 51-61.

Turkevich, J., Stevenson, P.C. and Hiller, J. 1951. A study of the nucleation and growth processes in the synthesis of colloidal gold. *Discuss. Faraday Soc.,* 11: 55-75.

Tyring, S.K. 2004. *Antiviral agents, vaccines, and immunotherapies*. CRC Press, Florida.

Uslu, B., Ozkan, S.A. 2007a. Electroanalytical application of carbon based electrodes to the pharmaceuticals. *Anal. Lett.,* 40(5): 817-853.

Van Heeswijk, R.P.G., Hoetelmans, R.M.W., Meenhorst, P.L., Mulder, J.W., Beijnen, J.H. 1998. Rapid determination of nevirapine in human plasma by ion-pair reversed phase high-performance liquid chromatography with ultraviolet detection. *J. Chromatogr. B*, 713: 395-399.

Vasantha, V.S., Chen, S.M. 2006. Electrocatalysis and simultaneous detection of dopamine and ascorbic acid using poly (3, 4-ethylenedioxy) thiophene film modified electrodes. *J. Electroanal. Chem.,* 592: 77-87.

Wang, L., Luo, J., Yin, J., Zhang, H., Wu, J., Shi, X., Crew, E., Xu, Z., Rendeng, Q., Lu, S. 2009. Flexible chemiresistor sensors: thin film assemblies of nanoparticles on a polyethylene terephthalate substrate. *J. Mater. Chem.,* 20: 907-915.

Wang, L., Mao, W., Ni, D., Di, J., Wu, Y., Tu, Y. 2008. Direct electrodeposition of gold nanoparticles of to indium/ tin oxide glass. *Electrochem. Commun.,* 10: 673-676.

Wang, Z.L., Ahmad, T.S., El-Sayed, M.A. 1997. Steps, ledges and kinks on the surfaces of platinum nanoparticles of different shapes. *Surf. Sci.,* 380: 302-310.

West, J.L., Halas, N.J. 2000. Applications of nanotechnology to biotechnology- Commentary. *Curr. Opin. Biotechnol.,* 11: 215-217.

Wilson, G.S., Gifford, R. 2005. Biosensors for real-time *in vivo* measurements. *Biosens. Bioelectron.,* 20: 2388-2403.

Wu, J.C., Warren, T.C., Adams, J., Proudfoot, J., Skiles, J., Raghavan, P., Perry, C., Potocki, I., Farina, P.R. and Grob, P.M. 1991. A novel dipyridodiazepinone inhibitor of HIV-1 reverse transcriptase acts through a nonsubtrate binding site. *Biochemistry,* 30(8): 2022-2026.

Xiao, F., Song, J., Gao, H., Zan, X., Xu, R., Duan, H. 2011. Coating graphene paper with 2d-assembly of electrocatalytic nanoparticles: a modular approach toward high- performance flexible electrodes. *ACS Nano*, 6: 100-110.

Xiong, Y.J., McLellan, J.M., Chen, J.Y., Yin, Y.D., Li, Z.Y., Xia, Y.N. 2005. Kinetically controlled synthesis of triangular and hexagonal nanoplates of palladium and their SPR/SERS properties. *J. Am. Chem. Soc.,* 127: 17118-17127.

Xu, C., Wang, X. 2009. Fabrication of flexible metal-nanoparticle films using graphene oxide sheets as substrates. *Small*, 5: 2212-2217.

Xu, J.J., Zhao, W., Luo, X.L. and Chen, H.Y. 2005. A sensitive biosensor for lactate based on layer-by-layer assembling $MnO_2$ nanoparticles and lactate oxidase on ion-sensitive field-effect transistors. *Chem. Commun.*, 792-794.

Yee, C., Scotti, M., Ulman, A., White, H., Rafailovich, M. and Sokolov, J. 1999. One-phase synthesis of thiol-functionalized platinum nanoparticles. *Langmuir*, 15(13): 4314-4316.

Yin, J., Hu, P., Luo, J., Wang, L., Cohen, M.F., Zhong, C.J. 2011. Molecularly mediated thin film assembly of nanoparticles on flexible devices: electrical conductivity versus device strains in different gas/vapor environment. *ACS Nano*, 5: 6516-6526.

Yogeswaran, U. and Chen, S.M. 2008. A review on the electrochemical sensors and biosensors composed of nanowires as sensing material. *Sensors,* 8: 290-313.

Yonezawa, T., Yasui, K., Kimizuka, N. 2001. Controlled formation of smaller gold nanoparticles by the use of four-chained disulfide stabilizer. *Langmuir,* 17: 271-273.

Yoo, S.H., Liu, L., Park, S. 2009. Nanoparticle films as a conducting layer for anodic aluminium oxide template-assisted nanorod synthesis. *J. Colloid Interface Sci.*, 339: 183-186.

Youn, H.C., Baral, S., Fendler, J.H. 1988. Dihexadecyl phosphate, vesicle-stabilized and *in situ* generated mixed cadmium sulfide and zinc sulfide semiconductor particles: preparation and utilization for photosensitized charge separation and hydrogen generation. *J. Phys. Chem.,* 92(22): 6320-6327.

Yuan, L., Dai, J., Fan, X., Song, T., Tao, Y.T., Wang, K., Xu, Z., Zhang, J., Bai, X., Lu, P. 2011. Self-cleaning flexible infrared nanosensor based on carbon nanoparticles. *ACS Nano*, 5: 4007-4013.

Zamborini, F.P., Bao, L., Dasari, R. 2011. Nanoparticles in measurement science. *Anal. Chem.*, 84: 541-576.

Zhang, F., Li, L., Luo, L., Ding, Y., Liu, X. 2013. Electrochemical oxidation and determination of antiretroviral drug nevirapine based on uracil-modified carbon paste electrode. *J. Appl. Electrochem*., 43: 263-269.

Zhang, S., Wang, N., Niu, Y., Sun, C. 2005. Immobilization of glucose oxidase on gold nanoparticles modified Au electrode for the construction of biosensor. *Sensors Actuat. B*, 109: 367-374.

Zhao, Y., Zhang, Z., Liu, W., Dang, H., Xie, Q. 2004. Controlling synthesis of BiIn dendritic nanocrystals by solution dispersion. *J. Am. Chem. Soc.,* 126(22): 6854-6855.

Zhou, M., Chen, S., Zhao, S., Ma, H. 2006. One-step synthesis of Au-Ag alloy nanoparticles by a convenient electrochemical method. *Physica E: Low dimens. Syst. Nanostruct.,* 33(1): 28-34.

Zhou, S.H., Varughese, B., Eichhorn, B., Jackson, G., McIlwrath, K. 2005. Pt-Cu core-shell and alloy nanoparticles for heterogeneous $NO_x$ reduction: anomalous stability and reactivity of a core-shell nanostructure. *Angew. Chem. Int. Ed.,* 44: 4539-4543.

Zhuo, Y., Yuan, R., Chai, Y., Tang, D., Zhang, Y., Wang, N., Li, X., Zhu, Q. 2005. A reagentless amperometric immunosensor based on gold nanoparticles/thionine/Nafion-membrane-modified gold electrode for determination of [alpha]-1-fetoprotein. *Electrochem. Commun.*, 7(4): 355-360.

# CHAPTER THREE
# RESEARCH RESULTS

## KINETICS AND MORPHOLOGICAL ANALYSIS OF NANOPARTICLES

### 3.1 Introduction

This chapter focuses on the synthesis, kinetics and morphology aspect of bimetallic nanoparticles with their respective monometallic counter parts. The systematic investigation on the formation of bimetallic nanoparticles between noble metals using a one-pot synthesis approach was done. Because the synthetic route is crucial in determining the final metal distributions of bimetallic nanoparticles, the synthesis rationally makes use of the difference in reduction kinetics of the various metal precursors. Nanoparticles have vast advantages including magnetic, catalytic and chemical properties. These properties have enabled their wide application in different fields including development of sensors. This insight provides details and understanding of the kinetics of particle formation, shapes, size and structural design. In this respect, the synthesis and kinetics approach is highlighted with much attention on the variation of the precursor concentrations.

The morphological properties of the synthesized bimetallic Ag-Pt NPs were investigated through transmission electron microscopy (TEM) techniques. The chapter elaborates further on the various contributions of monometallic Ag and Pt NPs in the bimetallic Ag-Pt nanoparticles formation and structural design. The need to control the composition and structure of metal nanoparticles in order to have certain desired property has been the major driving force for researchers to study bimetallic nanoparticles. Therefore, understanding the kinetics of the synthesis of these Ag and Pt metal nanostructures and their structural arrangement is extremely important considering their numerous potential applications. In this study, both silver and platinum were used to demonstrate a simple solution-phase method to synthesize nanoparticles. Further studies on the effect of morphology, size, composition, and structure of bimetallic Ag-Pt nanoparticles were done on the various synthesized molar ratios.

The last two decades have seen remarkable progress in nanoscience and nanotechnology, particularly in the synthesis of metallic nanomaterials, aiming at better materials that have the desired characteristics in terms of particle size, shape, elemental composition, and chemical stability, making them invaluable for many applications (Yang and Ying 2009; Sharma and

Pollet, 2012). Nanosized particles of metals have attracted considerable interest because of their potential application in catalysis, microelectronics, electronic, and magnetic devices (Zhu *et al.,* 2000) and as such, the synthesis and characterization of various metal nanoparticles of outstanding practical importance have come into the focus of cutting-edge research. The development of new nanostructured materials with optimal physicochemical characteristics for specific scientific and technological applications has promoted the use of chemical methods, which can obtain materials with good control on particle size and distribution (Morales *et al.,* 2010).

The study of bimetallic (BM) nanoclusters has received particular interest because of their myriad properties and applications in optics, magnetism, catalysis, and others, mainly because of their high tunability and superior features compared with those of their monometallic counterparts (Ferrando *et al.,* 2008; Greeley *et al.,* 2009; Khanal *et al.,* 2012). Bimetallic nanostructured materials such as alloy or core-shell nanoparticles (NPs), have attracted much recent attention because of their novel catalytic, magnetic, and optical properties, which could offer significant additional advantages over those of their constituent single metallic materials (Moghimi *et al.,* 2015). The presence of a second metal modifies the physical and chemical interactions, thus spatial distribution of atoms changes the chemical and physical properties of the nanoparticle (Shibata *et al.,* 2002; Feng *et al.,* 2010).

Depending on the elements, relative concentrations, and details of the synthesis method, the BM may form core-shell structures, heterostructures, and alloy nanocrystals, and this diversity potentiates the increase of the mass specific activity (MSA) of the nanoparticles while also minimizing the cost by using precious metals only on the surface of the particles (Khanal *et al.,* 2014). Based on the atomic arrangements, bimetallic nanoparticles can also exhibit the structures of ordered/random mixed-alloy (Ferrando *et al.,* 2008) and multishell nanoparticles (Baletto *et al.,* 2003; Cheng *et al.,* 2008). They have unique catalytic, electronic and optical properties distinct from those of the corresponding monometallic particles. The nature of the bimetallic particles depends on the mode of preparation and the miscibility, and kinetics of reduction of metal ions (Pal *et al.,* 2009).

The design and synthesis of bimetallic nanomaterials have attracted considerable attention, since there is a close relationship between structures and properties; the rational controlled synthesis of bimetallic nanocrystals is of vital importance for their applications (Wickman *et al.,* 2011; Kang *et al.,* 2012). Although significant progress has been made in the controllable synthesis of nanocrystals with well-defined composition, structure, size, and morphology in recent years (Zhang *et al.,* 2009; Cheng and Sun, 2010; Lim and Xia, 2011), more accurate control over nucleation and growth stages is required to achieve formation of bimetallic

nanocrystals (Banin, 2007; Hao *et al.,* 2010). Because the properties of bimetallic nanoparticles strongly depend on their size, structure and morphology (Habrioux *et al.,* 2009; Chen *et al.,* 2011), the design and control of the spatial arrangement of both metals in bimetallic nanoparticles are critical for exploiting their potential applications (Shi *et al.,* 2013). In the recent past, much effort has been devoted to the preparation of bimetallic nanoparticles with controlled composition distribution (Chen and Chen, 2002; Yashima *et al.,* 2003; Rodriguez-Gonzalz *et al.,* 2005; Camargo *et al.,* 2007; Fan *et al.,* 2008).

Besides UV-visible spectroscopy application in the characterization of metal and semiconductor nanoparticles with plasmon resonance lines in the visible range, it has been used to study the kinetics of particle formation (Cai *et al.,* 2004). The shift in characteristic absorption peaks monitored over time can be used to determine the rate of reaction involved. For example, Henglein monitored the stepwise growth of silver clusters by spectroscopic methods (Tausch-Treml *et al.,* 1978). According to his results; growth follows an autocatalytic reaction pathway that includes adsorption of metal ions and their subsequent reduction on the surface of the zero-valent metal cluster. These reactions could be described by a first-order rate equation (Papp *et al.,* 2007).

Solution based synthesis of NPs typically involves the reduction of precursor. However, the synthesis requires that nucleation and growth deviate from a thermodynamic to a kinetically controlled pathway by slowing down precursor decomposition or reduction via a weak reducing agent or by Ostwald ripening (Xia *et al.,* 2009). Furthermore, establishing control over the size and shape of nanoparticles requires a detailed understanding of the mechanism and kinetics of precursor reduction and particle growth (Polte *et al.,* 2010). Because of its simple preparation procedure, the classical citrate method (Polte *et al.,* 2010) remains one of the most reliable pathways of nanoparticle synthesis and was used as a model reaction in the present study on Ag-Pt NPs kinetics of formation.

According to a mechanism proposed by Watzky and Fink at the end of the nineteen-nineties, slow continuous nucleation followed by fast autocatalytic surface growth results in nearly monodisperse size distribution (Watzky and Finke, 1997). It has been experimentally proven that stronger reducing agents promote the formation of nuclei with smaller diameters, which then continue to grow (Leisner *et al.,* 1996). Growth may proceed in two different ways. Based on one conception, nuclei formed in the first stage join together, whereas another theory proposes that already solidified particles are further enlarged by collisions with freshly reduced metal ions. The notion accepted in special literature is that the final size is determined by the relative rates of nucleation and growth. This notion is the basis of the most efficient method of nanoparticle synthesis presently known that is controlled colloidal

synthesis (CCS), which allows arbitrary variation of particle size by varying the ratio of the rate of nucleation to that of particle growth. Previous studies (Magno *et al.,* 2010; Tojo *et al.,* 2009) concluded that the nanoparticle structure is defined by the difference in the reduction rates only if both reductions occur at the same rate (an alloy is obtained) or if both reductions have very different rates (a core-shell structure is obtained).

In the synthesis of bimetallic nanoparticles, the nucleus develops in a particle by building up new layers, so that the order of deposition of the metals defines the resulting structure. In most cases, when the synthesis takes place in a homogeneous media, it is assumed that the ions with a higher reduction potential are reduced first (Toshima and Yonezawa, 1998; Wu *et al.,* 2001; Feng *et al.,* 2006; Ferrando *et al.,* 2008; Langile *et al.,* 2012;), so the difference in the reduction potential of two metal ions is the main factor determining the final structure of the particles: when one of the reduction reactions is faster, the first nuclei are composed of the fastest reduction product and since the slower reduction product appears later, the outer layers show a progressive enrichment in the slower one. This effect is more pronounced as the difference between both reduction rates increases.

The morphology of nanoparticles can normally be studied using transmission electron microscopy (TEM) in order to establish nanoparticle arrangement and alignments. Past studies have focused on the control of particles' size and their self-assembly into various dimensional lattice structure with the kinetics of evolution, which play a very important role in self-assembly acquiring relatively less attention. The morphologies of nanomaterials play a critical role in determining their properties. Several physical properties of nanoparticles can be tailored for a specific application by controlling the size, shape and morphology of the nanoparticles (Alivisatos, 1996; Mubarakali *et al.,* 2011). Size provides important control over many of the physical and chemical properties of nanoscale materials including luminescence, conductivity, and catalytic activity (Lieber, 1998).

In this chapter, the synthesis of Ag (core)-Pt (shell) nanoparticles via citrate reduction method is described. The kinetics involved during formation of bimetallic Ag-Pt nanoparticles was studied and reported using the UV-visible absorption approach. In addition, the morphological studies of the BM NPs were investigated using TEM and energy dispersive X-ray (EDX) spectroscopy. The use of EDX line scans allowed us to study the atomic positions of Ag and Pt, and to compare the structure of the NPs. To the best of our knowledge, this work has not been reported elsewhere.

## 3.2 Experimental

### 3.2.1 Reagents and Materials

Silver nitrate; $AgNO_3$ (Aldrich, 99.9 %), hexachloroplatinate heptahydrate; $H_2PtCl_6.6H_2O$ (Aldrich, 99 %), trisodium citrate; ($Na_3C_6H_5O_7$) (Aldrich, 99 %) were used. Deionised water purified by a milli-QTM system (Millipore) was used for aqueous solution preparation.

### 3.2.2 Preparation of monometallic nanoparticles

Silver nanoparticles were synthesized by the reduction of $AgNO_3$ with trisodium citrate according to described procedures (Sileikaite *et al.,* 2006). A solution of 1.0 mM $AgNO_3$ was heated to boiling in an Erlenmeyer flask. To this solution, 0.1 M $Na_3C_6H_5O_7$ was added dropwise. During the process, the solution was mixed vigorously using a magnetic stirrer and heated until a pale yellow colour was observed. It was then removed from the heating surface and stirred until it cooled to room temperature. In the case of Pt NPs, the chemical reduction of $H_2PtCl_6{\cdot}6H_2O$ in aqueous solution was done according to the literature (Harriman *et al.,* 1988). A solution of 1.0 mM $H_2PtCl_6{\cdot}6H_2O$ was added to distilled water and heated to 80 °C with stirring in a 250 mL flask. Sodium citrate solution was then added dropwise with vigorous stirring. The resulting solution was maintained at 80 °C for about 1 hour until the pale yellow solution turned dark brown. It was then removed from the heating surface and stirred until it cooled at room temperature.

### 3.2.3 Preparation of bimetallic nanoparticles

A one-pot synthesis approach was used for the synthesis of bimetallic Ag-Pt NPs with various molar ratios. In brief, a solution mixture of 10 mM $H_2PtCl_6.6H_2O$ and $AgNO_3$, was added to distilled water followed by dropwise addition of sodium citrate and the reaction mixture refluxed with the temperature regulated between 90 °C and 95 °C for 1 hour. In continued synthesis steps, the volume of the mixture was adjusted in order to prepare Ag-Pt nanoparticles with molar ratios of 1:1, 1:3 and 3:1. A colourless solution was observed in each case indicating the formation of nanoparticles.

### 3.2.4 Kinetic studies

UV-visible absorption studies were performed with Cary 300 dual-beam spectrophotometer using 1 cm quartz cuvette in the wavelength range of 200-800 nm. In order to determine the rate of the nanoparticles formation, reactions were carried out in glass-stopper flasks fitted

with a condenser to minimize evaporation. Required amounts of $AgNO_3$, hexachloroplatinate and sodium citrate were introduced into the reaction vessel and thermally equilibrated. The growth process of the nanoparticles was monitored by measuring the UV-visible spectroscopy of the solution according to the method of Mie, 1908 by the sampling of aliquots of the aqueous component periodically and the absorbance noted. The progress of the reaction was followed by taking aliquots at definite time intervals (min) and measuring the absorbance at 450 nm for Ag NPs and 430 nm ($\lambda_{max}$ of yellow colour) for Pt NPs and Ag-Pt NPs (1:1, 1:3 and 3:1). The apparent rate constants ($k_{app}$, $s^{-1}$) were calculated from the initial part of the slopes (between 0 min and 40 min) with an absorbance and fixed time method as similarly discussed by Huang *et al.,* 1993 and Hussain *et al.,* 2011.

### 3.2.5 TEM and XRD measurements

The particle size distribution studies of the NPs were performed using a high resolution transmission electron microscope (HRTEM) from Tecnai G2F20 X-Twin MAT (US). For TEM, samples were prepared by placing a drop of working solution on a carbon-coated standard copper grid (300 mesh) operating at 80 kV. An EDX analyzer attached to the TEM operating in the transmission electron microscopy (TEM) mode was used to analyze the chemical compositions of the synthesized nanoparticles. The X-ray diffraction (XRD) studies of the NPs was performed by using a Bruker AXS D8 Advance diffractometer with Cu-Kα radiation over the scanning range $2\theta = 20° - 90°$ at a voltage of 40 kV and 40 mA. The nanoparticles were typical in slurry liquid forms. Approximately 2 mL of the nanoparticles were dropped on a copper plate and dried.

## 3.3 Results and discussion

### 3.3.1 Kinetic analysis of nanoparticles synthesis

The kinetics of particle formation was monitored based on the synthetic steps involved during formation of nanoparticles. Within 5 minutes (labelled as 5 min) of boiling, an absorption band developed around 450 nm in Ag NPs (Figure 3.1a). The peak was low in intensity and very broad. According to literature, broad peaks in the beginning of formation are attributed to very small particles (seeds) (Krylova *et al.,* 2005). The absorption band intensity increased with increase in time (Figure 3.1a) due to continuous reduction of $Ag^+$ ions. After about 25 minutes, $Ag^0$ formation slows down with maximum absorbance observed around 30 minutes similar observations have been reported (Sileikaite *et al.,* 2006). The wavelength of Ag NPs absorption band (450 nm) was not altered in the course of the reaction (Figure 3.1a).

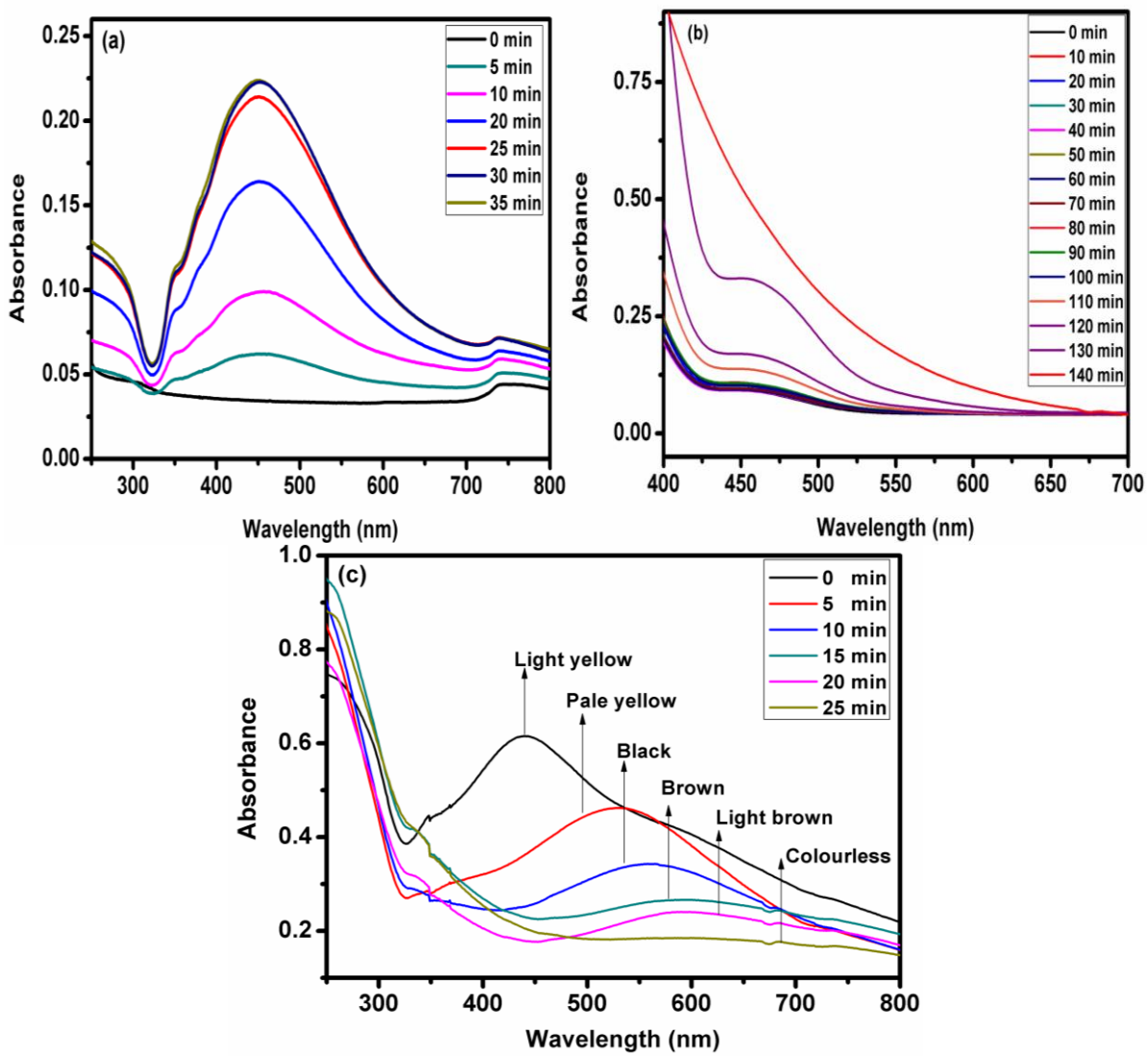


**Figure 3.1. UV-visible spectra displaying time evolution of the formation of (a) Ag NPs; (b) Pt NPs and; (c) Ag-Pt NPs 1:1.**

For the Pt NPs, the precursor peak observed during the beginning of reduction at around 430 nm was used to study the formation of Pt NPs by monitoring the decrease in its absorption. The disappearance of the $PtCl_6^{2-}$ absorption band successfully confirmed synthesis of the Pt NPs after 2 hour 20 minutes (Figure 3.1b) as similarly reported (Hrapovic *et al.,* 2006). In the case of the bimetallic Ag-Pt NPs 1:1 formation, the spectra readings were taken after every 5 minutes. Notable colour changes were observed during reduction from light yellow during initial mixture of both Ag and Pt precursors to colourless solution, which indicated formation of the BM Ag-Pt NPs 1:1 (Figure 3.1c). Further reduction resulted to no significant changes in the spectrum (Figure 3.1c). Although both Ag and Pt precursors were heated in one-pot synthesis, the Ag precursor was preferentially reduced because the reduction of Ag was kinetically more facile (Liu *et al.,* 2014). Fast kinetics resulted in the formation of Ag

nanoparticles, which seeded the subsequent deposition of Pt as similarly reported elsewhere (Liu *et al.,* 2014).

The surface plasmon absorption peak of Ag NPs is extremely sensitive to the presence of the transition metals and this explains the decreasing absorbance after 25 minutes of co-reduction with Pt precursor (Figure 3.2). This decreasing trend in absorption at 430 nm during reaction was monitored as a function of time in order to understand the sequence of steps that lead to the bimetallic Ag-Pt NPs 1:1 formation. The intensity of Pt precursor absorption band gradually decreased over the reaction time, indicating a possible gradual increase in the surface coverage by Pt NPs on the Ag NPs SPR. Weak but detectable peak could still be observed at 15 minutes (Figure 3.1a). This was associated with either a small fraction of exposed Ag surface or a damping effect on its SPR due to possible shelling of Pt NPs. Similar results to Ag-Pt NPs 1:1 was obtained with the formation of other BM Ag-Pt NPs.

### 3.3.2 Determination of the Rate of Reduction

From the UV visible analysis of each NP, plots of absorbances measured at specific wavelengths were made against time (Figure 3.2). We characterized the rate of the reduction process as a whole by the slope of the initial section of the absorbance versus time function.

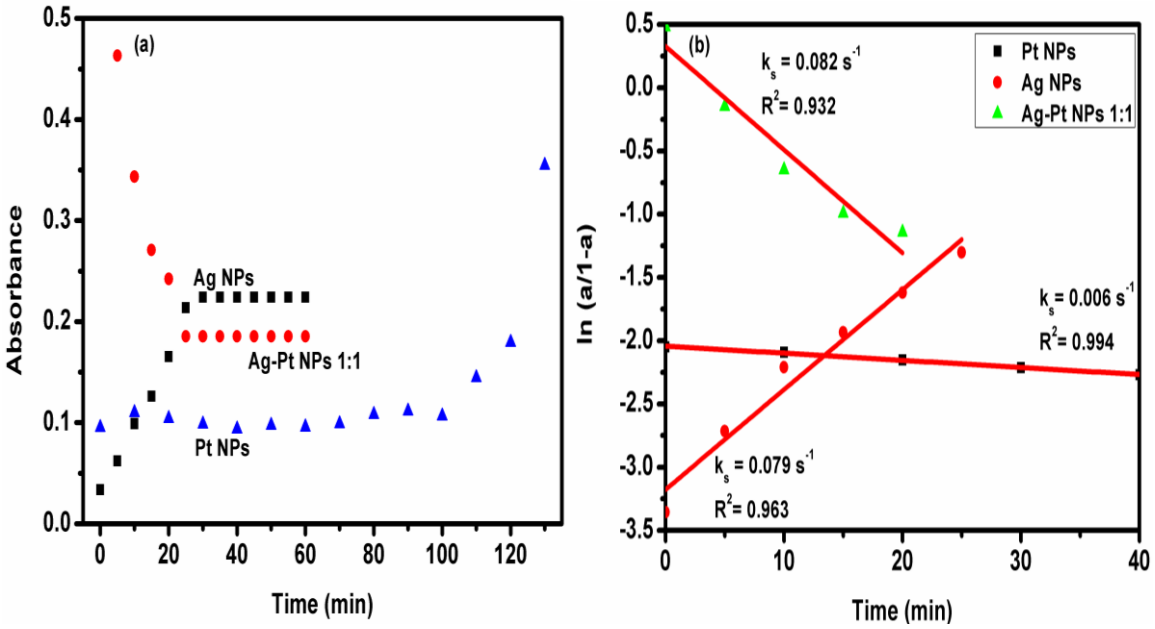


**Figure 3.2. (a) Absorbance versus time plots for various NPs, (b) Plots of $In(\frac{a}{1-a})$ as a function of reaction time (initial time of reduction).**

The apparent rate constants ($k_{app}$) of particle formation were determined and the absorbances versus time functions are summarized in Figure 3.2b where a represents absorbance. For a kinetic reduction of NPs formation reported in this study, the reduction rates were found to increase with increasing boiling time. Huang *et al.,* 1993, observed similar kinetic results. The apparent rate constant ($k_{app}$) was considerably high in the case of Ag-Pt NPs 1:1 (Figure 3.2b). The $k_{app}$ value was high in Ag NPs relative to Pt NPs with increasing time indicating fast reduction in Ag NPs with respect to monometallic NPs. The reaction time for the reduction process at boiling temperatures was found to be important for achieving complete reduction.

The kinetic data for all the NPs were fitted to first order rate equations as shown in Figure 3.2b and revealed that the reduction fit much better to first order kinetics with good correlation coefficients. The course of the Ag NPs kinetic curve in Figure 3.2, started with a sharp rising and finally reaching maximum as similarly reported (Papp *et al.,* 2007). Past study by De Dios *et al.,* 2009 reported similar time of particle formation at 30 minutes. The course of the function for Pt NPs revealed a slow induction process initially and later the process accelerated. The initial phase of the reaction was relatively slow and proposed to correspond to nucleation since no considerable increase in absorbance was observed. The process was complete in about 2 hours, since absorbance remained nearly constant. In the case of Ag-Pt NPs 1:1, the reduction process followed an exponential function (Figure 3.2). The decrease in the precursor absorbance ($\lambda_{max}$ of pale-yellow colour 430 nm) with boiling time was found to be relatively fast (30 minutes) in the particle formation.

### 3.3.3 Optical studies

The optical properties of nanoparticles vary with their composition, as observed in the photographs colour variations in Figure 3.3. During synthesis, the change of the colourless reaction mixture to characteristic pale yellow (Ag NPs) and dark brown (Pt NPs) colours clearly indicates the formation of the NPs (Figure 3.3). This confirmed that the sodium citrate moieties were attached to the surface of NPs in solution during synthesis. Metallic nanoparticles have characteristic optical absorption spectrums in the UV-visible region (Wang *et al.,* 2007). In the case of Ag NPs, the colour of the solution was due to the excitation of surface plasmon vibrations in the silver nanoparticles (Figure 3.3). Ag NPs are known to have a SPR band in the visible range. The broad peak at 450 nm was due to surface plasmon (Basak *et al.,* 2006), which arise from the collective oscillations of valence electrons in the electromagnetic field of incident radiation and is characteristic of Ag nanoparticles and was close to the values reported (Lu *et al.,* 2007).

In the case of Pt NPs, (Figure 3.3), the change in color of the solution from pale yellow to dark brown after the addition of reducing agent indicates the formation of Pt NPs. The precursor ion ($PtCl_6^{2-}$) exhibited a peak under UV-visible spectra (Figure 3.3) around 430 nm (Morales *et al.,* 2010) arising due to the d−d transition (Grant *et al.,* 2005) in the visible region, which disappeared upon complete reduction indicating no characteristic peak as similarly observed (Morales *et al.,* 2010), signifying complete reduction of Pt ions to metallic atoms.

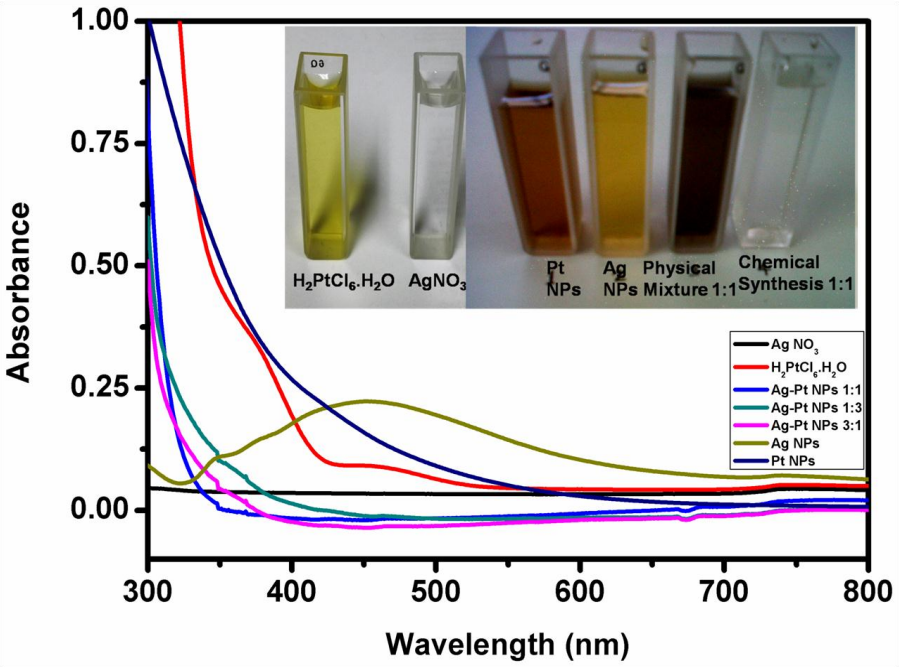


**Figure 3.3 Absorption spectra of Ag, Pt and Ag-Pt 1:1 nanoparticles and digital photographs (inset) of Ag, Pt and BM Ag-Pt 1:1 nanoparticles.**

Optical absorption spectra of BM Ag-Pt NPs 1:1 showed no plasmon band (Figure 3.3) depicting a chemical formation between the metals. The Ag-Pt NPs prepared in various molar ratios solutions were free of precipitates. This ruled out the formation of AgCl that could have resulted from addition of chlorine-containing compound like $H_2PtCl_6.6H_2O$ and solution containing $Ag^+$ ions. From the spectra of BM Ag-Pt NPs 1:1, it was observed that for all the studied molar ratios, the plasmon band at 430 nm vanished instantly as similarly discussed (Patel *et al.,* 2005). It was clear that the presence of Pt NPs even in small quantities strongly affects the spectrum of Ag NPs (Figure 3.3) since the surface plasmon resonance of Ag NPs is extremely sensitive to the presence of transition metals (Patel *et al.,* 2005).

Under these experimental conditions, the optical absorption measurement alone could not establish whether Ag NPs and Pt NPs formed an alloy or a core-shell structure and this did not rule out the possibility of either NPs structures. However, our optical absorption spectra rule out the possibility of the formation of isolated Ag NPs clusters, which would otherwise give rise to Ag surface plasmon absorption peak in the various ratios. Similar argument was noted by Patel *et al.,* 2005.

### 3.3.4 Transmission electron microscopy

Morphological studies of the prepared NPs were done to confirm particle size and structural alignment. Typical HR-TEM images with low magnifications for Ag, Pt and Ag-Pt BM NPs ratios (1:1, 3:1 and 1:3) samples are depicted in Figure 3.4a and b respectively. The Ag NPs showed uneven spheres of sphere-stacked aggregation (Hsieh *et al.,* 2011), as observed in Figure 3.4a. The aggregation in Ag NPs formation can be ascribed to the fact that as-grown Ag sphere easily combines with neighbouring spheres at higher temperatures during the reduction period, generating bulky silver islands (Hsieh *et al.,* 2011). Larger Ag nanoparticle aggregates were also present with the average diameter of 60 nm.

Even though Ag NPs had a larger particle size, BM Ag-Pt NPs ratios particle sizes were dependent on outer Pt NPs (shell). De Dios *et al.,* 2009 argued that slower reaction results to more NPs growth as longer time was taken during formation, which explains the high density of the Pt NPs (Figure 3.4a) in our case. TEM images of the bimetallic nanoparticles displayed a core-shell contrast and have a bright central part and dark out part indicating the formation of core-shell nanostructure, where the bold central part corresponds to the expected Ag core (seed) and the chain like out part to the Pt shell. The micrographs readily identified the components of bimetallic nanoparticles (core-shell).

The Pt shell particles are denser compared to the Ag core in all BM Ag-Pt nanostructures judging by its distribution with respect to the particles as shown in Figure 3.4. The Pt NPs particle size was much smaller than Ag NPs as observed (Figure 3.4). The reduction on the Pt precursor surface to the Pt shell around Ag NPs explains the effect of size variation majorly contributed by the Pt shelling effect. This leads to reduction in the particle sizes of BM Ag-Pt NPs ratios. This study reported the average sizes of Ag NPs, Pt NPs and bimetallic Ag-Pt NPs as shown in Table 3.1.

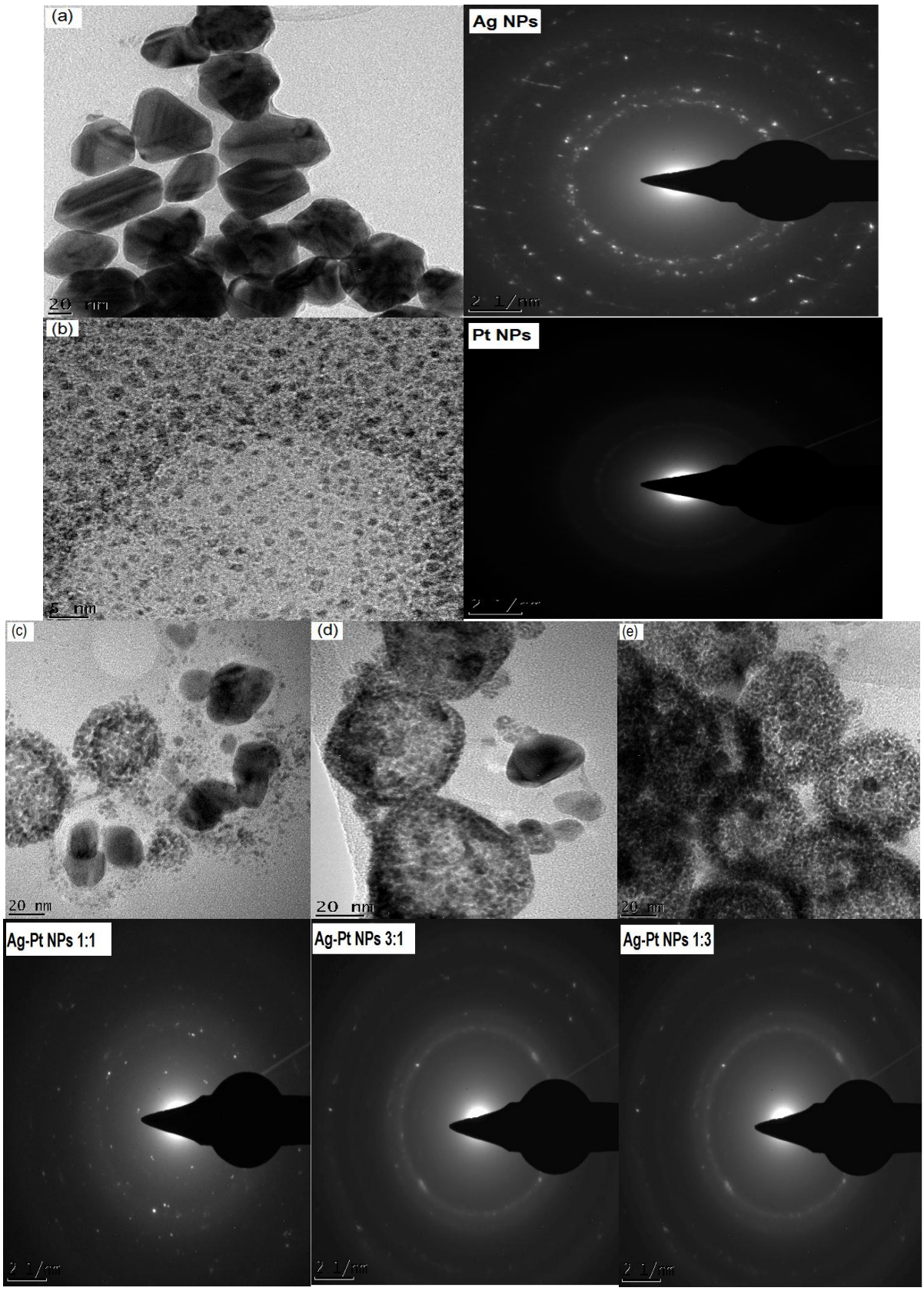


**Figure 3.4. TEM micrographs of (a) Ag NPs; (b) Pt NPs nanoparticles, Ag-Pt nanoparticles in the ratio; (c) 1:1; (d) 1:3; and (e) 3:1 with their corresponding SAED image patterns.**

**Table 3.1. Comparison of particle sizes of synthesised the NPs from TEM**

| Nanoparticles | Particle size ± SD (nm) |
|---|---|
| Ag | 60.0 ± 9.4 |
| Pt | 2.5 ± 0.5 |
| Ag-Pt (1:1) | 20.7 ± 9.0 |
| Ag-Pt (1:3) | 25.0 ± 5.0 |
| Ag-Pt (3:1) | 21.7 ± 7.6 |

A representative detailed section of the selected area electron diffraction (SAED) image in Figure 3.4a and b further corroborates the crystalline nature of these metal nanoparticles. At these higher magnifications, the crystalline nature of silver cores is visible by the appearance of lattice fringes. Electron diffraction reveals that the Ag and Pt bimetallic nanoparticle are crystalline with face-centred cubic (fcc) packing arrangements of bulk metals. As can be seen in Figure 3.4b, presence of rings patterns in the SAED reveals the single face-centred cubic (fcc) crystalline nature of the spherical nanoparticles with a preferential growth direction along the Ag (110), (200), (220), (311) and (331) planes as similarly reported (Hussain *et al.,* 2011; Vidhu and Philip, 2014). The SAED pattern from BM NPs show ring pattern of randomly overlapped and sharp diffraction spots, from the crystalline Ag-Pt nanoparticles. The rings observed in SAED patterns correspond to the (111), (200), (220) and (311) face-centred cubic (fcc) planes, which are similar to the reported planes in Pt-based alloys (Leteba and Lang, 2013).

The size of the particles obtained from TEM analyses were in the range of 2 nm to 60 nm. However, when $AgNO_3/PtCl_6^{2-}$ molar ratio was introduced, the particles obtained had a slightly larger average diameter of about 20 nm in the final particles formed with core shell aligned pattern. The large difference in particle morphology could be due to the surface segregation for the different compositions or a change in the growth kinetics with $AgNO_3/PtCl_6^{2-}$ molar ratios. Such interaction can be sensitive to the concentration of precursors and reaction condition.

EDX analyses together with elemental composition of the elongated nanoparticles were carried out using the TEM showing characteristic peaks of the nanoparticles. In this study, EDX was used to verify the presence of silver and platinum NPs in their respective suspensions purified by ultracentrifugation. Sharp strong signal in the silver region of between 2 and 4 keV (Jang *et al.,* 2011) due to SPR confirmed the presence of elemental silver of the Ag NPs (Figure 3.5) thus giving confidence that silver has been correctly

identified. The emission energy at 3 keV indicates the reduction of silver ions to element of silver.

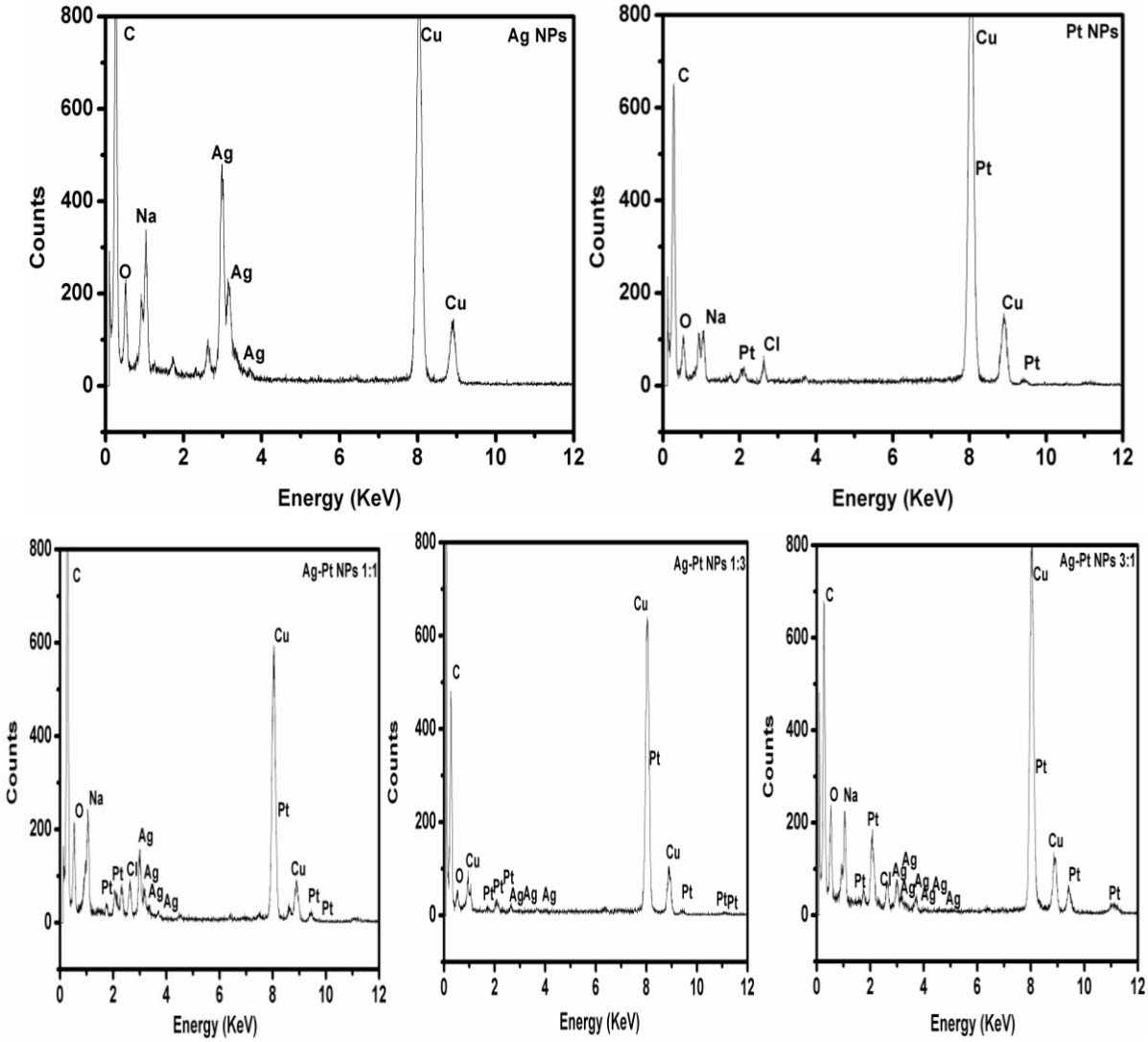


**Figure 3.5. EDX characterization spectra obtained for Ag, Pt and Ag-Pt 1:1, 1:3 and 3:1 nanoparticles.**

For Pt NPs EDX spectra, characteristic signals around 10 keV was noted as similarly observed (Jang *et al.,* 2011; Feng *et al.,* 2014), which confirmed presence in the NPs suspension. In EDX for Ag-Pt core-shell (1:1, 1:3 and 3:1) NPs spectra, one can clearly see five peaks located between 2 keV and 4 keV. The maximum located on the left part of the spectrum at 0.2 keV clearly comes from carbon. The hardly visible maximum located at 0.5 keV is connected with the oxygen characteristic line. The carbon and oxygen spots in the examined samples confirm the presence of stabilizers composed of alkyl chains. The peak was obtained at the energy of 3 keV for silver and some of the weak signals for C, O, Cl, Al,

and Na were observed. The characteristic signal for Pt was equally visible confirming presence of Pt NPs. The EDX results clearly showed the nanoparticle suspensions were composed of the synthesized metal nanoparticles.

**Table 3.2. Compositions of Ag-Pt core-shell nanostructures based on atomic weights from EDX**

| $AgNO_3/(PtCl_4)^{2+}$ feeding molar ratio | Ag-Pt core-shell NPs | | |
|---|---|---|---|
| | Ag (atomic %) | Pt (atomic %) | Atomic Composition |
| 1:1 | 1.12 | 0.81 | $Ag_5Pt_2$ |
| 1:3 | 0.03 | 0.16 | $Ag_1Pt_3$ |
| 3:1 | 0.87 | 1.31 | $Ag_6Pt_5$ |

The atomic percentage and composition of the bimetallic NPs were obtained based on EDX analysis. The atomic percentage of Ag and Pt in the resultant $Ag_xPt_y$ nanoparticles was slightly higher than that in the precursors fed into the reaction mixtures, suggesting the amount of unreacted precursors was fairly low (Table 3.2). Although the atomic ratios of Ag and Pt in the core shell nanoparticles were found to vary, core shell formation was good, as evidenced by TEM micrographs.

### 3.3.5 X-ray Diffraction studies

Figure 3.6 shows the XRD patterns of monometallic silver, platinum nanoparticles and bimetallic Ag-Pt nanoparticles. The phase of prepared films has been investigated by X-ray diffraction method and corresponding XRD pattern is shown in Figure 3.6 (a to e). XRD pattern of Ag NPs (Figure 3.6 a) has shown clear peaks of characteristic face centered cubic planes at 30.08° (111), 44.18° (200), 64.30° (220), 77.23° (311) and 81.59° (222) as similarly reported (Peng and Yang, 2008). Thus indicating the crystalline structure of silver nanoparticles. The XRD spectrum of Pt NPs contains multiple peaks that are clearly distinguishable, the peaks with 2θ values of 33.89°, 45.78°, 66.58° and 84.22° corresponding to the 111, 200, 220, and 222 crystal planes of face-centered cubic (fcc) structure respectively as reported (Jingyu *et al.,* 2007; Yang *et al.,* 2008). In the Pt NPs diffraction pattern the broad peak observed at about 24° 2θ belonged to the graphitic carbon used as the support. In contrast, the XRD patterns of the bimetallic Ag-Pt NPs (Figure 3.6 c to e) are a superimposition of the two components of Ag core and a relatively crystalline Pt shell.

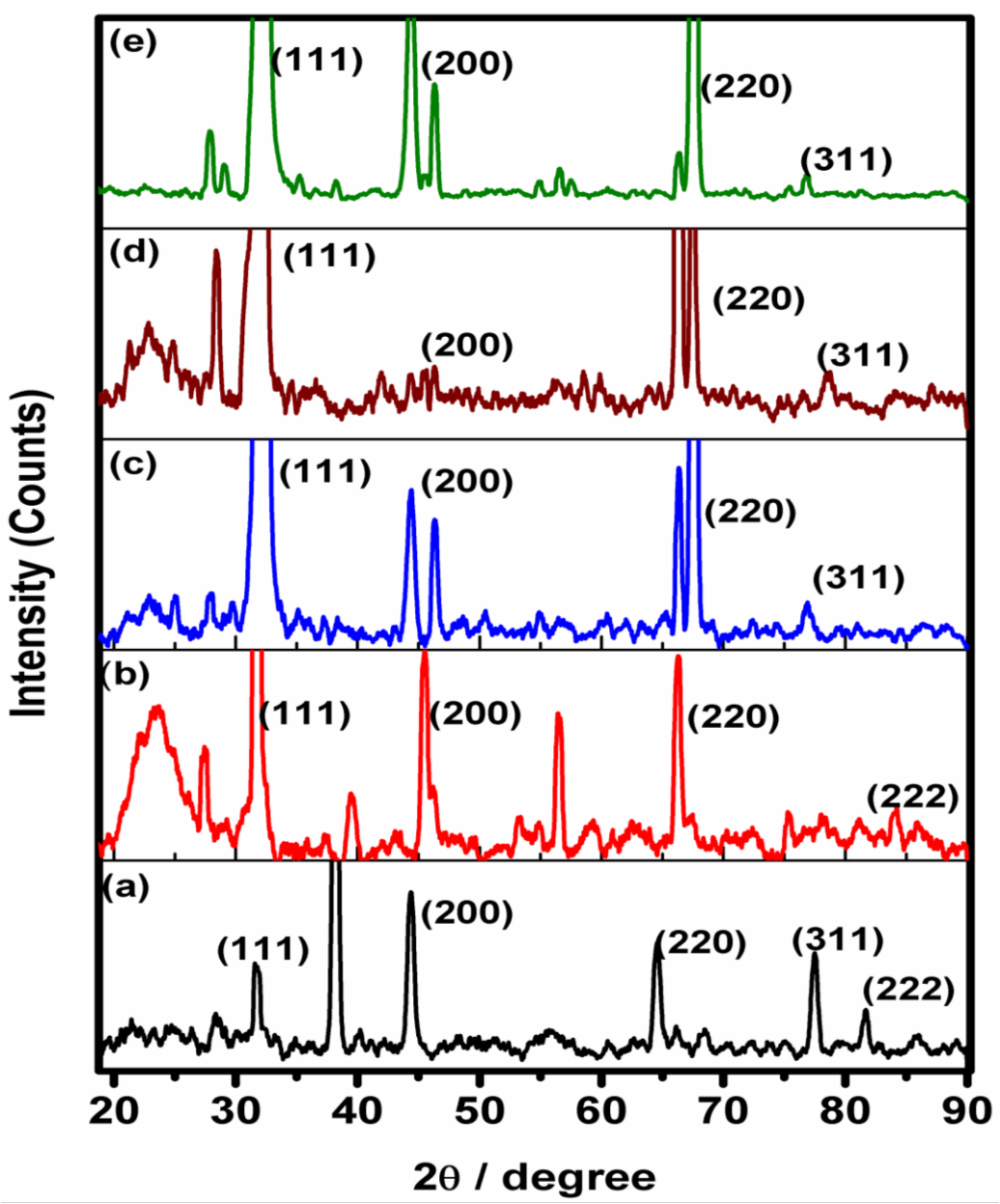


Figure 3.6. XRD patterns of (a) Ag NPs (b) Pt NPs and BM Ag-Pt NPs (c to e) (1:1, 1:3 and 3:1) respectively.

All three bimetallic Ag-Pt nanoparticles showed common diffraction peaks around 2θ angles 32.85°, 45.77°, 66.58° and 76.85° that could be indexed to (111), (200), (220) and (311) planes of a face-centered cubic (fcc) lattice. In the XRD patterns for BM NPs, all the peaks were double peaks except the (111) planes as a result of the close proximity of the Ag and Pt peaks. Which reflected the fact that the resultant crystalline phase of the bimetallic NPs was intact throughout. Other diffraction peaks observed were attributed to the support material used during analysis. The diffraction pattern of the three bimetallic Ag-Pt nanoparticles displayed mostly the reflection characteristics of both Ag and Pt NPs fcc structure, and the diffraction peaks were shifted slightly to higher 2θ values relative to the same reflections on

monometallic factions. The relative peak intensities increased in the diffraction patterns of BM Ag-Pt nanoparticles. The peak positions were slightly shifted in the BM NPs ratios, suggesting some atomic interaction in Ag-Pt bimetallic. The diffraction peaks of bimetallic NPs had higher 2θ angles than those for pure monometallics and moved to high angles with the increase of Ag in the molar ratio (3:1). This shift to higher 2θ angles was indexed to lower d spacing possibly due to the inter-atomic interactions, which result in structural transformation in the bimetallic NPs altering the d-spacing arrangement.

## 3.4 Conclusion

Synthesis of bimetallic Ag-Pt NPs ratios was successfully achieved by varying amounts of silver nitrate and hexachloroplatinate precursors resulting in core-shell morphologies consisting of Ag core and Pt shell. Fast kinetics based on rate constants was observed in both Ag NPs and Ag-Pt NPs 1:1 formation relative to Pt NPs with the kinetics of particle formation best fitted to first order reaction. The bimetallic NPs were chemically formed as confirmed by optical absorption spectroscopy. The optical band gap of the Ag-Pt NPs was found to be within 3.75 to 3.77 eV range, which was higher than that corresponding monometallics indicating the existence of strong quantum confinement. Size dependence of efficient UV absorption spectra of various NPs sizes give evidence for the quantum confinement effect. A size-dependent opening of the band gap for nanoparticles gives numerous new opportunities for their use in industrial applications. The TEM data confirmed the formation of Ag-Pt core-shell nanoparticles with Ag (core)-Pt (shell) alignment while EDX analysis confirmed the chemical nature of synthesized Ag-Pt core shell nanoparticles. XRD results confirmed the formation of bimetallic Ag-Pt NPs with crystallinity observed in all the synthesized nanoparticles.

## 3.5 References

Alivisatos, A.P. 1996. Semiconductor clusters, nanocrystals, and quantum dots. *Science*, 271: 933-937.

Baletto, F., Mottet, C. and Ferrando, R. 2003. Growth of three-shell onion like bimetallic nanoparticles. *Phys. Rev. Lett.,* 90: 135504.

Banin, U. 2007. Nanocrystals: Tiny seeds make a big difference. *Nat. Mater.,* 6: 625-626.

Basak, D., Karan, S. and Mallik, B. 2006. Size selective photoluminescence in poly (methyl methacrylate) thin solid films with dispersed silver nanoparticles synthesized by a novel method. *Chem. Phys. Lett.,* 420(1-3): 115-119.

Cai, M., Chen, J. and Zhou, J. 2004. Reduction and morphology of silver nanoparticles via liquid-liquid method. *Appl. Surf. Sci.* 226(4): 422-426.

Camargo, P.H.C., Xiong, Y., Ji, L., Zuo, J.M., Xia, Y. 2007. Facile synthesis of tadpole-like nanostructures consisting of Au heads and Pd tails. *J. Am. Chem. Soc.*, 129: 15452-15453.

Chen, D.H., Chen, C.J. 2002. Formation and characterization of Au-Ag bimetallic nanoparticles in water-in-oil microemulsions. *J. Mater. Chem.*, 12: 1557-1562.

Chen, G.D., Stefano, D., Nechache, R., Rosei, R., Rosei, F., Ma, D.L. 2011. Bifunctional catalytic/magnetic Ni@Ru core-shell nanoparticles. *Chem. Commun.*, 47: 6308-6310.

Cheng, D., Wang, W., Huang, S. and Cao, D. 2008. Atomistic modelling of multishell onion-ring bimetallic nanowires and clusters. *J. Phys. Chem. C,* 112(13): 4855-4860.

Cheng, K., Sun, S. 2010. Recent advances in syntheses and therapeutic applications of multifunctional porous hollow nanoparticles. *Nano Today*, 5(3): 183-196.

De Dios, M., Barroso, F., Tojo, C. and López-Quintela, M.A. 2009. Simulation of the kinetics of nanoparticle formation in microemulsions. *J. Colloid Interface Sci.*, 333: 741-748.

Fan, F.R., Liu, D.Y., Wu, Y.F., Duan, S., Xie, Z.X., Jiang, Z.Y., Tian, Z.Q. 2008. Epitaxial growth of heterogeneous metal nanocrystals: From gold nano-octahedra to palladium and silver nanocubes. *J. Am. Chem. Soc.*, 130: 6949-6951.

Feng, J., Zhang, C. 2006. Preparation of Cu-Ni alloy nanocrystallites in water-in-oil microemulsions. *J. Coll. Interface Sci.*, 293: 414-420.

Feng, L., Gao, G., Huang, P., Wang, K., Wang, X., Luo, T., Zhang, C. 2010. Optical properties and catalytic activity of bimetallic gold-silver nanoparticles. *Nano Biomed. Eng.,* 2: 258-267.

Feng, Y., Liu, H., Wang, P., Ye, F., Tan, Q. and Yang, J. 2014. Enhancing the electrocatalytic property of hollow structured platinum nanoparticles for methanol oxidation through a hybrid construction. *Sci. Rep.,* 4: 6204.

Ferrando, R., Jellinek, J. and Johnston, R.L. 2008. Nanoalloys: from theory to applications of alloy clusters and nanoparticles. *Chem. Rev.*, 108: 845-910.

Grant, G.J., Chen, W., Goforth, A.M., Baucom, C.L., Patel, K., Repovic, P., VanDerveer, D.G. and Pennington, W.T. 2005. Anion and solvent effects upon the structures of platinum (II) complexes with thiacrown ligands: the crystal structures of $[Pt(9S3)_2](PF_6)_2 \cdot 2\ CH_3NO_2$, $[Pt(9S3)_2](BF_4)_2 \cdot 2\ CH_3NO_2$, $[Pt(9S3)_2](OTf)_2 \cdot 2\ CH_3NO_2$, and $[Pt(18S6)](BF_4)_2$. *Eur. J. Inorg. Chem.*, 2005(3): 479-485.

Greeley, J., Stephens, I.E., Bondarenko, A.S., Johansson, T.P., Hansen, H.A., Jaramillo, T.F., Rossmeisl, J., Chorkendorff, I., Nørskov, J.K. 2009. Alloys of platinum and early transition metals as oxygen reduction electrocatalysts. *Nat. Chem.,* 1(7): 552-556.

Habrioux, A., Vogel, W., Guinel, M., Guetaz, L., Servat, K., Kokoh, B., Alonso-Vante, N. 2009. Structural and electrochemical studies of Au-Pt nanoalloys. *Phys. Chem. Chem. Phys.*, 11: 3573-3579.

Hao, R., Xing, R., Xu, Z., Hou, Y., Gao, S., Sun, S. 2010. Synthesis, functionalization, and biomedical applications of multifunctional magnetic nanoparticles. *Adv. Mater.,* 22: 2729-2742.

Harriman, A., Millward, G.R., Neta, P. and Richoux, M.C. 1988. Interfacial electron-transfer reactions between platinum colloids and reducing radicals in aqueous solution. *J. Phys. Chem.,* 92(5): 1286-1290.

Hrapovic, S., Majid, E., Liu, Y., Male, K. and Luong, J.H.T. 2006. Metallic nanoparticle-carbon nanotube composites for electrochemical determination of explosive nitroaromatic compounds. *Anal. Chem.,* 78: 5504-5512.

Hsieh, C.T., Pan, C. and Chen, W.Y. 2011. Synthesis of silver nanoparticles on carbon papers for electrochemical catalysts. *J. Power Sources*, 196: 6055-6061.

Huang, Z.Y., Mills, G. and Hajek, B. 1993. Spontaneous formation of silver particles in basic 2-propanol. *J. Phys. Chem.*, 97: 11542-11550.

Hussain, J.I., Kumar, S., Hashmi, A.A. and Khan, Z. 2011. Silver nanoparticles: preparation, characterization, and kinetics. *Adv. Mater. Lett.*, 2(3): 188-194.

Jang, J.H., Kim, J., Lee, Y.H., Kim, I.Y., Park, M.H., Yang, C.W., Hwang, S.J. and Kwon, Y.U. 2011. One-pot synthesis of core-shell-like $Pt_3Co$ nanoparticle electrocatalyst with Pt-enriched surface for oxygen reduction reaction in fuel cells. *Energy Environ. Sci.,* 4: 4947-4953.

Jingyu, S., Jianshu, H., Yanxia, C., Xiaogang, Z. 2007. Hydrothermal synthesis of Pt-Ru/MWCNTs and its electrocatalytic properties for oxidation of methanol. *Int. J. Electrochem. Sci.,* 2: 64-71.

Kang, Y., Qi, L., Li, M., Diaz, R.E., Su, D., Adzic, R.R., Stach, E., Li, J., Murray, C.B. 2012. Highly active $Pt_3Pb$ and core-shell $Pt_3Pb$-Pt electrocatalysts for formic acid oxidation. *ACS Nano*, 6: 2818-2825.

Khanal, S., Casillas, G., Velazquez-Salazar, J.J., Ponce, A. and Jose-Yacaman, M. 2012. Atomic resolution imaging of polyhedral PtPd core-shell nanoparticles by Cs-corrected STEM. *J. Phys. Chem. C,* 116(44): 23596-23602.

Khanal, S., Spitale, A., Bhattarai, N., Bahena, D., Velazquez-Salazar, J.J., Mejía-Rosales, S., Mariscal, M.M. and José-Yacaman, M. 2014. Synthesis, characterization, and growth simulations of Cu-Pt bimetallic nanoclusters. *Beilstein J. Nanotechnol.,* 5*:* 1371-1379.

Krylova, G., Eremenko, A., Smirnova, N. and Eustis, S. 2005. Structure and spectra of photochemically obtained nanosized silver particles in presence of modified porous silica. *Int. J. Photoenergy*, 7(4): 193-198.

Langille, M.R., Personick, M.L., Zhang, J., Mirkin, C.A. 2012. Defining rules for the shape evolution of gold nanoparticles. *J. Am. Chem. Soc.*, 134: 14542-14554.

Leisner, T., Rosche, C., Wolf, S., Granzer, F. and Woste, L. 1996. The catalytic role of small coinage-metal clusters in photography. *Surf. Rev. Lett.* 3(1): 1105-1108.

Leteba, G.M., Lang, C.I. 2013. Synthesis of bimetallic platinum nanoparticles for biosensors. *Sensors,* 13(8): 10358-10369.

Lieber, C.M. 1998. One-dimensional nanostructures: chemistry, physics & application. *Solid State Commun.,* 107(11): 607-616.

Lim, B., Xia, Y. 2011. Metal nanocrystals with highly branched morphologies. *Angew. Chem. Int. Ed.,* 50: 76-85.

Liu, H., Ye, F., Yao, Q., Cao, H., Xie, J., Lee, J.Y. and Yang. J. 2014. Stellated Ag-Pt bimetallic nanoparticles: An effective platform for catalytic activity tuning, *Sci. Rep*. 4: 3969-3973.

Lu, X.M., Tuan, H.Y., Chen, J.Y., Li, Z.Y., Korgel, B.A. and Xia, Y.N. 2007. Mechanistic studies on the galvanic replacement reaction between multiply twinned particles of Ag and $HAuCl_4$ in an organic medium. *J. Am. Chem. Soc.,* 129: 1733-1742.

Magno, L.M., Sigle, W., Aken, P.A.V., Angelescu, D.G., Stubenrauch, C. 2010. Microemulsions as reaction media for the synthesis of bimetallic nanoparticles: Size and composition of particles. *Chem. Mater.,* 22: 6263-6271.

Mie, G. 1908. Contributions to the optics of turbid media, especially colloidal metal solutions. *Ann. Phys.*, 25: 377-445.

Moghimi, N., Mohapatra, M. and Leung, K.T. 2015. Bimetallic nanoparticles for arsenic detection. *Anal. Chem.,* 87: 5546-5552.

Morales, B.E., Gamboa, S.A., Pal, U., Guardian, R., Acosta, D., Magan, C. and Mathew, X. 2010. Synthesis and characterization of colloidal platinum nanoparticles for electrochemical applications. *Int. J. Hydrogen Energy*, 35: 4215-4221.

Mubarakali, D., Thajuddin, N., Jeganathan, K. and Gunasekharan, M. 2011. Plant extract mediated synthesis of silver and gold nanoparticles and its antibacterial activity against clinically isolated pathogens. *Colloids Surf. B,* 85: 360-365.

Pal, A., Shaha, S., Kulkarni, V., Murthy, R.S.R. and Devi, S. 2009. Template free synthesis of silver-gold alloy nanoparticles and cellular uptake of gold nanoparticles in Chinese Hamster Ovary cell. *Mater. Chem. Phys.*, 113: 276-282.

Papp, S., Patakfalvi, R. and Dékánya, I. 2007. Formation and stabilization of noble metal nanoparticles. *Croat. Chem. Acta*, 80(3-4): 493-502.

Patel, K., Kapoor, S. and Dave, D.P. 2005. Synthesis of Pt, Pd, Pt/Ag and Pd/Ag nanoparticles by microwave-polyol method. *J. Chem. Sci.*, 117(4): 311-316.

Peng, Z. Yang, H. 2008. Ag-Pt alloy nanoparticles with the compositions in the miscibility gap. *J. Solid State Chem*., 181: 1546-1551.

Polte, J.R., Ahner, T.T., Delissen, F., Sokolov, S., Emmerling, F., Thünemann, A.F. and Kraehnert, R. 2010. Mechanism of gold nanoparticle formation in the classical citrate synthesis method derived from coupled *in situ* XANES and SAXS Evaluation. *J. Am. Chem. Soc.,* 132: 1296-1301.

Rodríguez-González, B., Burrows, A., Watanabe, M., Kiely, C.J., Liz-Marzán, L.M. 2005. Multishell bimetallic AuAg nanoparticles: Synthesis, structure and optical properties. *J. Mater. Chem.*, 15: 1755-1759.

Sharma, S. and Pollet, B.G. 2012. Support materials for PEMFC and DMFC electrocatalysts-A review. *J. Power Sources*, 208: 96-119.

Shi, L., Wang, A., Zhang, T., Zhang, B., Su, D., Li, H., Song, Y. 2013. One-step synthesis of Au-Pd alloy nanodendrites and their catalytic activity. *J. Phys. Chem. C*, 117: 12526-12536.

Shibata, T., Bunker, B.A., Zhang, Z., Meisel, D., Vardeman, C.F., Gezelter, J.D. 2002. Size-dependent spontaneous alloying of Au-Ag nanoparticles. *J. Am. Chem. Soc.*, 124: 11989-11996.

Sileikaite, A., Prosycevas, I., Puiso, J., Juraitis, A. and Guobiene, A. 2006. Analysis of silver nanoparticles produced by chemical reduction of silver salt solution. *J. Mater. Sci.,* 12(4): 287-291.

Tausch-Treml, R., Henglein, A. and Lilie, J. 1978. Reactivity of Silver Atoms in Aqueous Solution II. A Pulse Radiolysis Study. *Ber. Bunsen-Ges. Phys. Chem.,* 82(12): 1335-1343.

Tojo, C., De Dios, M., López-Quintela, M.A. 2009. On the structure of bimetallic nanoparticles synthesized in microemulsions. *J. Phys. Chem. C*, 113: 19145-19154.

Toshima, N., Yonezawa, T. 1998. Bimetallic nanoparticles-Novel materials for chemical and physical applications. *New J. Chem.*, 22*:* 1179-1201.

Vidhu, V.K., Philip, D. 2014. Spectroscopic, microscopic and catalytic properties of silver nanoparticles synthesized using Saraca indica flower. *Spectrochim. Acta Part A: Mol. Biomol. Spectrosc.,* 117: 102-108.

Wang, G., Shi, C., Zhao, N. and Du, X. 2007. Synthesis and characterization of Ag nanoparticles assembled in ordered array pores of porous anodic alumina by chemical deposition. *Mater. Lett.*, 61: 3795-3797.

Watzky, M.A. and Finke, R.G. 1997. Nanocluster size-control and “magic number” investigations. experimental tests of the “living-metal polymer” concept and of mechanism-based size-control predictions leading to the syntheses of iridium(0) nanoclusters centering about four sequential magic numbers. *Chem. Mater.* 9: 3083-3095.

Wickman, B., Seidel, Y.E., Jusys, Z., Kasemo, B., Behm, R.J. 2011. Fabrication of Pt/Ru nanoparticle pair arrays with controlled separation and their electrocatalytic properties. *ACS Nano*, 5: 2547-2558.

Wu, M., Chen, D., Huang, T. 2001. Synthesis of Au/Pd bimetallic nanoparticles in reverse micelles. *Langmuir,* 17: 3877-3883.

Xia, Y., Xiong, Y., Lim, B. and Skrabalak, S.E. 2009. Shape-controlled synthesis of metal nanocrystals: simple chemistry meets complex physics? *Angew. Chem. Int. Ed*., 48(1): 60-103.

Yang S., Peng, Z. and Yang, H. 2008. Platinum Lead Nanostructures: Formation, Phase Behavior, and Electrocatalytic Properties. *Adv. Funct. Mater.,* 18, 2745-2753.

Yang, Y. and Ying, J.Y. 2009. A general phase-transfer protocol for metal ions and its application in nanocrystals synthesis. *Nat. Mater.*, 8: 683-689.

Yashima, M., Falk, L.K.L., Palmqvist, A.E.C., Holmberg, K. 2003. Structure and catalytic properties of nanosized alumina supported platinum and palladium particles synthesized by reaction in microemulsion. *J. Colloid Interface Sci.,* 268: 348-356.

Zhang, Q., Wang, W., Goebl, J., Yin, Y. 2009. Self-templated synthesis of hollow nanostructures: review. *Nano Today*, 4(6): 494-507.

Zhu, J., Liu, S., Palchik, O., Koltypin, Y. and Gedanken, A. 2000. Shape-controlled synthesis of silver nanoparticles by pulse sonoelectrochemical methods. *Langmuir*, 16(16): 6396-6399.

# CHAPTER FOUR

# ELECTROCHEMICAL CHARACTERIZATION OF NANOPARTICLES MODIFIED ELECTRODE

## 4.1 Introduction

This chapter focuses on the electrochemical behaviour of synthesized nanoparticles (NPs) by paying attention on their ability to undergo various redox reactions. This insight opens up to the possible exploitation of these NPs as potential chemical sensor materials based on their electroactivity. Many of the unique physicochemical properties at the nanoscale, such as optical, magnetic and electrical properties can be explored in various applications such as development of sensors. This can be achieved through the fabrication of a wide range of electrochemical sensors that exhibit improved analytical capacities. In this chapter, the fabrication and characterization studies of such electrodes are outlined, and described. Further studies in this chapter looked into the electrochemical band gap of bimetallic nanofilms and provide an insight into its correlation with optical band gap. The energy gap between valence and conduction band is of fundamental importance for the properties of a material. Most of a material's behaviour, such as intrinsic conductivity, optical transitions, or electronic transitions, depends on it. Any change of the gap may significantly alter the material's physics and chemistry. This occurs when the size of a material is reduced to the nanometer length scale (Sattler, 2002). Therefore, the science and the technology of nanomaterials need to take into account a band gap, which is different from that of the bulk.

Surface modification of conventional electrodes for enhanced current response is very important in developing a stable and highly target specific interface. Fundamental studies of such modified electrodes have also provided a better insight into the nature of charge transfer, charge transport processes in the thin films and changes in diffusion towards their altered surfaces amongst other properties. Chemically modified electrodes (CMEs) have sparked considerable interest in analytical chemistry with respect to catalysis, electrochemical detection of organic compounds, and chemical sensor development. With the pioneering work by Lane and Hubbard, over 20 years ago, involving chemisorbed metals on platinum electrode surfaces, numerous methods have been developed to immobilize compounds on electrode surfaces (Lane and Hubbard, 1973).

Several modification techniques of electrode surfaces include covalent attachment, spin coating, and electropolymerization. Deliberate chemical alteration of the electrode surface may result in a more favourable interaction between an analyte and electrode surface by changing the thermodynamic and kinetic behaviour of reactants, products, or intermediates involved in the redox transformation (Brown and Gray, 2010). Controlled modification of the electrodes produce surfaces with new and interesting properties that may form the basis of new applications in electrochemistry and novel devices. These new electrodes possess properties, which can be exploited to lay a foundation for new and interesting applications and devices such as electrochromic displays and sensors (Wang, 1996).

The electrochemical methods using chemically modified electrodes (CMEs) have been widely used as sensitive and selective analytical methods for the detection of the trace amounts of biologically important compounds (Zheng and Song, 2009; Ganjali *et al.,* 2010). One of the most important properties of CMEs has been their ability to catalyze the electrode process via significant decreasing of overpotential with respect to unmodified electrodes. By relatively selective interaction of the electron mediator with the target analyte in a coordination fashion, these electrodes are capable of considerably enhancing the selectivity in the electroanalytical methods (Mazloum-Ardakani *et al.,* 2010). Modified electrodes have been developed to minimize large overpotentials (AitRamdane-Terbouche *et al.,* 2014). In addition, CMEs have helped overcome problems arising due to electrode fouling (Manjunatha *et al.,* 2009). Electrodeposited metal nanoparticles modified electrodes possess interesting electrochemical activities for the detection of various types of chemical compounds and biomolecules (Selvaraju and Ramaraj, 2005). Not only limited to single metal nanoparticles, bimetallic nanoparticles also hold the special electrochemical behaviour for the detection of important compounds (Luo *et al.,* 2006). Noble metal nanoparticles have been more favourable and much utilized for the electrode modification process (Thiagarajan and Chen, 2007).

The rapid development of new nanomaterials and nanotechnologies has provided many new opportunities for electroanalysis. In electrochemical sensing techniques, the development of nanomaterials (Aragay *et al.,* 2012) and signal amplification strategies (Justino *et al.,* 2013) has significantly improved their detection capability. Nanoparticles exhibit high electrocatalytic activity because of their miniaturized size. The surface area increases due to the reduction in size. Materials with high surface area to volume ratio react at much faster rate as more surface area is exposed for reaction and have an effect on enhanced mass transport characteristics (D'Souza *et al.,* 2015). Redox active metal nanoparticles such as Ag, Pt, Pd and Ir have been used as catalyst for the electro-oxidation of $H_2O_2$ (Chakraborty

and Raj, 2009: Ojani *et al.,* 2010). These unique properties of nanoparticulate materials can be exploited to enhance the response of electroanalytical techniques.

Metal nanoparticles provide three important functions for electroanalysis. These include the roughening of the conductive sensing interface, the catalytic properties of the nanoparticles permitting their enlargement with metals and the amplified electrochemical detection of the metal deposits and the conductivity properties of nanoparticles at nanoscale dimensions that allow the electrical contact of redox-centers (Zheng *et al.,* 2009) with electrode surfaces. In addition, metal and semiconductor nanoparticles provide versatile labels (Jingyu *et al.,* 2007) for enhancement of sensitivity in electroanalysis. These unique functions of nanoparticles were employed for developing electrochemical gas sensors, electrochemical sensors based on molecular or polymer functionalized nanoparticles sensing interfaces, and for the construction of different biosensors including immunosensors and DNA sensors (Gao *et al.,* 2009) and enzyme based electrodes (Can *et al.,* 2009).

Generally, nanoparticle modified electrodes present advantages when compared with macro electrodes: High effective mass transport catalyzes and controls the local environment (Katz *et al.,* 2004). Nanoparticle modified electrodes allow convergent rather than linear diffusion, which results in a higher rate of mass transport to the electrode surface (Simm *et al.,* 2005). On the other hand, the catalytic properties of some nanoparticles cause a decrease in the overpotential needed for a redox reaction to occur (Raj *et al.,* 2003). Metal nanoparticles, especially noble metal nanoparticles-modified electrodes usually exhibit high electrocatalytic activities towards the compounds, which have sluggish redox process at bare electrodes (Huang *et al.,* 2008). Besides provision of more active sites on the electrodes surface, NPs have exceptional electrocatalytic characteristics, which make them suitable modifiers for the construction of electrodes. The properties of NPs such as enhanced mass transport and the promotion of electron transfer in redox reactions in combination with the proposed synergistic adsorption property of modifiers contribute to the enhancement of current in NPs modified electrodes.

The modification of electrode surfaces with redox-active metal nanoparticles has led to the development of various electrochemical sensors. For example, silver nanoparticles have attracted growing interest in constructing electrochemical sensors due to its conductivity and excellent catalytic activity (Lu *et al.,* 2011). Previous studies indicated that, Pt nanoparticles could increase the surface area and are conducive for electron transfer with strong catalytic properties. As a result, platinum nanoparticles have been an intensive research subject for the design of electrodes (Pronkin *et al.,* 2001). Electrodeposited nanostructured Pt films onto microelectrodes enhanced mass transport characteristics (Birkin *et al.,* 2000) and are shown

to be excellent amperometric sensors for $H_2O_2$ over a wide range of concentrations (Evans *et al.,* 2002). Kim *et al.* developed a composite hybrid electrode containing Pt-based nanoparticles and nanowires, which they characterized in terms of its electrocatalytic activities (Kim *et al.,* 2010), and have attracted more and more interests as transducer in sensors (Birkin *et al.,* 2000; Hrapovic *et al.,* 2004).

Electrochemical sensors based on nanomaterials such as, silver (Rena *et al.,* 2005) and platinum (You *et al.,* 2003) have been widely used in environmental, food and clinical fields owing to the inherent properties such as portable size, high sensitivity, and high selectivity (Wu *et al.,* 2006). For example, Chen *et al.* (2007) deposited Pt nanoparticles on carbon nanotubes by pulsed electrodeposition, the prepared electrode maintained a good catalytic activity to oxygen and hydrogen peroxide; Selvaraj *et al.* (2009) prepared electrodes by mixing the Pt or Pt-Pd nanoparticles with carbon nanotubes, the modified electrode exhibits well electrocatalytic activity towards formic acid and formaldehyde oxidation. Various nanoparticles of Pt (Rong *et al.,* 2007), Au/Ag (Tominaga *et al.,* 2008), Au/Pt (Jin and Chen, 2007) and Pt/Ir (Hindle *et al.,* 2008) have been used to fabricate non-enzymatic glucose sensors, and have shown good catalytic activity.

Various electrochemical properties such as the kinetic characteristics of the modified electrodes have been investigated using cyclic voltammetry (CV). The importance of surface coverage in the electrochemical behaviour of our modified electrodes as well as its effects on standard rate constant of the surface reaction ($k_s$) and $\Delta E_p$ obtained from Laviron's equation are important parameters in their various applications. These parameters are commonly used as criteria for the effectiveness of a mediator since their values determine the electron transfer kinetics between the modifier and the electrode, observed current limitations (kinetic or diffusion limited), status of the immobilised species or their interaction with the support (Prodromidis *et al.,* 2000). Furthermore, uneven surface coverage would passivate the electrode surface and slow down the electron transfer processes at the electrode surface unlike uniform surfaces. Therefore, knowledge on these parameters is of great need.

Nanoparticles have most of their atoms at surface positions. A surface is a strong perturbation to any lattice, creating many dangling bonds. These unsaturated bonds are energetically unfavourable. The particles can lower their free energy by side- and back-bonding of these bonds. A high concentration of deep and shallow levels can occur at the surface of nanoparticles, and these may act as electron hole recombination centers (Sattler, 2002). The distribution of surface states is discontinuous for small clusters, but can be continuous for nanoparticles, where the surface consists of several facets. When electrons or holes are within a diffusion length of the surface, they will recombine, with transitions through

a continuum of states being non-radiative (Sattler, 2002). Nanoparticle films are interesting from many points of view. They still may have many properties of the free nanoparticles. The coupling between the particles however leads to interface formation, which can result in changes of electronic and optical properties. The particles in the films can form ordered lattices with translational symmetry. The type of order can be due to the coupling to the substrate or due to the interaction between the particles.

Cyclic voltammetry (CV) is an easy and effective technique for studying the electroactivity of nanofilms and to determine the oxidation and reduction potential values. Cyclic voltammetry is also one of the most useful methods to estimate the band gap energies (D'Andrade *et al.,* 2005). Under CV, the oxidation and reduction peaks can be correlated directly to electron transfer at highest occupied molecular orbital (HOMO) and lowest unoccupied molecular orbital (LUMO), respectively (Haram *et al.*, 2001). These processes can be measured using CV method by measuring the redox potentials $E_{red}$ and $E_{ox}$. These values can be used to evaluate the ionisation potential ($I_p$), the electron affinity ($E_a$), and the gap between the HOMO and LUMO, often called the band gap. Knowledge of such values is important in selection of suitable materials for solar cell devices. Selection of hole- or electron-transporting materials in the fabrication of light emitting diodes will also benefit (Bredas *et al.,* 1983; Janietz *et al.,* 1998; Meng *et al.,* 1999; Liu *et al.,* 2000; Inbasekaran *et al.,* 2000; Pei *et al.,* 2000; Liu *et al.,* 2001; Pei *et al.,* 2001; Charas *et al.,* 2003).

Optical spectroscopy studies of nanoparticles demonstrate their atom like discrete level structure by showing very narrow transition line widths (Norris *et al.,* 1994; Leon *et al.,* 1995; Empedocles *et al.,* 1996; Norris and Bawendi, 1996; Banin *et al.,* 1997; Banin *et al.,* 1998). Optical techniques probe the allowed transitions between valence band and conduction band states for nanoparticles, which do not have defect or impurity states in the energy gap. Interpretation of optical spectra often is not straightforward and needs correlation with theoretical models (Ekimov *et al.,* 1993; Fu and Zunger, 1998; Fu *et al.,* 1998). A method for probing the band structure of nanoparticles is to measure the optical absorption or luminescence spectrum. In the absorption process, a photon of known energy excites an electron from a lower to a higher energy state (Sattler, 2002).

The comparison of the band gap determined from the CV data with those obtained from other simple methods like optical absorption spectroscopy has been reported in literatures (Cervini *et al.,* 1997; Beaupre and Leclerc, 2002; Johansson *et al.,* 2003; Muhlbacher *et al.,* 2003;). Murray and co-workers observed a similar correlation between the optical band-gap and the electrochemical potentials for quantized thiol-protected gold particles (Chen *et al.,* 1998; Templeton *et al.,* 2000). Detailed understanding of the electrochemical and optical

properties of metal nanoparticles band gap is important from a fundamental science point of view and knowledge gain such as valuable insight into the structural size effects of the new materials as possible conductors or electrocatalysts. Quantum confinement that manifests itself in widening of the band gap increases with decreasing crystallite size and its implications on the electronic structure of the crystallites has generated considerable interest (Fujishima and Honda, 1972). Generally, band gap is reported to be size dependent and increases with smaller particle diameter (Wang *et al.,* 2000). The quantum size effect (QSE) predicts the formation of a band gap with decreasing particle size for metals and widening of the intrinsic gap for semiconductors (Sattler, 2002). In this chapter, we investigate the influence of the nature of the nanofilms on the optical and electrochemical properties of band gap systems. Their optical absorption spectra, oxidation and reduction potentials, were investigated in detail. Clear correlations between the nature of the band gap and the HOMO and LUMO levels are affirmed. The band gaps were determined by electrochemical and optical absorption measurements and both compared with the theoretical calculation from the Tauc and Bredas models. However, direct observation of the band gap variation upon particle size from UV-visible and electrochemistry is relatively rare.

This study reports and explores the various electrochemical properties due to surface modification of GCE electrode by comparison with bare GCE. The contribution of each monometallic nanofilm in the bimetallic ratios was investigated at the GCE surface and discussed. These bimetallic Ag-Pt core shell nanoparticles exhibit the desired properties whose effects on electron transfer within the nanofilms were examined in phosphate buffer solutions. Each experiment in alkaline solution shows distinct redox characteristic, indicating that these nanoparticles prepared by simple drop-cast method can be used as potential electrode modifiers for enhanced sensitive in electrodes. To the best of our knowledge, no study has reported the electrochemical characterization of Ag-Pt core shell nanoparticles modified glassy carbon electrodes.

In this work, we determine experimentally and by comparison, the variation of the energy gap for the bimetallic nanoparticles. We consider nanoparticles of metals, with sizes typically smaller than 10 nm, which is the range where size effects become observable. To demonstrate the quantum size effects in these metal nanoparticles, the particles were suspended in water and the UV absorption spectra recorded. To substantiate our results an attempt is also being made to estimate the size dependent band gap shift, Thus, the band structure parameters for Ag-Pt BM NPs in the size range of 20 nm to 25 nm were determined using CV and the results were compared with Tauc calculations for the optical gaps.

## 4.2 Experimental

### 4.2.1 Reagents and materials

Silver nanoparticles (Ag NPs), Platinum nanoparticles (Pt NPs) and bimetallic Ag-Pt NPs ratios (1:1, 1:3 and 3:1) were used as synthesized in chapter 3. The solutions were prepared from analytical grade reagents and water distilled and purified in a Millipore system. Alumina micropowder and polishing pads were purchased from United Scientific (SA) and used for polishing of the GCE. Analytical grade nitrogen (Afrox, South Africa) was bought and used for electrochemical studies.

### 4.2.2 Instrumentation

Electrochemical measurements were done using Autolab PGSTAT 101 (Metrohm, South Africa). All electrochemical experiments were carried out in 0.1 M Phosphate buffer solution (PBS) pH 7.0, purged with high purity nitrogen gas for 5 min and blanketed with nitrogen atmosphere during measurements. A conventional three-electrode system consisting of glassy carbon electrode (GCE) was used as the working electrode (A = 0.071 $cm^2$), a platinum wire (3 mm diameter) from Metrohm SA and Ag/AgCl (3 M KCl) electrodes from BAS were used as auxiliary and reference electrodes respectively. All potentials were quoted with respect to Ag/AgCl. The experiments were carried out at room temperature (25 °C).

### 4.2.3 Optical band gap measurements

UV-visible absorption studies were performed in a Cary 300 dual-beam spectrophotometer using 1 cm quartz cuvette in the wavelength range of 200-800 nm. The nanoparticle samples were run and their plots analysed using Tauc's model. During the band gap study, the nanoparticles were suspended in water and the UV absorption spectra recorded.

### 4.2.4 Electrochemical band gap measurements

Nanoparticles suspensions were drop coated on the surface of polished GCE and their CV run in 0.1 M PBS pH 7.0 as a supporting electrolyte. The corresponding voltammograms were analysed using Breda's equation.

### 4.2.5 Preparation of bare and modified GCE

Silver, platinum and bimetallic (BM) nanoparticles were synthesized by the chemical reduction of their metal precursors as described in this chapter 3. During electrochemical characterization, modified electrode was prepared by drop coating GCE surface using NPs suspensions and left for 3 hours in order to allow for the maximum adsorption of the NPs onto the electrode surface and for the solvent to evaporate at room temperature. This process yielded GCE/Ag NPs, GCE/Pt NPs and GCE/Ag-Pt NPs ratios (1:1, 1:3 and 3:1). This fabrication process yielded stable modified electrodes. Prior to modification by drop cast method, GCE was polished repeatedly with 1, 0.3 and 0.05 µm alumina slurries. After each polishing, electrode cleaning adopted was as follows; successive 5 minutes rinsing with doubly distilled water, ultrasonication in ethanol and finally with another doubly distilled water to remove any adsorbed substances on the electrode surface.

## 4.3 Results and discussion

### 4.3.1 Electrochemical characterization of modified GCE/Ag-Pt NPs

The modified GCEs were investigated using cyclic voltammetry (CV) in the potential range of -600 to 1000 mV at 20 $mVs^{-1}$ as shown in Figure 4.1. Typical peaks of the respective NPs were observed in the voltammograms. Cyclic voltammetry was used to characterize the NPs to investigate their electroactivity as shown in Figure 4.1. The synthesized Ag NPs, Pt NPs and Ag-Pt bimetallic nanoparticle (1:1, 1:3 and 3:1) ratios were modified on the GCE surfaces to give; GCE/Ag NPs, GCE/Pt NPs and GCE/Ag-Pt NPs ratios (1:1, 1:3 and 3:1) and characterized using CV. The CV responses of GCE/Ag NPs showed both oxidation (A) and reduction (B) peaks of Ag nanoparticles at 100 mV and -320 mV (corresponding to the $Ag/Ag^+$ redox couple), respectively (Figure 4.1) (versus Ag/AgCl). The absence of this peak in the CV of bare GCE suggests that, this peak corresponds to the oxidation of the $Ag^0$ species to $Ag^+$ on the surface of the modified electrode as indicated by the redox reaction equation 4.1 and 4.2. This was similarly reported elsewhere (Wang *et al.,* 2009).

The CV responses of GCE/Pt NPs showed oxidation (-465 mV, -250 mV and 515 mV shown as peaks a, b and c) and reduction peaks d of Pt nanoparticles at -15 mV (Figure 4.1). These peaks did not appear on the CV of bare GCE, suggesting that they correspond to the electroactivity of Pt ion species on the surface of the modified electrode. In this voltage range, GCE/Pt NPs faced several oxidation changes. Initially, the peaks a and b were observed at more negative voltages near -465 and -250 mV due to platinum's excess electrons, which resulted in hydrogen atoms bonding to Pt. On the anodic sweep, Pt reacted

with oxygen in water, forming PtO. A small peak c was formed at 515 mV, which was assigned to PtO formation (Hudak *et al.,* 2010). Each Pt atom could be bound to a maximum of two oxygen atoms, resulting in $Pt^{+4}$. On the cathodic sweep, as the voltage falls below 100 mV, the platinum oxide was reduced to elemental Pt (Figure 4.1). The peak d at -15 mV corresponded to PtO reduction. Both hydrogen desorption and adsorption occurred within lower $E_p$ values. Finally, the peak e at -450 mV indicates hydrogen desorption. Similar to the literature (Hudak *et al.,* 2010; Lee *et al.,* 2010), not perfectly but roughly symmetrical CV plots along the potential axis have been observed for Pt.

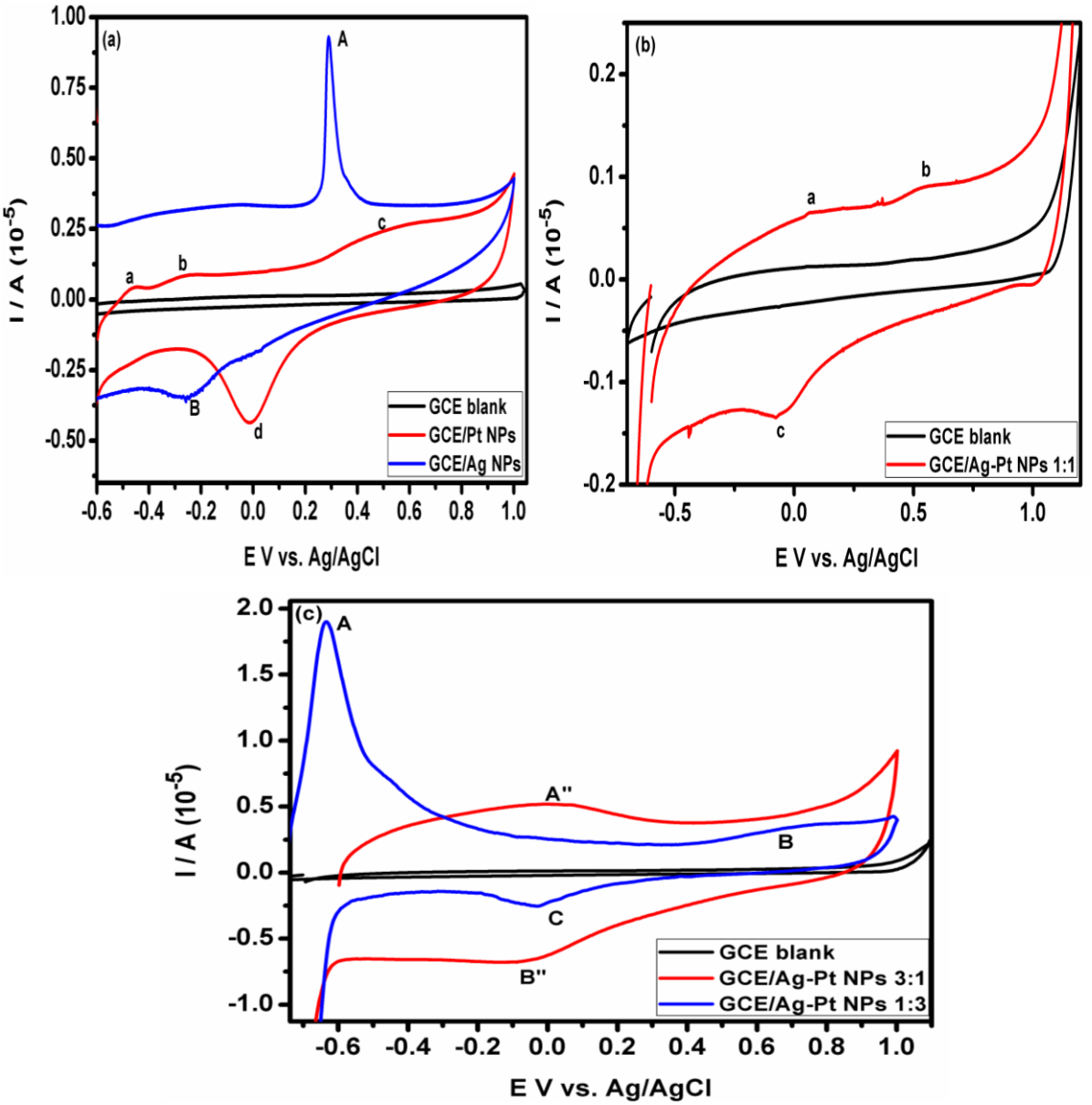


**Figure 4.1. Cyclic voltammograms of (a) monometallic modifications, (b) Ag-Pt NPs 1:1 modification and (c) Ag-Pt NPs (1:3 and 3:1) bimetallic modification on GCE in 0.1 M PBS pH 7.0. Scan rate: 20 mV $s^{-1}$.**

In the PBS solution, the CVs of GCE/Pt NPs (Figure 4.1) was characterized by well-known hydrogen adsorption/desorption peaks at negative potentials, a flat double layer region at intermediate potentials, and platinum oxide formation and reduction peaks at positive potentials (Guo *et al.,* 2012). The fact that hydrogen adsorption/desorption and the oxide formation peaks of bulk Pt were readily observed, indicating that Pt was effectively loaded on the electrodes (Gao *et al.,* 2011). Equation 4.3 to 4.6 shows the various Pt NPs redox reactions involved in each step.

For the GCE/Ag-Pt NPs 1:1, a cathodic peak c was observed around -54 mV while two anodic peaks a and b were observed at 70 mV and 535 mV (Figure 4.1) respectively. This showed significant Ag NPs peak contribution due to the redox couple (54 mV and 70 mV) with 535 mV attributed to Pt NPs. The CV of GCE/Ag-Pt NPs 1:3 showed two anodic peaks A and B at -630 mV and 710 mV respectively and one cathodic peak C at -30 mV. The two peaks A and B were attributed to the characteristic peaks of Pt NPs (equation 4.5) with a high current profile while peak C at -30 mV was due to the presence of Ag NPs that formed part of the BM NPs. On the other hand, GCE/Ag-Pt NPs 3:1 showed two peaks (A" and B"), which are typical of Ag NPs redox couple (equation 4.1 and 4.2) suggesting major contribution by Ag as similarly shown in the molar ratio. The fact that the Ag-Pt bimetallic nanoparticles showed contributions of individual monometallic peaks in their respective ratios suggest that the BM NPs were composed of atomically mixed Ag and Pt atoms and not composed of Ag and Pt metal domains. The equations showing the various reactions taking place for the redox peaks observed were deduced as follows;

$$Ag^{0} \rightarrow Ag^{+} + e^{-} \quad \text{.....Equation 4.1}$$

$$Ag^{+} + e^{-} \rightarrow Ag^{0} \quad \text{.....Equation 4.2}$$

$$Pt + H^{+} + e^{-} \rightarrow Pt - H_{ads} \quad \text{.....Equation 4.3}$$

$$Pt - H_{ads} \rightarrow Pt + H^{+} + e^{-} \quad \text{.....Equation 4.4}$$

$$Pt + O^{2-} + 2e^{-} \rightarrow PtO \quad \text{.....Equation 4.5}$$

$$PtO \rightarrow Pt + O^{2-} + 2e^{-} \quad \text{.....Equation 4.6}$$

Furthermore, the oxidation peak potentials in GCE/Pt NPs and GCE/Ag NPs shifted to less positive potential in the GC BM NPs modified electrodes. This shift was a result of the high electroactivity of Ag and Pt nanoparticles attributed to the electron transfer facilitated by both Ag and Pt NPs. Similar argument on NPs ability to facilitate electron transfer was reported by (Brown *et al.,* 1996; Hrapovic *et al.,* 2004). These results were in agreement with other reported work on metal particles-based electrodes (Raj *et al.,* 2003; Sulak *et al.,* 2006). In

addition, the modification in electronic and geometric structures of surface platinum due to the formation of Ag-Pt bimetallic contributed to the observed enhancement in electroactivity in the BM NPs ratios. Such characteristics together with an ease of miniaturization of sensing devices to nanoscale dimensions make nanoparticles suitable for important applications in chemical/biochemical sensing (Hrapovic *et al.,* 2004).

### 4.3.2 Electrochemical band gaps

Cyclic voltammetry (CV) is recognized as an important technique for measuring band gaps (Al-Ibrahim *et al.,* 2005) and electron affinities (Ahn *et al.,* 2001). In this study, CV was used to confirm the formation of the NPs as shown in Figure 4.1. The CV of each NP was run in the potential range of -600 and 1000 mV versus Ag/AgCl reference electrode as shown below (Figure 4.1).

The oxidation process corresponds to the removal of electron from the HOMO energy level, while the reduction corresponds to the electron addition to the LUMO energy level of the nanoparticles. The current arises from transfer of electrons between the energy levels of the electrode and the energy levels of the nanoparticles under study. The onset potentials of oxidation and reduction of the nanoparticles can be correlated to the ionization potential ($I_p$) and electron affinity ($E_a$) respectively according to the empirical relationship proposed by Bredas *et al.,* 1983 based on a detailed comparison between valence effective Hamiltonian calculations and experimental electrochemical measurements. The correlation can be expressed as:

$$I_p = -\left[E_{ox}^{onset} + 4.4\right]eV \qquad E_a = -\left[E_{red}^{onset} + 4.4\right]eV \quad \text{.....Equation 4.7}$$

$$E_g = \left(I_p - E_a\right)eV \quad \text{.....Equation 4.8}$$

Where $\left[E_{ox}^{onset}\right]$ is the onset oxidation and $\left[E_{red}^{onset}\right]$ is the onset reduction potential versus the Ag/AgCl reference electrode. The onset values were estimated by taking the intersection point between the baseline and the tangent line drawn to the rising portion of the current. The difference in energy levels of HOMO and LUMO gave the band gaps (equation 4.8).

The CV regarding Ag NPs behaviour depicted a reversible reaction system with respect to Ag/AgCl (Figure 4.1a). From the CV curve, the shape of CV curve of Pt NPs (Figure 4.1a) is similar to that of Ag NPs, except with a wider band gap (Table 4.1). In the bimetallic Ag-Pt

NPs ratios of 1:1, 1:3 and 3:1, much larger band gap values were noted with Ag-Pt 1:3 showing more quantum confinement in the ratios.

**Table 4.1. Electrochemical band gap data of synthesised NPs**

| NPs | $E_{ox}^{onset}$ | $E_{red}^{onset}$ | E (LUMO) | E (HOMO) | $E_g^{CV}$ (eV) |
|---|---|---|---|---|---|
| Ag | -0.50 | 0.95 | -3.90 | -5.35 | 1.45 |
| Pt | -0.60 | 0.95 | -3.40 | -5.35 | 1.55 |
| Ag-Pt 1:1 | -0.60 | 1.00 | -3.40 | -5.00 | 1.60 |
| Ag-Pt 1:3 | -0.90 | 0.90 | -3.50 | -5.30 | 1.80 |
| Ag-Pt 3:1 | -0.60 | 0.90 | -3.50 | -5.30 | 1.50 |

It is interesting to note that, for the Ag-Pt bimetallic nanoparticles, only one reduction and one oxidation peak was observed. This suggests that the Ag-Pt bimetallic nanoparticles were composed of atomically mixed Ag and Pt atoms and not composed of Ag and Pt metal domains.

It is clear from the figure that significant shift to higher band energies were observed in the case of bimetallic nanoparticles relative to Pt NPs. The increase in the band gap energies may arise due to the formation of small sized nanoparticles with little or no aggregation during synthesis as similarly reported (Niquet *et al.,* 2000). The increase in the band gap of the Ag-Pt NPs with the decrease in particle size may be due to a quantum confinement effect (Yang *et al.,* 1995). The data listed in Table 4.1 indicates that increasing the ratio of either Ag or Pt in the mixture increases the band gap to higher values than the monometallics.

### 4.3.3 Optical band gap studies

UV-visible spectroscopy is an important tool for characterization of materials. It provides useful information about the optical band gap of various materials. To correlate nanoparticles with the optical properties of Ag, Pt and Ag-Pt bimetallic NPs (1:1, 1:3 and 3:1), systematic optical absorption studies were carried out on the samples. The fundamental absorption corresponding to electron excitation from the valence band to conduction band was used to determine the nature and the value of the band gap while the value of the band gap, $E_g$ was determined by using Tauc's relation (Tauc *et al.,* 1966),

$$(\alpha h\nu) = A(h\nu - E_g)^n \quad \text{.....Equation 4.9}$$

where α is the absorption coefficient, h*v* is the photon energy, A is a fixed constant and exponent n whose value depends upon the type the transition, which may have the values 1/2, 2, 3/2 and 3 for allowed direct, allowed indirect, forbidden direct, and forbidden indirect transitions, respectively (Pankove, 1971). In this study, the allowed direct transition of n=1/2 was used to calculate the band gaps as shown in the y-axis component. The band gap, $E_g$, values were derived when the straight portion of the $(\alpha h\nu)^2$ versus h*v* plot is extrapolated to the *x*-axis. Band gap for all the samples lie in the range of 3.55 to 4.02 eV and are shown in Table 4.2.

The band gap energies of the nanoparticles calculated from the Tauc plots were tabulated as shown (Table 4.2). Moreover, the optical band gap, calculated with Tauc's equation, shows an increase from about 3.96 eV for Ag NPs, to about 4.02 eV for the BM nanoparticles at higher concentration of silver. This drastic increase in optical band can explain the changes in UV-visible absorption and clearly indicate a progressive metallization of samples caused by the Ag doping. This suggests that the band gap is mainly determined by the lateral confinement. Similarly, Pt NPs with 3.55 eV had a blue shift at higher concentration of the BM nanoparticles at 3.97 eV. From Figure 4.2, we observed that an increase in Ag molar concentration resulted in increased Ag-Pt NPs 3:1 band gap energy. Similar observation was noted by Salem, (2014) in Ag-doped CdO nanoparticles. The $E_g$ values for BM Ag-Pt NPs 1:1 were found to be lower than Ag NPs. This decrease in the value of $E_g$ was attributed to the formation of bonds between Ag and Pt NPs, which form the trap levels between the HOMO and LUMO energy states, making the lower energy transitions feasible and resulting in the reduction of optical band gap in line with past-discussed work (Chahal *et al.,* 2011).

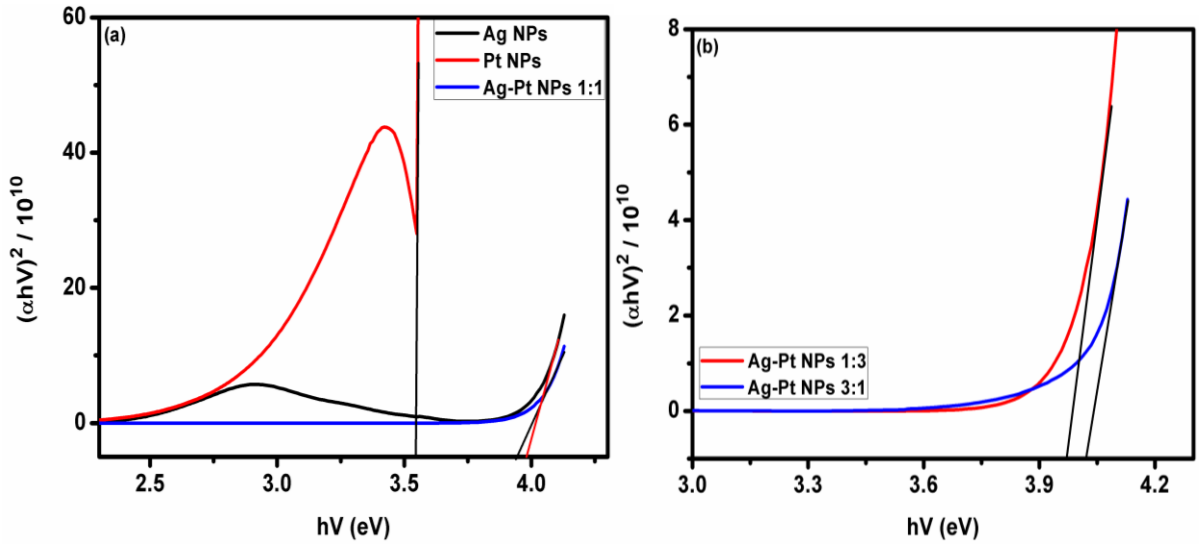


**Figure 4.2. Tauc plots for the determination of band gaps (straight lines are linear extrapolation to the x-axis).**

From our results, the optical band gap increased on average in the final BM NPs as shown in $E_g$ values (Table 4.2) relative to their monometallic counterpart. This indicates that the BM NPs exhibited strong quantum confinement, which shifts the energy levels of the conduction and valence bands apart. This gives rise to a blue shift in the transition energy as the particle size decreases (Lin *et al.,* 2005). Similar trend has been reported in other related studies (Bhargava *et al.,* 1994). From this observation, we can report that the combination of Pt nanoparticles with Ag NPs did significantly influence the band gap energy of the bimetallic Ag-Pt NPs. The blue shift of the absorption spectra for different ratio of nanoparticles arises due to the quantum size effect (Bhargava *et al.,* 1994; Banerjee *et al.,* 2000) in the nanoparticles. This phenomenon causes the continuous band of the solid to split into discrete, quantized levels and the band gap to increase as similarly noted (Revaprasadu and Mlondo, 2006). The obtained band gap values are in close agreement with those reported in monometallic nanoparticles (Budhiraja *et al.,* 2013; Kumar and Rani, 2013), core-shell nanoparticles (Chahal *et al.,* 2011), doped nanoparticles (Sankara *et al.,* 2013) and bimetallic NPs (Nkosi *et al.,* 2012).

**Table 4.2. Optical band gap data of synthesised NPs**

| Nanopartcles | $E_g^{opt}$ (eV) |
|---|---|
| Ag | 3.96 |
| Pt | 3.55 |
| Ag-Pt 1:1 | 3.94 |
| Ag-Pt 1:3 | 3.97 |
| Ag-Pt 3:1 | 4.02 |

Besides the quantum confinement effect, the blue shift in the bimetallic ratios can be attributed either to the decreasing grain size or to strain present in the nanoparticles. This has been supported by past work where factors such as impurity, lattice strain, surface effect (Smith *et al.,* 2009) have been reported to contribute to band gap shifts. In addition, the increase in band gap energy might be due to the charge transfer transitions (Fang *et al.,* 2008) between the Ag atom and Pt atom. To our knowledge, no work has reported the calculations of the band gap of bimetallic Ag-Pt NPs using Tauc's calculations in this manner.

### 4.3.4 Determination of electron-transfer kinetic parameters

The investigation of the kinetic parameters characteristic of the electron-transfer reactions at electrode surfaces helps get a better definition of the electrode surfaces and the electrode/solution interface thereby determining fast and slow reactions on the electrode surfaces. Generally, the current is measured both by the rate of the electrochemical reaction and by the transport of the reacting species to the interface. For this purpose, it is convenient to define a few quantities that affects these reactions. In this regard, the electrode potential is the most important variable that is controlled and thus these quantities can be determined using Laviron's equation (Laviron, 1979) which also considers the changes in scan rates.

Scan rates were studied in 0.1 M PBS of pH 7.0 at modified GCE surfaces as shown (Figure 4.3). Both anodic and cathodic peak currents were found to be proportional to the scan rate in the range between 10 and 150 mV $s^{-1}$ and a corresponding linear correlation values reported as shown in Figure 4.3. The CVs of the modified GCEs at different scan rates (Figure 4.3) showed shifts in oxidation peak potential with increasing scan rates towards more positive potentials confirming the kinetic limitation of the electrochemical reaction (Mazloum-Ardakani *et al.,* 2011). Which maybe due to: (i) chemical interactions between the electrolyte ions and the modifier film, (ii) dominance of electrostatic factors, (iii) the lateral interactions of the redox couples present on the surface and/or (iv) non-equivalent sites present in the film (Karim-Nezhad *et al.,* 2009). When the potential was scanned at increasing rates from 10 to 150 mV $s^{-1}$ under the same experimental conditions, a linear relationship was observed between the peak current, $I_p$ and both scan rate, v and the square root of v (Figure 4.4).

In voltammetry, the nature of the surface reaction taking place at the electrodes can be determined by the linear plot analysis of both $I_p$ versus $v^{1/2}$ and plot of $I_p$ versus v. Generally, a linear plot of $I_p$ versus $v^{1/2}$ is obtained when the electrode process is diffusion controlled, whereas the adsorption-controlled process results in a linear plot of $I_p$ versus v (Bard and Faulkner, 1980). In this work (Figure 4.4), a mixture of both adsorption and diffusion controlled processes was evident based on the correlation values. However linear plots of $I_p$ versus v gave better correlation coefficient values, which indicates that the surface redox reaction at the modified GCE is an adsorption controlled (Xu *et al.,* 2012) process.

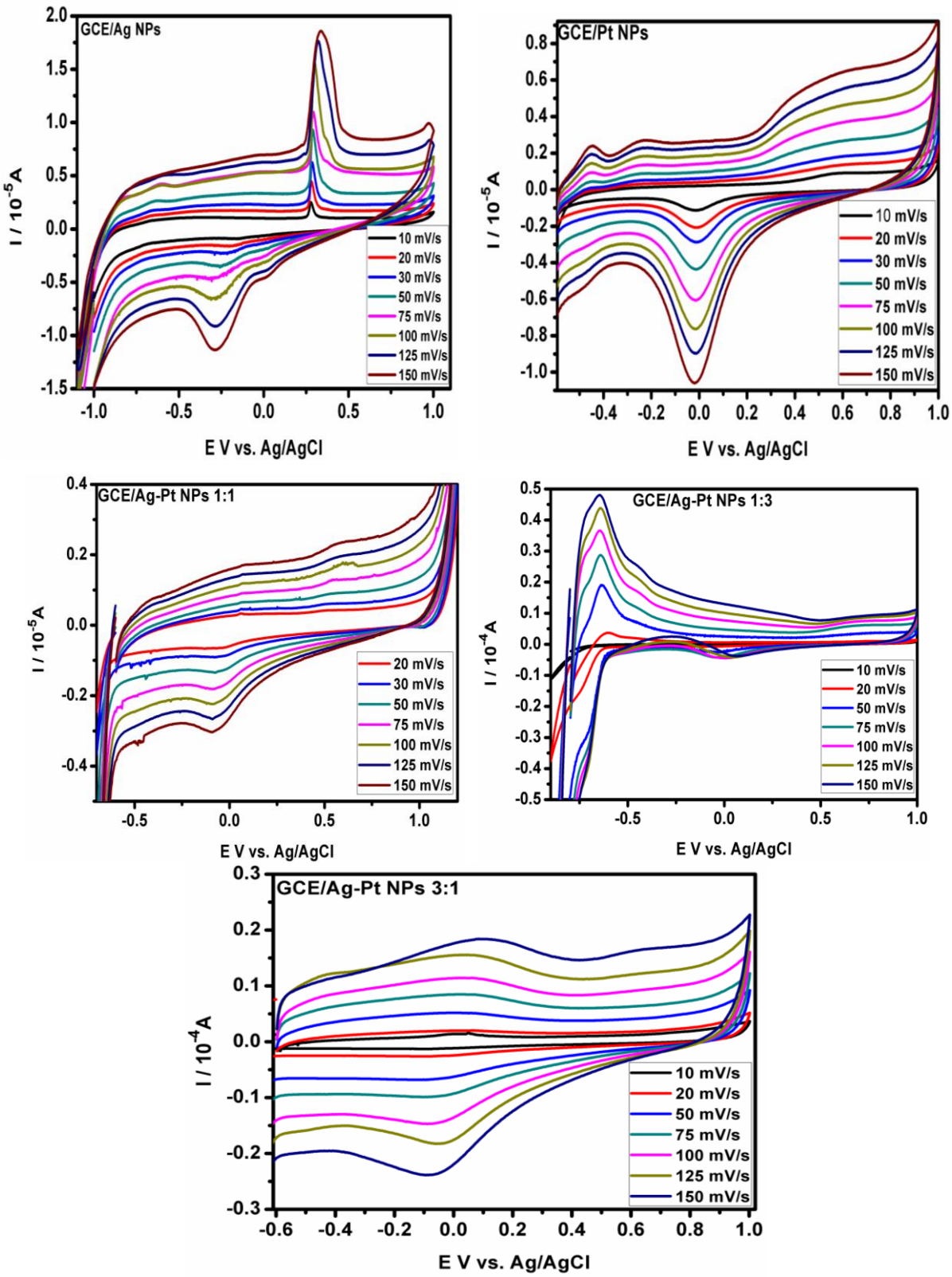


**Figure 4.3. Plots of scan rates for monometallic and bimetallic modified electrodes in 0.1 M PBS pH 7.0.**

From the cyclic voltammograms of GCE/Metal NPs in 0.1 M PBS of pH 7.0 at various scan rates, the relationships of the redox peak potentials with the scan rate were applied to

calculate the electrochemical parameters using the following Laviron's equations (Laviron, 1979):

$$E_{pa} = E^{O} + \frac{2.3RT}{(1-\alpha)nF}\log v \quad \text{.....Equation 4.10}$$

$$E_{pc} = E^{O} - \frac{2.3RT}{\alpha nF}\log v \quad \text{.....Equation 4.11}$$

$$\log ks = \alpha\log(1-\alpha) + (1-\alpha)\log\alpha - \log(\frac{RT}{nF}) - (1-\alpha)\alpha nF\frac{\Delta E_p}{2.3RT} \quad \text{.....Equation 4.12}$$

Where $E_{pa}$ and $E_{pc}$ are the anodic and cathodic peak potentials, respectively, α is the electron transfer coefficient, $k_s$ the standard rate constant of the surface reaction, *v* the scan rate, R is the universal gas constant (8.314 J $mol^{-1}$ $K^{-1}$), T is the absolute temperature (273.15 K), *F* the Faraday constant (96485 C/mol), $E^0$ the formal potential and n is the electron transfer number. According to above equation, if the $E^0$ is known, $E_p$ is in linear with ln *v* and the αn value can be calculated from the slope and $k_s$ from the intercept. The $E^0$ value can be deduced from the intercept of $E_p$ *vs. v* plot on the ordinate by extrapolating the line to v = 0, when v was approached to zero, then $E_p$ was approached to $E^0$.

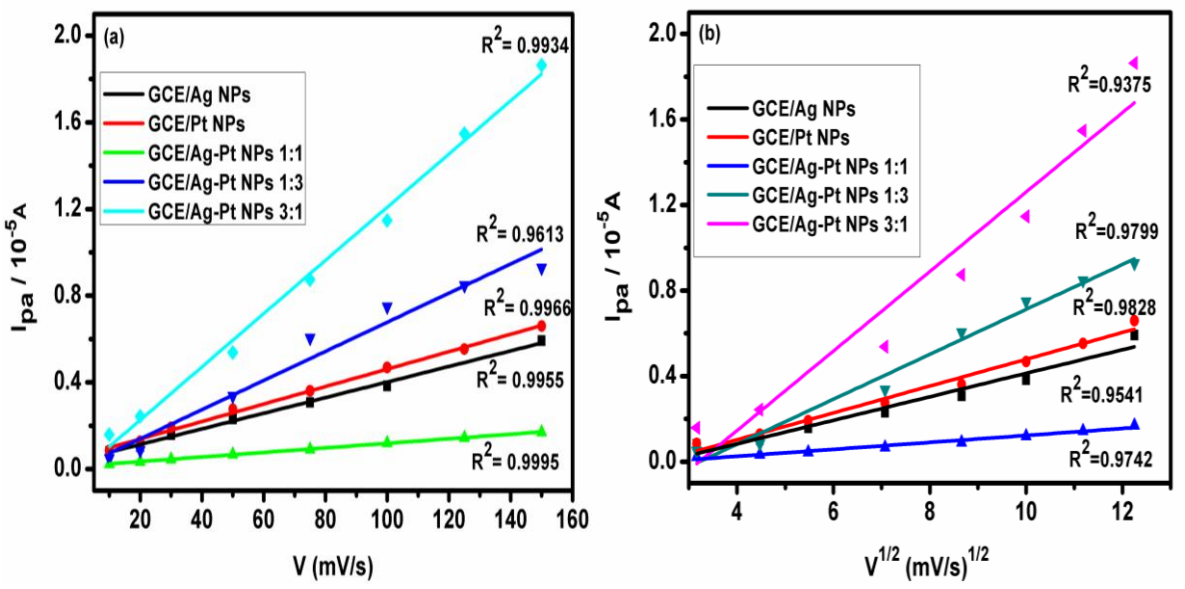


**Figure 4.4. The peak current of modified electrodes versus (a) scan rates, (b) square root of scan rate at 5 to 150 mV $s^{-1}$.**

Figure 4.5 shows the linearity of $E_{pa}$ and $E_{pc}$ versus log v respectively. The linear regression equations of $E_{pa}$ and $E_{pc}$ versus log v were deduced with better correlations as shown (Table 4.3). Using Equations (4.10) and (4.11), the values of α was calculated as shown (Table 4.4). The charge transfer coefficient (α) suggests a fraction of the interfacial potential at an electrode-electrolyte interface, which helps in lowering the free energy barrier for the electrochemical reaction. Furthermore, based on Equation (4.12), the value of apparent heterogeneous rate constant $k_s$ were calculated (Table 4.3) and found to vary from 0.10 to 31.13 $s^{-1}$ as evaluated from the experimental results. Small values of $k_s$ were observed in GCE/Ag NPs, GCE/Pt NPs and GCE/Ag-Pt NPs 1:3 indicating the existence of some nanoparticles domains, which are not directly adsorbed onto the surface of the electrode (Prodromidis *et al.,* 2000). The $k_s$ values were found to be within range of reported values (Pankratov *et al.,* 2014; D'Souza *et al.,* 2015). For GCE/Ag-Pt NPs 1:1, higher $k_s$ value was obtained, which was about 40 times higher than most of the values reported on GCE (Karim-Nezhad *et al.,* 2009; Zheng *et al.,* 2013) indicating that functionalized nanoparticles provide fast electron transfer at the surface of electrode as similarly argued (Kang *et al.,* 2009) and showed significantly high reversibility also contributed by its stability on the GCE surface. This further suggests that the electronic structure and the surface physicochemistry of GCE/Ag-Pt 1:1 NPs is beneficial for electron transfer as similarly reported with other modified electrodes (Fischer *et al.,* 2004; Tang *et al.,* 2009).

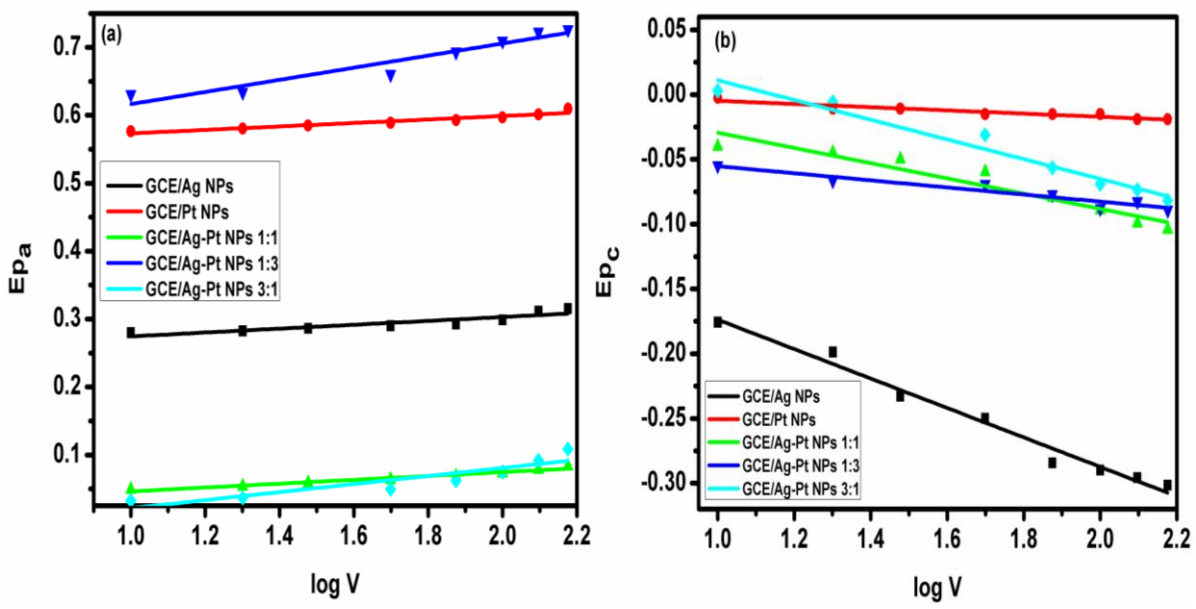


**Figure 4.5. Variation of (a) $E_{pa}$ versus logarithm of scan rate and (b) $E_{pc}$ versus logarithm of scan rate for the modified GC electrodes in 0.1 M PBS pH 7.0.**

From Table 4.3, the voltammograms of the modified GCE/Ag-Pt NPs 1:1, exhibited small separation of peak potentials indicating that the electrode process was reversible (Wang, 2000) while the rest of the modified GCEs had greater peak separation potentials ($\Delta E_p >$ 59/n mV) than the expected range for a reversible system suggesting that the redox processes had quasi-reversible behaviour. Furthermore, from the slope of the linear plot of $I_p$ versus v, the surface coverage of the electrode (Γ) in mol $cm^{-2}$ was determined using the equation 4.13, where Q is the charge in coulombs, A is the area of the electrode surface in $cm^2$, and n is the number of electrons transferred during redox transformation. The surface concentration of the electroactive species of each modified electrode was estimated as shown (Table 4.4) using anodic peak as similarly discussed (Shap *et al.,* 1979).

**Table 4.3. The electrochemical parameters of modified electrodes using Laviron's equation (Equation 4.10-4.12)**

| Electrode | Peaks $E_{pa}$ (mV) | used $E_{pc}$ (mV) | $\Delta E_p^0$ (mV) | αn | $k_s$ ($s^{-1}$) |
|---|---|---|---|---|---|
| GCE/Ag | 100 | -32 | 310 | 0.52 | 0.99 |
| GCE/Pt | 515 | -15 | 540 | 1.96 | 0.74 |
| GCE/Ag-Pt (1:1) | 535 | -54 | 10 | 1.00 | 31.13 |
| GCE/Ag-Pt (1:3) | 630 | -30 | 550 | 1.74 | 0.10 |
| GCE/Ag-Pt (3:1) | 28 | -28 | 120 | 0.90 | 3.43 |

From the plots in Figure 4.4, varying trend in diffusion coefficient was reported with GCE/Ag NPs showing high diffusion in the monometallic NPs while GCE/Ag-Pt NPs 3:1 gave a higher D value (Table 4.4). Higher D values exhibited by GCE/Ag NPs was attributed to its high film thickness on the electrode surface. This difference was supported by the nature of the surface redox reactions, which are mainly adsorption controlled as earlier discussed. The surface concentration of the electroactive species was higher in the GCE/Ag-Pt NPs 1:3 partly contributed by concentration of Pt NPs shell per unit Ag NP core. The fact that the surface coverages were much lower in their nmol $cm^{-2}$ range showed that the electron transfer in each electrode is fast as similarly observed (Murray, 1984). From this observations, GCE/Ag-Pt NPs 1:1 exhibited fast electron transfer relative to other modified GCEs.

The degree of surface coverage is a very important parameter in the construction of CMEs and its value is strictly depended on the morphology (roughness, homogeneity) of the

surface of the electrode (Prodromidis *et al.,* 2000). The charge contribution of electroactive modified GCE were estimated based on the charge associated with the film oxidation or reduction in 0.1 M PBS pH 7.0 and was calculated from integrated charge (Q) of the anodic peak as shown in Equation 4.14.

**Table 4.4. Electrochemical properties of modified electrodes based on Equation (4.10-4.11)**

| Electrode | α | Γ ($10^{-10}$ mol $cm^{-2}$) | Q ($10^{-6}$ C) | Slopes $I_{pa}$ vs. v | Slopes $I_{pa}$ vs. $v^{1/2}$ | D ($10^{-5}$ $cm^2$ $s^{-1}$) |
|---|---|---|---|---|---|---|
| GCE/Ag | 0.5 | 25.79 | 4.23 | 0.0036 | 0.0550 | 6.10 |
| GCE/Pt | 0.1 | 2.30 | 0.75 | 0.0040 | 0.0627 | 2.16 |
| GCE/Ag/Pt (1:1) | 0.7 | 1.85 | 0.61 | 0.0011 | 0.0163 | 0.62 |
| GCE/Ag/Pt (1:3) | 0.1 | 54.49 | 17.88 | 0.0067 | 0.1051 | 1.15 |
| GCE/Ag/Pt (3:1) | 0.4 | 19.13 | 6.27 | 0.0123 | 0.1858 | 1.87 |

$$I_p = \left(\frac{n^2F^2}{4RT}\right)\Gamma AV \quad \text{.....Equation 4.13}$$

$$\Gamma = Q/nFS \quad \text{.....Equation 4.14}$$

where Q is the charge obtained from the integration of the baseline corrected area under the oxidation or reduction peak, F is the Faraday constant (96485 $Cmol^{-1}$), n the number of electrons exchanged per electroactive molecule, and S the geometric area of the electrode (0.017 $cm^2$). Charge contribution per each NPs was higher in the BM NPs modified GCE values indicating enhanced conductivity observed mostly in the case of GCE/Ag-Pt NPs 1:3 with GCE/Ag-Pt NPs 1:1 depicting low conductivity. As shown in Figure 4.4, the anodic peak currents were linearly proportional to the square root of scan rate. This gave various values of diffusion coefficient as shown (Table 4.4).

## 4.4 Conclusion

This work demonstrates successful modification of GCE surface with the bimetallic silver-platinum nanoparticles in various ratios. The results presented a clear contribution of Pt NPs on Ag NPs as well as its distribution in the resulting bimetallic structures as characterized by CV analysis. Band gap of nanoparticles were found in the range of 2.48 eV to 3.84 eV for

optical and 1.45 eV to 1.80 eV for electrochemical measurements. The band gap increase in the BM NP ratios was consistent in both electrochemical and optical results relative to monometallics. The electrochemical band gaps were found to have an average factor difference of 1 with the optical band gaps. Although the electrochemically determined band gaps were found to be lower than the optical band gap, in most cases values portrayed similar trends. These results depict nanoparticles with band gaps within semiconductor range for most materials. The cyclic voltammetry based conclusion of interaction was supplemented by the results obtained from band gap energy. The CV data allowed us to quantitatively determine the changes in band gap energies of Ag NPs in the presence of Pt NPs. The Ag-Pt nanoparticles in suspension show the quantum size effect and the absorption edge shifts to lower wavelength when the particle size falls into nanometer range (<10 nm). The fact that electrochemical band gaps were found to be smaller than the optical band gaps with an average factor difference above 1 was attributed to solvation and electrode surface coverage effects. The electroactive surface coverage, the transfer coefficient, standard rate constant and diffusion coefficient were calculated from CV responses. The modified electrodes were found to have better surface attributes that influence the kinetics of electron transfer on the GCE with significant surface coverages determined in each case. The nanofilms exhibit facile electron transfer properties in the 0.1 M PBS pH 7.0 and offers good electrical functionality and thus offer broad opportunities in catalysis and chemical detection. From these results, GCE/Ag-Pt NPs 1:3 depicted improved properties and therefore proposed as a more efficient platform in electrochemical sensing amongst other potential applications.

## 4.5 References

Ahn, T., Choi, B., Ahn, S.H., Han, S.H., Lee, H. 2001. Electronic properties and optical studies of luminescent polythiophene derivatives. *Synth. Met.,* 117: 219-221.

AitRamdane-Terbouche, C., Terbouche, A., Djebbar, S., Hauchard, D. 2014. Electrochemical sensors using modified electrodes based on copper complexes formed with Algerian humic acid modified with ethylenediamine or triethylenetetramine for determination of nitrite in water. *Talanta,* 119: 214-225.

Al-Ibrahim, M., Roth, H.K., Schroedner, M., Konkin, A., Zhokhavets, U., Gobsch, G., Scharff, P., Sensfuss, S. 2005. The influence of the optoelectronic properties of poly (3-alkylthiophenes) on the device parameters in flexible polymer solar cells. *Org. Electron.,* 6: 65-77.

Aragay, G., Pino, F., Merkoçi, A. 2012. Nanomaterials for sensing and destroying pesticides. *Chem. Rev.,* 112(10): 5317-5338.

Banerjee, R., Jayakrishnan, R. and Ayyub, P. 2000. Effect of the size-induced structural transformation on the band gap in CdS nanoparticles. *J. Phys. Condens. Matter*, 12: 10647-10654.

Banin, U., Lee, J.C., Guzelian, A., Kadavanich, A.V. and Alivisatos, A.P. 1997. Exchange interaction in InAs nanocrystal quantum dots. *Superlattices Microst.,* 22: 559-568.

Banin, U., Lee, J.C., Guzelian, A.A., Kadavanich, A.V., Alivisatos, A.P., Jaskolski, W., Bryant, G.W., Efros, A.L. and Rosen, M. 1998. Size-dependent electronic level structure of INAS nanocrystal quantum dots - test of multiband effective-mass theory. *J. Chem. Phys.* 109(6): 2306-2309.

Bard, A.J., Faulkner, L.R. 1980. *Electrochemical methods fundamentals and applications*. Wiley New York, 1980, 522.

Beaupre, S., Leclerc, M. 2002. Fluorene-based copolymers for red-light-emitting diodes. *Adv. Funct. Mater.,* 12(3): 192-196.

Bhargava, R.N., Gallagher, D., Hong, X., Nurmikko, A. 1994. Optical properties of manganese-doped nanocrystals of ZnS. *Phys. Rev. Lett.,* 72(3): 416-419.

Birkin, P.R., Elliot, J.M., Watson, Y.E. 2000. Electrochemical reduction of oxygen on mesoporous platinum microelectrodes. *Chem. Commun.,* 17: 1693-1694.

Bredas, J.L., Silbey, R., Boudreux, D.S. and Chance, R.R. 1983. Chain-length dependence of electronic and electrochemical properties of conjugated systems: polyacetylene, polyphenylene, polythiophene, and polypyrrole. *J. Am. Chem. Soc.*, 105(22): 6555-6559.

Brown, K.L. and Gray, S.B. 2010. Cyclic voltammetric studies of electropolymerized films based on Ruthenium (II/III) Bis (1, 10 phenanthroline) (4-methyl-4'vinyl-2, 2'-bibyridine). *Int. J. Chem.,* 2(2): 3-9.

Brown, K.R., Fox, A.P., Natan, M.J. 1996. Morphology-dependent electrochemistry of cytochrome *c* at Au colloid-modified $SnO_2$ electrodes. *J. Am. Chem. Soc.,* 118(5): 1154-1157.

Budhiraja, N., Sharma, A., Dahiya, S., Parmar, R. and Vidyadharan, V. 2013. Synthesis and optical characteristics of silver nanoparticles on different substrates. *Int. Lett. Chem. Phys. Astron.,* 14: 80-88.

Can, K., Ozmen, M., Ersoz, M. 2009. Immobilization of albumin on aminosilane modified superparamagnetic magnetite nanoparticles and its characterization. *Colloids Surf. B,* 71(1): 154-159.

Cervini, R., Li, X.C., Spencer, G.W., Holmes, A.B., Moratti, S.C., Friend, R.H. 1997. *Synthetic Met*., 84: 359-360.

Chahal, R.P., Mahendia, S., Tomar, A.K. and Kumar, S. 2011. Effect of ultraviolet irradiation on the optical and structural characteristics of *in-situ* prepared PVP-Ag nanocomposites. *Dig. J. Nanomater. Bios.*, 6(1): 299-306.

Chakraborty. S., Raj, R.C. 2009. Pt nanoparticles-based highly sensitive platform for the enzyme-free amperometric sensing of $H_2O_2$. *Biosens. Bioelectron*., 24: 3264-3268.

Charas, A., Morgado, J., Martinho, J.M.G., Alcacer, L., Lim, S.F., Friend, R.H., Cacialli, F. 2003. Synthesis and luminescence properties of three novel polyfluorene copolymers. *Polymer,* 44: 1843-1850.

Chen, S. Ingrma, R. S. Hostetler, M. J. Pietron, J. J. Murray, R. W. Schaaff, T. G. Khoury, J. T. Alvarez, M. M. and Whetten, R. L. 1998. Gold nanoelectrodes of varied size: transition to molecule-like charging. *Science*, 280(5372): 2098-2101.

Chen, X.X., Li, N., Eckhard, K., Stoica, L., Xia, W., Assmann, J., Muhler, M., Schuhmann, W. 2007. Pulsed electrodeposition of Pt nanoclusters on carbon nanotubes modified carbon materials using diffusion restricting viscous electrolytes. *Electrochem. Commun.,* 9(6): 1348-1354.

D'Andrade, B.W., Datta, S., Forrest, S.R., Djurovich, P., Polikarpov, E. and Thompson, M.E. 2005. Relationship between the ionization and oxidation potentials of molecular organic semiconductors. *Org. Electron.*, 6: 11-20.

D'Souza, O.J., Mascarenhas, R.J., Thomas, T., Basavaraja, B.M., Saxena, A.K., Mukhopadhyay, K., Roy, D. 2015. Platinum decorated multi-walled carbon nanotubes/Triton

X-100 modified carbon paste electrode for the sensitive amperometric determination of Paracetamol. *J. Electroanal. Chem.,* 739: 49-57.

Ekimov, A.I., Hache, F., Schanne-Klein, M.C., Ricard, D., Flytzanis, C., Kudryavtsev, I.A., Yazeva, T.V., Rodina, A.V. and Efros, A.L. 1993. Absorption and intensity-dependent photoluminescence measurements on CdSe quantum dots: assignment of the first electronic transitions. *J. Opt. Soc. Am*. *B*, 10(1): 100-107.

Empedocles, S.A., Norris, D.J. and Bawendi, M.G. 1996. Photoluminescence spectroscopy of single CdSe nanocrystallite quantum dots. *Phys. Rev. Lett*., 77(18): 3873-3876.

Evans, S.A.G., Elloit, J.M., Andrews, L.M., Barlett, P.N., Doyle, P.J., Denuault, G. 2002. Detection of hydrogen peroxide at mesoporous platinum microelectrodes. *Anal. Chem.,* 74(6): 1322-1326.

Fang, M.M., Zu, X.T., Li, Z.J., Zhu, S., Liu, C.M., Zhou, W.L. and Wang, L.M. 2008. Synthesis and characteristics of $Fe^{3+}$-doped $SnO_2$ nanoparticles via sol-gel-calcination or sol-gel-hydrothermal route. *J. Alloys Compd.,* 454: 261-267.

Fischer, A.E., Show, Y., Swain, G.M. 2004. Electrochemical performance of diamond thin-film electrodes from different commercial sources. *Anal. Chem.,* 76(9): 2553-2560.

Fu, H. and Zunger, A. 1998. Excitons in InP quantum dots. *Phys. Rev. B,* 57: R15064-R15067.

Fu, H., Wang, L.W. and Zunger, A. 1998. Applicability of the k.p method to the electronic structure of quantum dots. *Phys. Rev. B,* 57: 9971-9987.

Fujishima, A., Honda, K. 1972. Electrochemical photolysis of water at a semiconductor electrode. *Nature*, 238: 37-38.

Ganjali, M.R., Motakef-Kazami, N., Faridbod, F., Khoee, S., Norouzi, P. 2010. Determination of $Pb^{2+}$ ions by a modified carbon paste electrode based on multi-walled carbon nanotubes (MWCNTs) and nanosilica. *J. Hazard. Mater.,* 173(1-3): 415-419.

Gao, H., Xiao, F., Ching, C.B., Duan, H. 2011. One-step electrochemical synthesis of PtNi nanoparticle-graphene nanocomposites for non-enzymatic amperometric glucose detection. *ACS Appl. Mater. Interfaces*, 3: 3049-3057.

Gao, H., Zhong, J., Qin, P., Lin, C., Sun, W. 2009. Microplate electrochemical DNA detection for phosphinothricin acetyltransferase gene sequence with cadmium sulfide nanoparticles. *Microchem. J.,* 93(1): 78-81.

Guo, M.Q., Hong, H.S., Tang, X.N., Fang, H.D., Xu, X.H. 2012. Ultrasonic electrodeposition of platinum nanoflowers and their application in nonenzymatic glucosesensors. *Electrochim. Acta*, 63: 1-8.

Haram, S.K., Quinn, B.M. and Bard, A.J. 2001. Electrochemistry of CdS nanoparticles: a correlation between optical and electrochemical band gaps. *J. Am. Chem. Soc.,* 123: 8860-8861.

Hindle, P.H., Nigro, P.H.S., Asmussen, M., Chen, A. 2008. Amperometric glucose sensor based on platinum-iridium nanomaterials. *Electrochem. Commun.,* 10(10): 1438-1441.

Hrapovic, S., Liu, Y.L., Male, K.B. and Luong. J.H.T. 2004. Electrochemical biosensing platforms using platinum nanoparticles and carbon nanotubes. *Anal. Chem.,* 76: 1083-1088.

Huang, J., Liu, Y., Hou, H. and You, T. 2008. Simultaneous electrochemical determination of dopamine, uric acid and ascorbic acid using palladium nanoparticle-loaded carbon nanofibers modified electrode. *Biosens. Bioelectron.,* 24: 632-637.

Hudak, E.M., Mortimer, J.T. and Martin, H.B. 2010. Platinum for neural stimulation: Voltammetry considerations. *J. Neural Eng.,* 7(2): 026005-026012.

Inbasekaran, M., Woo, E., Wu, W., Bernius, M., Wujkowski, L. 2000. Fluorene homopolymers and copolymers. *Synth. Met*., 112-113: 397-401.

Janietz, S., Bradley, D.D.C., Grell, M., Giebeler, C., Inbasekaran, M., Woo, E.P. 1998. Electrochemical determination of the ionization potential and electron affinity of poly (9, 9-dioctylfluorene). *Appl. Phys. Lett*., 73: 2453-2455.

Jin, C.C., Chen, Z.D. 2007. Electrocatalytic oxidation of glucose on gold-platinum nanocomposite electrodes and platinum-modified gold electrodes. *Synth. Met.,* 157: 592-596.

Jingyu, S., Jianshu, H., Yanxia, C., Xiaogang, Z. 2007. Hydrothermal synthesis of Pt-Ru/MWCNTs and its electrocatalytic properties for oxidation of methanol. *Int. J. Electrochem. Sci.,* 2: 64-71.

Johansson, T., Mammo, W., Svensson, M., Anderson, M.R., Inganas, O. 2003. Electrochemical bandgaps of substituted polythiophenes. *J. Mater. Chem*., 13: 1316-1323.

Justino, C.I.L., Rocha-Santos, T.A.P., Cardoso, S., Duarte, A.C. 2013. Strategies for enhancing the analytical performance of nanomaterial-based sensors. *TrAC-Trends Anal. Chem.,* 47: 27-36.

Kang, X.H., Wang, J., Wu, H., Aksay, A.I., Liu, J., Lin, Y.H. 2009. Glucose oxidase-graphene-chitosan modified electrode for direct electrochemistry and glucose sensing. *Biosens. Bioelectron.,* 25: 901-905.

Karim-Nezhad, G., Hasanzadeh, M., Saghatforoush, L., Shadjou, N., Earshad, S. and Khalilzadeh, B. 2009. Kinetic study of electrocatalytic oxidation of carbohydrates on cobalt hydroxide modified glassy carbon electrode. *J. Braz. Chem. Soc.,* 20(1): 141-151.

Katz, E., Willner, I. and Wang, J. 2004. Electroanalytical and Bioelectroanalytical Systems Based on Metal and Semiconductor Nanoparticles. *Electroanalysis,* 16: 19-44.

Kim, H.J., Kim, Y.S., Seo, M.H., Choi, S.M., Cho, J., Huber, G.W., Kim, W.B. 2010. Highly improved oxygen reduction performance over Pt/C-dispersed nanowire network catalysts. *Electrochem. Commun.,* 12(1): 32-35.

Kumar, H. and Rani, R. 2013. Structural characterization of silver nanoparticles synthesized by micro emulsion route. *Int. J. Eng. Innov. Technol.*, 3(3): 344-348.

Lane, R.F., Hubbard, A.T. 1973. Electrochemistry of chemisorbed molecules. I. Reactants connected to electrodes through olefinic substituents*. J. Phys. Chem.,* 77(11): 1401-1410.

Laviron, E. 1979. General expression of the linear potential sweep voltammogram in the case of diffusionless electrochemical systems. *J. Electroanal. Chem.,* 101: 19-28.

Lee, S.H., Jung, J.H., Chae, Y.M., Suh, J.F. and Kang, J.Y. 2010. Fabrication and characterization of implantable and flexible nerve cuff electrodes with Pt, Ir and IrOx films deposited by RF sputtering. *Micromech. Microeng.,* 20(3): 035015-035023.

Leon, M., Petroff, P.M., Leonard, D. and Fafard, S. 1995. Spatially resolved visible luminescence of self-assembled semiconductor quantum dots. *Science,* 267: 1966-1968.

Lin, K.F., Cheng, H.M., Hsu, H.C., Lin, L.J., Hsieh, W.F. 2005. Band gap variation of size-controlled ZnO quantum dots synthesized by sol-gel method. *Chem. Phys. Lett.,* 409: 208-211.

Liu, B., Chen, Z.K., Yu, W.L., Lai, Y.H., Huang, W. 2000. Poly [9-methyl-9-(4-cyanobutyl) fluorene] synthesis towards water-soluble polyfluorenes. *Thin Solid Films,* 363: 332-335.

Liu, B., Yu, W.L., Lai, Y.H., Huang, W. 2001. Blue-light-emitting fluorene-based polymers with tunable electronic properties. *Chem. Mater*., 13(6): 1984-1991.

Lu, W., Chang, G., Luo, Y., Liao, F. and Sun, X. 2011. Method for effective immobilization of Ag nanoparticles/graphene oxide composites on single-stranded DNA modified gold electrode for enzymeless $H_2O_2$ detection. *J. Mater. Sci.,* 46: 5260-5266.

Luo, J., Njoki, P.N., Mott, D., Wang, L., Zhong, C.J. 2006. Characterization of carbon-supported AuPt nanoparticles for electrocatalytic methanol oxidation reaction. *Langmuir,* 22(6): 2892-2898.

Manjunatha, J.G., Kumara, B.E., Mamatha, S.G.P., Chandra, U., Niranjana, E., Sherigara, B.S. 2009. Cyclic voltammetric studies of dopamine at lamotrigine and TX-100 modified carbon paste electrode. *Int. J. Electrochem. Sci.,* 4: 187-196.

Mazloum-Ardakani, M., Beitollahi, H., Taleat, Z., Salavati-Niasar, M. 2011. Fabrication and characterization of molybdenum (VI) complex-$TiO_2$ nanoparticles modified electrode for the electrocatalytic determination of L-cysteine. *J. Serb. Chem. Soc.,* 76(4): 575-589.

Mazloum-Ardakani, M., Rajabi, H., Beitollahi, H., Mirjalili, B.B.F., Akbari, A., Taghavinia, N. 2010. Voltammetric determination of dopamine at the surface of $TiO_2$ nanoparticles modified carbon paste electrode. *Int. J. Electrochem. Sci.,* 5: 147-157.

Meng, H., Chen, Z.K., Huang, W. 1999. Spectroscopic and electrochemical study of a novel blue electroluminescent p-n diblock conjugated copolymer. *J. Phys. Chem. B,* 103(31): 6429-6433.

Muhlbacher, D., Neugebauer, H., Cravino, A., Sariciftci, N.S. 2003. Comparison of the electrochemical and optical bandgap of low-bandgap polymers. *Synthetic Met*., 137: 1361-1362.

Murray, R.W. 1984. In: Bard, A.J. ed. *Electroanalytical Chemistry*. Marcel Dekker, New York, 13, pp. 191-368.

Niquet, Y.M., Allan, G., Deleue, C. and Lannoo, M. 2000. Quantum confinement in germanium nanocrystals. *Appl. Phys. Lett.*, 77(8): 1182-1184.

Nkosi, S.S., Mwakikunga, B.W., Sideras-Haddad, E. and Forbes, A. 2012. Synthesis and characterization of potential iron-platinum drugs and supplements by laser liquid photolysis. *Nanotechnol. Sci. Appl.*, 5: 27-36.

Norris, D.J. and Bawendi, M.G. 1996. Measurement and assignment of the size-dependent optical spectrum in CdSe quantum dots. *Phys. Rev. B,* 53(24): 16338-16346.

Norris, D.J., Sacra, A., Murray, C.B. and Bawendi, M.G. 1994. Measurement of the size dependent hole spectrum in CdSe quantum dots. *Phys. Rev. Lett*., 72: 2612-2615.

Ojani, R., Raoof, J., Babazadeh, R. 2010. Electrocatalytic oxidation of hydrogen peroxide on poly (*m*-toluidine)-nickel modified carbon paste electrode in alkaline medium. *Electroanalysis*, 22(14): 1607-1616.

Pankove, J.I. 1971. *Optical process in semiconductors*. Prentice-Hall, Englewood Cliffs, New Jersey.

Pankratov, D.V., Zeifman, Y.S., Dudareva, A.V., Pankratova, G.K., Khlupova, M.E., Parunova, Y.M., Zajtsev, D.N., Bashirova, N.F., Popov, V.O. and Shleev, S.V. 2014. Impact of surface modification with gold nanoparticles on the bioelectrocatalytic parameters of immobilized bilirubin oxidase. *Acta naturae*, 6(1): 102-106.

Pei, J., Yu, W.L., Huang, W., Heeger, A.J. 2000. A novel series of efficient thiophene-based light-emitting conjugated polymers and application in polymer light-emitting diodes. *Macromolecules,* 33(7): 2462-2471.

Pei, J., Yu, W.L., Ni, J., Lai, Y.H., Huang, W., Heeger, A.J. 2001. Thiopene based conjugated polymers for light emitting electrodes: Effect of aryl a groups on photoluminescence efficiency and redox behaviour. *Macromolecules*, 34: 7241-7248.

Prodromidis, M.I., Florou, A.B., Tzouwara-Karayanni, S.M. and Karayannis, M.I. 2000. The importance of surface coverage in the electrochemical study of chemically modified electrodes. *Electroanalysis,* 12: 1498-1501.

Pronkin, S.N., Tsirlina, G.A., Petrii, O.A., Yu, S. 2001. Vassiliev, Nanoparticles of Pt hydrosol immobilised on Au support: an approach to the study of structural effects in electrocatalysis. *Electrochim. Acta,* 46: 2343-2351.

Raj, C.R., Okajima, T., Ohsaka, T. 2003. Gold nanoparticle arrays for the voltammetric sensing of dopamine. *J. Electroanal. Chem.,* 543: 127-133.

Rena, X.L., Menga, X.W., Chena, D., Tanga, F., Jiao, J. 2005. Using silver nanoparticles to enhance current response of biosensor. *Biosens. Bioelectron.,* 21(3): 433-437.

Revaprasadu, N, Mlondo, S.N. 2006. Use of metal complexes to synthesize semiconductor nanoparticles. *Pure Appl. Chem.,* 78(9): 1691-1702.

Rong, L.Q., Yang, C., Qian, Q.Y., Xia, X.H. 2007. Study of the nonenzymatic glucose sensor based on highly dispersed Pt nanoparticles supported on carbon nanotubes. *Talanta,* 72(2) (2007) 819-824.

Salem, A. 2014. Silver-doped cadmium oxide nanoparticles: Synthesis, structural and optical properties. *Eur. Phys. J. Plus*, 129: 263.

Sankara, R.B., Venkatramana, R.S., Koteeswara, R.N. and Pramoda, K.J. 2013. Synthesis, structural, optical properties and antibacterial activity of codoped (Ag, Co) ZnO nanoparticles. *Res. J. Mater. Sci.*, 1(1): 11-20.

Sattler, K. 2002. *Handbook of Thin Films, Nanomaterials and Magnetic Thin Films*, vol. 5, Academic Press, New York. p. 61-97.

Selvaraj, V., Grace, A.N., Alagar, M. 2009. Electrocatalytic oxidation of formic acid and formaldehyde on nanoparticle decorated single walled carbon nanotubes. *J. Colloids Interf. Sci.,* 333(1): 254-262.

Selvaraju, T., Ramaraj, R. 2005. Electrochemically deposited nanostructured platinum on Nafion coated electrode for sensor applications. *J. Electroanal. Chem*., 585(2): 290-300.

Shap, M., Petersson, M. and Edstrom, K. 1979. Preliminary determinations of electron transfer kinetics involving ferrocene covalently attached to a platinum surface. *J. Electroanal. Chem.,* 95(1): 123-130.

Simm, A.O., Ward-Jones, S., Banks, C.E, Compton, R.G. 2005. Novel methods for the production of silver microelectrode-arrays: their characterisation by atomic force microscopy and application to the electro-reduction of halothane. *Anal Sci.,* 21(6): 667-71.

Smith., M., Mohs, A.M., and Nie, S. 2009. Tuning the optical and electronic properties of colloidal nanocrystals by lattice strain. *Nat. Nanotechnol.*, 4: 56-63.

Sulak, M.T., Gokdogan, O., Gulce, A., Gulce, H. 2006. Amperometric glucose biosensor based on gold deposited PVF film on Pt electrode. *Biosens. Bioelectron.,* 21: 1719-1726.

Tang, L.H., Wang, Y., Li, Y.M., Feng, H.B., Lu, J., Li, J.H. 2009. Preparation, structure, and electrochemical properties of reduced graphene sheet films. *Adv. Funct. Mater.,* 19: 2782-2789.

Tauc, J., Grigorovici, R. and Vancu, A. 1966. Optical properties and electronic structure of amorphous germanium. *Phys. Status Solidi(b)*, 15: 627-637.

Templeton, A.C., Wuelfing, W.P. and Murray, R.W. 2000. Monolayer-protected cluster molecules. *Accounts Chem. Res.*, 33(1): 27-36.

Thiagarajan, S., Chen, S.M. 2007. Preparation and characterization of PtAu hybrid film modified electrodes and their use in simultaneous determination of dopamine, ascorbic acid and uric acid. *Talanta*, 74(2): 212-22.

Tominaga, M., Shimazoe, T., Nagashima, M., Taniguchi, I. 2008. Composition-activity relationships of carbon electrode-supported bimetallic gold-silver nanoparticles in electrocatalytic oxidation of glucose. *J. Electroanal. Chem.,* 615(1): 51-61.

Wang, B., Xiao, X., Huang, X., Sheng, P. and Hou, J.G. 2000. Single-electron tunneling study of two-dimensional gold clusters. *Appl. Phys. Lett.,* 77: 1179-1181.

Wang, G.F., Wang, W., Wu, J.F., Liu, H.Y., Jiao, S.F. and Fang, B. 2009. Self-assembly of silver nanoparticles modified electrode and its electrocatalysis on neutral red. *Microchimica Acta,* 164(1-2): 149-155.

Wang, J. 1996. Electrocatalytic reduction and flow injection analysis of organic peroxides at polymeric tetra-amino Iron phthalocyanine modified electrode. *Anal. Lett.,* 29(9): 1575-1587.

Wang, J. 2000. *Analytical Electrochemistry*. 2nd ed., Wiley-VCH, New York.

Wu, S., Zhao, H.T., Ju, H.X., Shi, C.G., Zhao, J.W. 2006. Electrodeposition of silver-DNA hybrid nanoparticles for electrochemical sensing of hydrogen peroxide and glucose. *Electrochem. Commun.,* 8: 1197-1203.

Xu, P., Zeng, G.M., Huang, D.L., Feng, C.L., Hu, S., Zhao, M.H., Lai, C., Wei, Z., Huang, C., Xie, G.X., Liu, Z.F. 2012. Use of iron oxide nanomaterials in wastewater treatment: a review. *Sci. Total Environ.,* 424: 1-10.

Yang, P., Meldrum, F.C. and Fendler, J.H. 1995. Epitaxial-growth of size quantized cadmium sulphide crystals under arachnid acid monolayer. *J. Phys. Chem.*, 99: 5500-5504.

You, T.Y., Niwa, O., Tomita, M., Hirono, S. 2003. Characterization of platinum nanoparticle-embedded carbon film electrode and its detection of hydrogen peroxide. *Anal. Chem.,* 75(9): 2080-2085.

Zheng, L., Song, J.F. 2009. Nickel (II)-baicalein complex modified multiwall carbon nanotube paste electrode and its electrocatalytic oxidation toward glycine. *Anal. Biochem.,* 391(1): 56-63.

Zheng, M., Gao, F., Wang, Q., Cai, X., Jiang, S., Huang, L., Gao, F. 2013. Electrocatalytical oxidation and sensitive determination of acetaminophen on glassy carbon electrode modified with graphene-chitosan composite. *Mater. Sci. Eng. C Mater. Biol. Appl.,* 33(3): 1514-1520.

Zheng, N., Zhou, X., Yang, W., Li, X., Yuan, Z. 2009. Direct electrochemistry and electrocatalysis of haemoglobin immobilized in a magnetic nanoparticles-chitosan film. *Talanta,* 79(3): 780-786.

# CHAPTER FIVE

# DEVELOPMENT OF ELECTROCHEMICAL NEVIRAPINE SENSOR

## 5.1 Introduction

This chapter focuses on the potential usage of bimetallic nanoparticles and MWCNT's nanocomposite platforms in the development of an electrochemical nevirapine (NVP) sensor. The need to monitor and analyse pharmaceuticals such as NVP has continued to be of great concern to most researchers due to its wide usage as an ARV in the treatment of HIV infection. Electrochemical techniques have been utilised in analyses of various drug molecules since they offer very low detection limits for electroactive molecules (Dogan-Topal *et al.,* 2010; Castro *et al.,* 2011). From 2010, much of the studies on the electrochemical determinations of nevirapine has been on bare GCE (Teradal *et al.,* 2012), gold electrode (Esteva *et al.,* 2014), mercury electrode (Castro *et al.,* 2011), carbon paste electrode (Zhang *et al.,* 2010) with few done on modified electrodes. Some of the reported modifications on electrodes for NVP detection include CuO NPs/GCE platform (Shahrokian *et al.,* 2015). These platforms have provided good detection probes though with challenges such as electrode fouling and low sensitivity. Therefore, there is need to establish highly sensitive platforms for the determination of nevirapine. Various electrodes were used to detect nevirapine and the mechanism of reaction proposed based on the electrode interaction with NVP as an electron transfer process (Teradal *et al.,* 2012; Esteva *et al.,* 2014) with an irreversible behaviour. This study however, pays attention to the detection of NVP exhibited on Ag and Pt bimetallic electrode platforms.

Metallic nanoparticles are capable of increasing the activities for many chemical reactions due to the high ratio of surface atoms with free valences to the cluster of total atoms. In addition to a high surface area-to-volume ratio for nanoparticle derivatized materials, the size controllability, chemical stability, and surface tenability provide an ideal platform for exploiting such nanostructures in sensing/biosensing and catalytic applications (Hrapovic *et al.,* 2006). The use of metal NPs as modifiers during detection studies significantly enhances the kinetics of the electrode reaction (Shahrokian *et al.,* 2015) which helps in obtaining well resolved redox peaks. For example, bimetallic Ag-Pt NPs has been used in the detection of dopamine (Huang *et al.,* 2014). However, from the literature, little work has been done to the present date to investigate the electrochemical behaviour of nevirapine on bimetallic Ag-Pt NPs platforms.

Metal nanoparticles are comprehensively displayed for the detection methodology of drug biomolecules in chemical control process, due to their advantages over conventional chemical analysis methods. In conventional method, the unmodified electrodes for nevirapine detection have exhibited slower response, surface fouling (Teradal *et al.,* 2012), noise, unstable signals, and lower dynamic range as well as lower sensitivity. Hence, the modification of the sensor surface with nanomaterials is very significant in order to achieve higher sensitivity with repeatable and stable responses. Lately, studies on the sensing properties of bimetallic NPs have been reported (Li *et al.,* 2013; Liu *et al.,* 2013; Yan *et al.,* 2013). However, very few modified electrodes have been explored on NVP detection.

In this work, MWCNTs were incorporated on the BM NPs as a result of the relatively unstable signal resolutions due to the bimetallic Ag-Pt NPs modifications. MWCNT containing bimetallic Ag-Pt NPs electrode was used for nevirapine detection in order to enhance the adsorptive accumulation of the analyte increasing the signal resolution thus offering significant improvement in the electrochemical detection (Hrapovic *et al.,* 2006). In particular, MWCNTs have much higher stability against electromigration than other small metallic structures and therefore they find applications as possible links on modified electrodes. For example, multi-walled carbon nanotubes (MWCNTs) have been mixed with silver (Ghalkhani *et al.,* 2009) or cobalt (Shahrokian *et al.,* 2009) nanoparticles to measure sumatriptan and thioridazine, respectively. In this regard, part of this chapter highlights a brief discussion on the fabrication of GCE with metal (Ag-Pt) NPs together with MWCNT to form a nanocomposite modifier, and its usage as sensor probe for the detection of NVP. Nanocomposites are combinations of nanomaterials with other molecules or nanoscaled materials, such as nanoparticles or nanotubes. In order to increase the application areas of nanoparticles, multi-functionalised materials have been developed (Breuer and Sundararaj, 2004) such as nanocomposites. These nanocomposites combine excellent physical and chemical properties of their components, but may also provide novel properties (Datta *et al.,* 2007; Zhang *et al.,* 2010c). Among the nanocomposites, metal NPs-carbon nanotube composites are of great interests, due to their easy fabrication protocols and broad potential applications.

Carbon nanotubes (CNTs) are one of the most intensively explored nanostructured materials. In particular, CNTs are unique and ideal templates onto which nanoparticles can be immobilized to allow construction of designed nanoarchitectures that are extremely attractive. CNTs have been used in many different types of sensors as a way of increasing the analytical signal and investigating possible electrocatalytic properties, exploiting the fact that the reaction sites on the carbon nanotube surface are, in principle, different from those at a macroscopic glassy carbon electrode (Jacobs *et al.,* 2010). Several advantages of CNTs

have been noted, such as enhanced mass transport, high effective surface area, high porosity, more adsorption capability and reactive sites with control over the electrode macro-environment (Binks *et al.,* 2006; Amiri *et al.,* 2007; Ho *et al.,* 2009). These play a crucial role in the construction of sensitive, selective and quick responsive biosensors for the detection of some important analyte molecules (Shahmiri *et al.,* 2013). Both, the CNTs as well as NPs have exceptional electrocatalytic characteristics, which make them suitable modifiers for the construction of electrodes (Li and Lin, 2007; Sreeja *et al.,* 2011, Mohan *et al.,* 2015). These unique properties of CNTs have been explored in this study.

Many ingenious methods of depositing metal nanoparticles onto CNT substrates have been reported including direct and linked deposition of nanoparticles on CNT. These include electrochemical deposition (Guo *et al.,* 2004; He *et al.,* 2004) using noble metals like Pt, Pd and also bimetallic Pt-Ru (He *et al.,* 2004), and physical and chemical methods (Wildgoose *et al.,* 2006), which have been reported to offer varying degrees of control of particle size and distribution along the CNT. During deposition, the acid-treated carbon nanotubes are decorated with nanoparticles by employing several procedures. The nature and extent of metal coverage can be varied by changing the concentration of the metal compound or by mild sonication (treatment with ultrasound) (Satiskumar *et al.,* 1996). The metal clusters are deposited on the acidic surface sites of the nanotubes. The ease in modification surfaces of metal NPs and the excellent conductivity of carbon nanotube as well as the high surface area, offers a broad range of applications. Various nanocomposites have been developed, such as gold-carbon nanotube (Au-CNT) nanocomposites (Choi *et al.,* 2002; Kim and Sigmund, 2004; Raghuveer *et al.,* 2006; Zhang and Wang, 2007; Zhang *et al.,* 2009b). These composites are used in a number of applications, such as sensors (Zhang *et al.,* 2006a; Shimada *et al.,* 2007; Chen *et al.,* 2008; De Oliveira *et al.,* 2009), optics (Ispasoiu *et al.,* 2000; Qu *et al.,* 2001; Zijlstra *et al.,* 2007), and in the medical area (Bielinska *et al.,* 2002; Mishra *et al.,* 2007; Lee *et al.,* 2008).

A simple, direct electroanalytical method for determination of nevirapine at MWCNT/Ag-Pt NPs electrode was developed. A series of experiments were performed to optimize the conditions with acceptable signal response. Much attention was on the optimization of the detection platform to achieve the best results. The effect of supporting electrolyte, scan rates and the bimetallic ratios were investigated. The electrochemical study on MWCNT/Ag-Pt NPs/GCE, as well as its efficiency for the electrooxidation of nevirapine using differential pulse voltammetry (DPV) technique is described. Cyclic voltammetry (CV) was used to study the redox behaviour of NVP and further characterize its reaction on the electrode surface through analysis of its diffusion and kinetic limitations. Common point sources of interferences with NVP electrooxidation were studied and discussed. The proposed DPV

method was further applied in real sample analysis of human urine, milk and application in the analysis of pharmaceutical NVP tablets. The electroanalytical method exhibited a very reliable and highly sensitive detection of nevirapine using MWCNT/bimetallic Ag-Pt nanocomposite. The present approach also depicts a sensitive, easy to handle electrochemical technique over the existing reported methods. To the best of our knowledge, this is the first report of a highly sensitive electrochemical detection of nevirapine with MWCNT/bimetallic Ag-Pt nanocomposite as a detection platform.

## 5.2 Experimental

### 5.2.1 Materials, reagents and Instrumentation

Nevirapine standard was purchased from Industrial Analytical South Africa (SA). Sodium hydroxide and ethanol were purchased from the Sigma Aldrich (SA). MWCNT was bought from Signa Aldrich (SA). Sodium hydroxide solutions were used to prepare the supporting electrolyte. Electrochemical measurements were done using Autolab PGSTAT 101 (Metrohm, SA). All electrochemical experiments were carried out in solutions purged with high purity nitrogen gas for 5 min and blanketed with nitrogen atmosphere during measurements. A conventional three-electrode system consisting of glassy carbon electrode (GCE) was used as the working electrode (A = 0.071 $cm^2$). A platinum wire (3 mm diameter) from Metrohm SA and Ag/AgCl (3 M KCl) electrodes from BAS were used as auxiliary and reference electrodes respectively. All potentials were quoted with respect to Ag/AgCl and the experiments were carried out at room temperature (25 °C).

### 5.2.2 Electrode preparation and modification

GCE was fabricated with monometallic NPs (Ag and Pt), bimetallic NPs (Ag-Pt ratios 1:1, 1:3 and 3:1) and MWCNT/bimetallic Ag-Pt nanocomposites via drop casting method. The electrodes were left to dry at room temperature before use. Prior to each modification, the MWCNT was codeposited with the Ag-Pt NPs and GCE was polished repeatedly with 1, 0.3 and 0.05 µm alumina slurries. After each polishing, electrode cleaning adopted was as follows; successive 5 minutes rinsing with doubly distilled water, ultrasonication in ethanol and finally with another doubly distilled water to remove any adsorbed substances on the electrode surface. The reference electrode, Ag/AgCl (3 M NaCl) was rinsed thoroughly with distilled water and used. The counter electrode, platinum (Pt) wire was cleaned by burning in a gas flame.

### 5.2.3 Detection of Nevirapine

Stock solutions of nevirapine (NVP) were prepared in methanol to water 80:20 % v/v solution. All the stock solutions were kept in the refrigerator. The working solutions of NVP were freshly diluted from their stocks. 15.0 mL of NaOH solution was kept constant during measurements. The ratio of voltage versus current (slope of calibration curve) was used to measure NVP sensitivity while detection limit was measured from the (3 x standard deviation of blank) in the linear dynamic range of calibration plot.

## 5.3 Results and discussion

### 5.3.1 Electrochemical behaviour of Nevirapine at bare and modified GCEs

To investigate the electrochemical behaviour of NVP on different electrodes, both CV and differential pulse voltammetry (DPV) scans were run with the same experimental conditions of potential range and scan rate. Different voltammograms were obtained using various NPs/GC electrodes in 0.01 mol $L^{-1}$ NaOH solution containing known amounts of NVP as shown in Figure 5.1 and 5.2. The voltammograms showed an irreversible oxidation peak between 550 mV and 600 mV, corresponding to the oxidation of NVP.

In order to determine the electrochemical behaviour of NVP, cyclic voltammetry was carried out at various GCE surfaces (Figure 5.1). From this study, the potential range of electrooxidation was observed at around 550 to 600 mV in most detection platforms labelled as “NVP” which denoted the electrooxidation of NVP as shown in all Figure 5.1. This was within the range of reported work elsewhere (Zhang *et al.,* 2013). All other peaks observed were characteristic of the modified electrodes as discussed in chapter 4. From Figure 5.1, better signal resolution due to electrooxidation of NVP was observed in the MWCNT/bimetallic NPs/GCE platforms than in the corresponding MWCNT/monometallic NPs/GCE platforms. The CVs also showed the respective peaks of MWCNT/NPs modifiers, which were intact as observed in the voltammograms. Figure 5.1b on the other hand, the NPs/GCE platforms exhibited electrooxidation with similar unresolved peak signals. This peak behaviour was uniform in all of the platforms investigated and was mainly due to the film stability which reduced with time and affected the conductivity on the electrode surface during runs. However, by comparison MWCNT/Ag-Pt 3:1 NPs/GCE portrayed a better detection platform based on its well resolved signal coupled with minimum interference due to both the monometallic and bimetallic character signals.

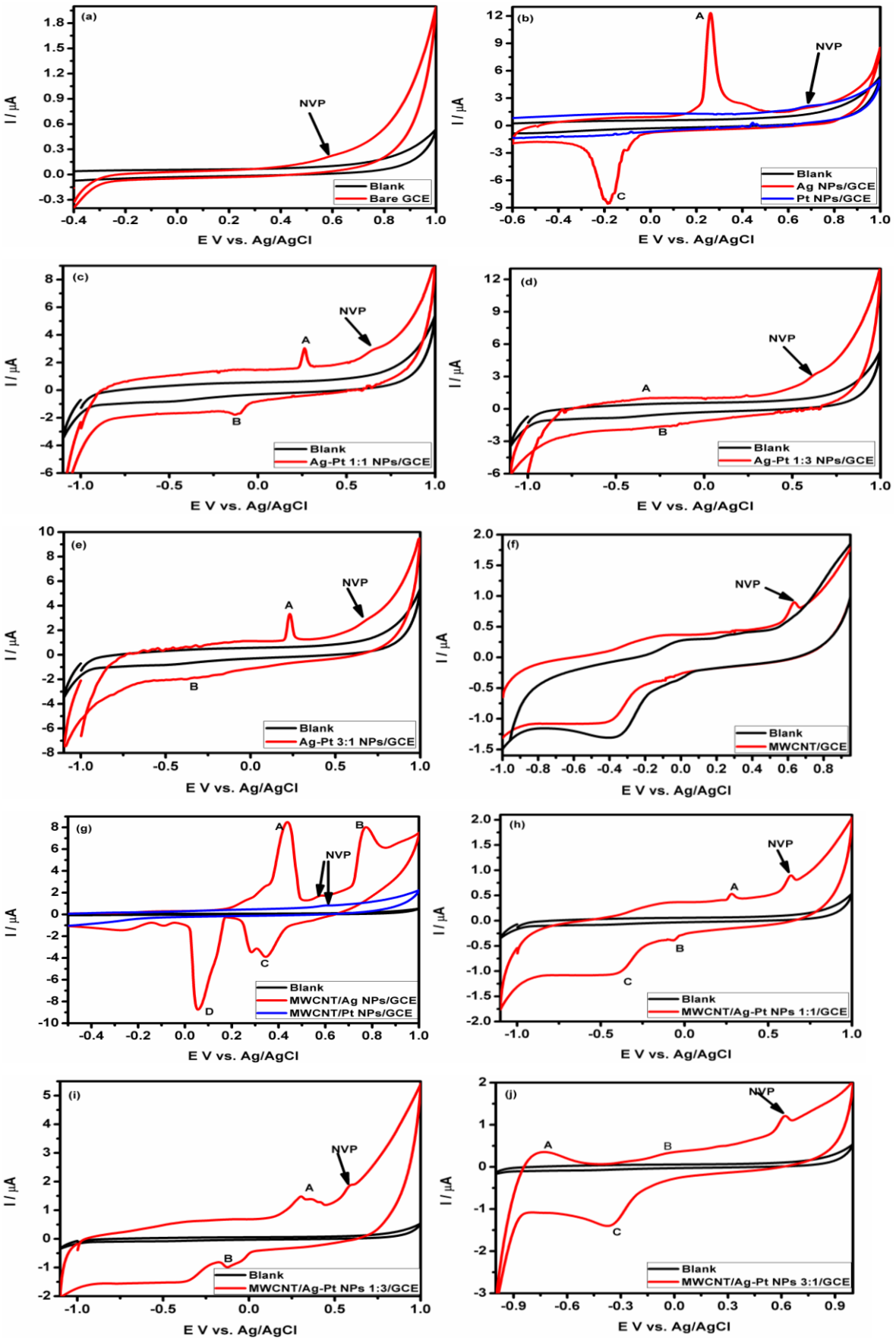


**Figure 5.1. Detection of 1.52 µM NVP at various GCE surfaces using CV at 20 mV $s^{-1}$.**

The intensity of the oxidation peak current of NVP on MWCNT/Ag-Pt NPs 3:1/GCE was equally higher than those determined with the other modified electrodes (Figure 5.1a-h). The analysis of Figure 5.5 shows that the oxidation peak potential of NVP on the GCE modified electrode shifted negatively to 550 mV (I, 24.5 µA) compared to 620 mV (I, 10.28 µA) obtained with bare glassy carbon electrode. This result indicates an effective electrooxidation of NVP on the MWCNT/Ag-Pt NPs 3:1/GC electrode. This is probably due to the large surface area of the electrode, which leads to an increased heterogeneous electron transfer and to a high electron transfer capacity as similarly discussed (Zhang *et al.,* 2013).

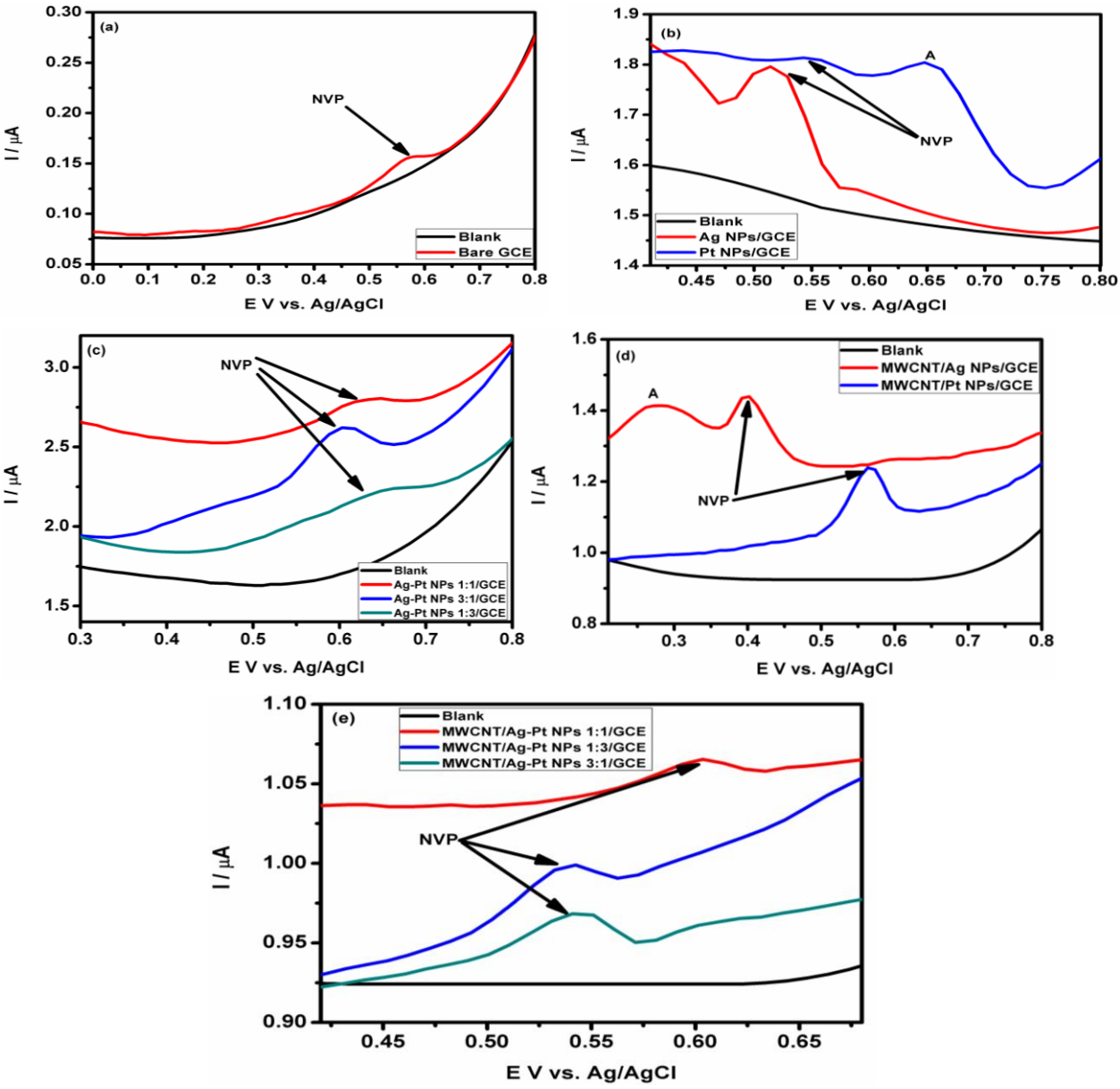


**Figure 5.2. DPV voltammograms for the detection of 1.52 µM NVP in 0.01 M NaOH at 20 mV $s^{-1}$ on GCEs.**

The largest current response was obtained at MWCNT/Ag-Pt NPs 3:1/GC electrode, while the lowest response was observed at GCE bare electrode (Figure 5.1a and b). Compared to the peak current response of bare GCE electrode (Figure 5.1a and b), there was a more than 50 % increase in the current response observed at MWCNT/Ag-Pt NPs 3:1/GC modified electrode using 0.01 M NaOH. The fact that all current responses were positive signifies all nanofilms irrespective of their nature i.e. monometallic and bimetallic or nanotubes brought about the improvement in detection. This suggests that the modifiers amplified the detection signal response with notable magnitudes. Although a higher peak current was observed in most Ag NPs modified GCE, the best electrode was chosen as MWCNT/Ag-Pt NPs 3:1/GCE due to the formation of well defined peak with stable peak signal throughout the run.

**Table 5.1. Detection of 1.52 µM NVP on various GCE surfaces using DPV at 20 mV $s^{-1}$.**

| Type of electrode | Peak potential ($E_p$ / V) | Peak current ($I_{pa}$ / µA) |
|---|---|---|
| GCE | 0.5672 | 0.1714 |
| GCE/Ag NPs | 0.5154 | 1.7944 |
| GCE/Pt NPs | 0.6486 | 1.8053 |
| GCE/Ag-Pt NPs 1:1 | 0.6335 | 2.8218 |
| GCE/Ag-Pt NPs 1:3 | 0.6543 | 2.2425 |
| GCE/Ag-Pt NPs 3:1 | 0.6047 | 2.6445 |
| GCE/MWCNT | 0.6333 | 8.8846 |
| GCE/MWCNT/Ag NPs | 0.6008 | 12.6056 |
| GCE/MWCNT/Pt NPs | 0.5666 | 12.5495 |
| GCE/MWCNT/Ag Pt NPs 1:1 | 0.6028 | 10.6508 |
| GCE/MWCNT/Ag Pt NPs 1:3 | 0.5416 | 9.9962 |
| GCE/MWCNT/Ag Pt NPs 3:1 | 0.5456 | 9.6951 |

Using both CV and DPV as shown in Figure 5.3 a and b, a study was done to determine the best technique for the detection of NVP and MWCNT/Ag-Pt 3:1 NPs/GCE was used in this study as the platform of choice. In Figure 5.3a the CV showed the characteristic peaks due to the Ag-Pt NPs 3:1 while the electrooxidation of NVP was observed at peak “NVP”. However, the peak signal due to NVP oxidation was not well resolved. From Figure 5.3b, DPV technique showed a better signal response for the electrooxidation of NVP due to well resolved, stable signals with relatively high currents (Table 5.1). From both Figures, the peaks due to the MWCNT/NPs modifiers were equally intact throughout the electrooxidation confirming minimum interference. The DPV technique was further used to optimize various

parameters in the detection of NVP at the MWCNT/Ag-Pt 3:1 NPs/GCE surface. From these results, it was clear and evident that the incorporation of the MWCNT onto BM Ag-Pt NPs 3:1 films facilitated electron transfer thereby improving the signal identity and response.

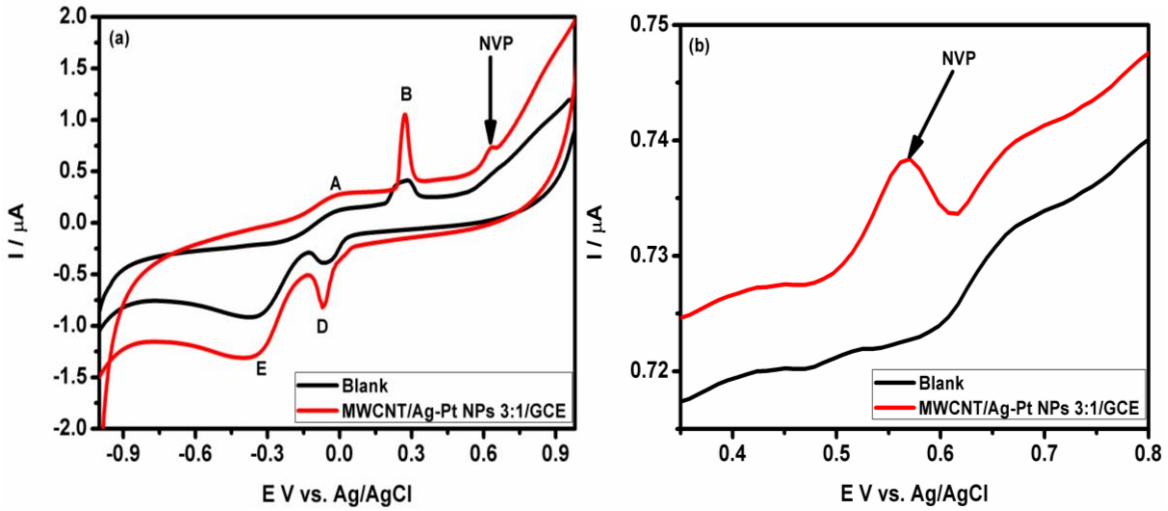


**Figure 5.3. Detection of 0.76 µM NVP on MWCNT/Ag-Pt 3:1 NPs/GCE using both CV and DPV at 20 mV $s^{-1}$.**

Scheme 5.1 shows the behaviour of NVP during electrooxidation. In the presence of hydroxide ions, the NVP was deprotonated to radical ions using 2-electron transfer. This electrochemical process occurred with same number of protons and electrons.

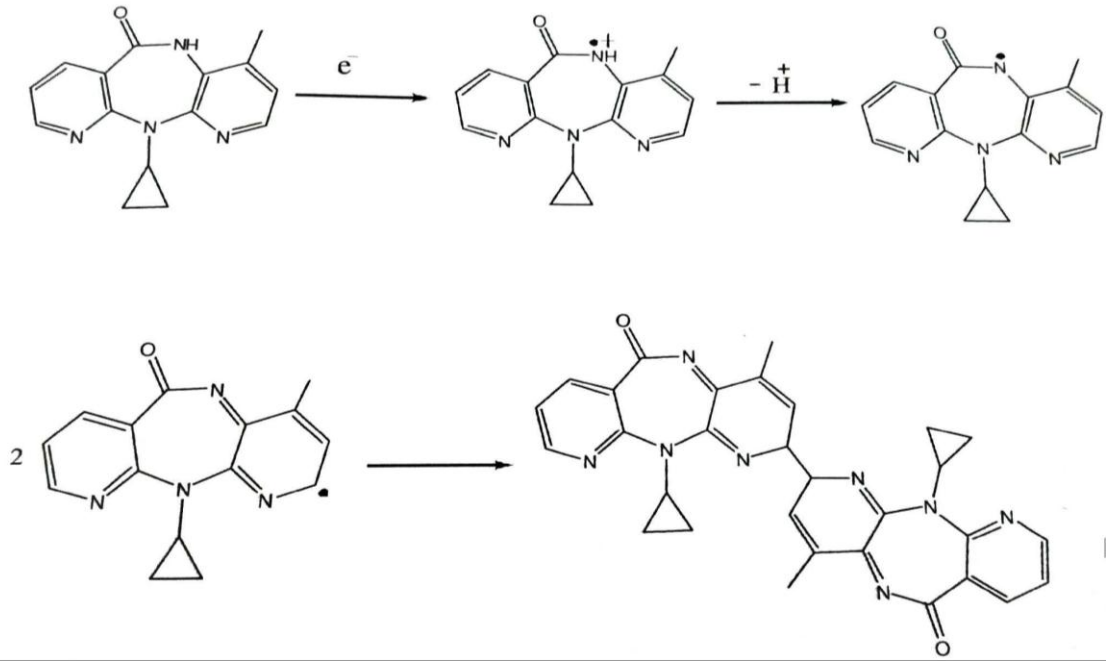

**Scheme 5.1. Electrooxidation of nevirapine.**

The probable electrochemical reaction process for nevirapine oxidation at MWCNT/Ag-Pt NPs 3:1/GCE was summarized in Scheme 5.1 as similarly proposed (Heli *et al.,* 2010; Antunes *et al.,* 2011; 2012; Zhang *et al.,* 2013).

### 5.3.2. Choice of supporting electrolyte concentration

The influence of supporting electrolyte on electrochemical behaviour of 1.52 µM NVP at MWCNT/Ag-Pt 3:1 NPs/GCE was investigated as shown in Figure 5.4. The electrochemical response of MWCNT/Ag-Pt 3:1 NPs/GCE to nevirapine was further studied by means of DPV in series of concentrations ranging from 0.001 to 0.1 M as supporting electrolytes.

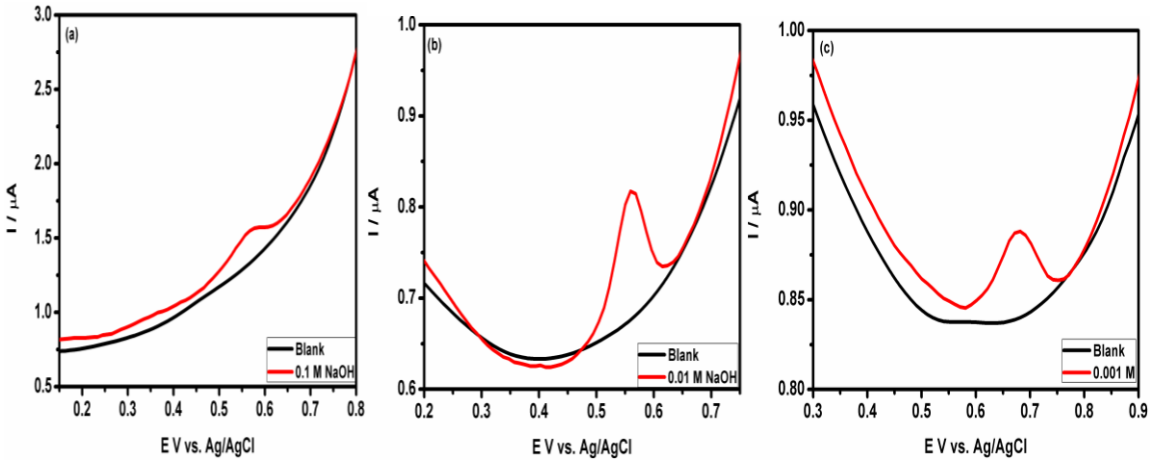


**Figure 5.4. DPV of 1.52 µM NVP in various NaOH concentrations at 20 mV $s^{-1}$ on MWCNT/Ag-Pt 3:1 NPs/GCE surface.**

Based on the ionic strength of each supporting electrolyte, 0.01 M NaOH was supportive for good conductivity as evident by a low background current. In addition, the oxidation peak signal was well resolved and stable (Figure 5.4b). Therefore, this concentration was chosen and used as supporting electrolyte in all further experiments.

### 5.3.3 Optimization parameters of detection

#### 5.3.2.1 Effect of pulse amplitude and starting potential

The impact of varying the pulse amplitude on the voltammetric current intensity was determined. This was studied over the range of 5-60 mV (Figure 5.5a) and it was concluded that in order to assure maximum peak current with well resolved signals, 25 mV pulse

amplitude was the ideal choice for this operational parameter. The variation of the initial potential (from -0.03 to 0.50 V) on the nevirapine detection is shown in Figure 5.5b. Several parameters including the peak potential ($E_p$), and peak current ($I_p$) were analyzed. When an initial potential of 0.20 V was used, a well-defined nevirapine peak ($E_p$) at -0.557 V ($I_p$ = 12.87 µA) with best background resolution was obtained. Although other initial potential ranges used showed significant peaks of nevirapine oxidation, they had poor resolution. From Figure 5.5b, beyond 0.20 V, we can conclude that the peak current of NVP decreases as we increase the initial potential towards more positive potentials (Figure 5.5b). The initial potential of 0.20 V versus Ag/AgCl was therefore selected and used for further experimental measurements.

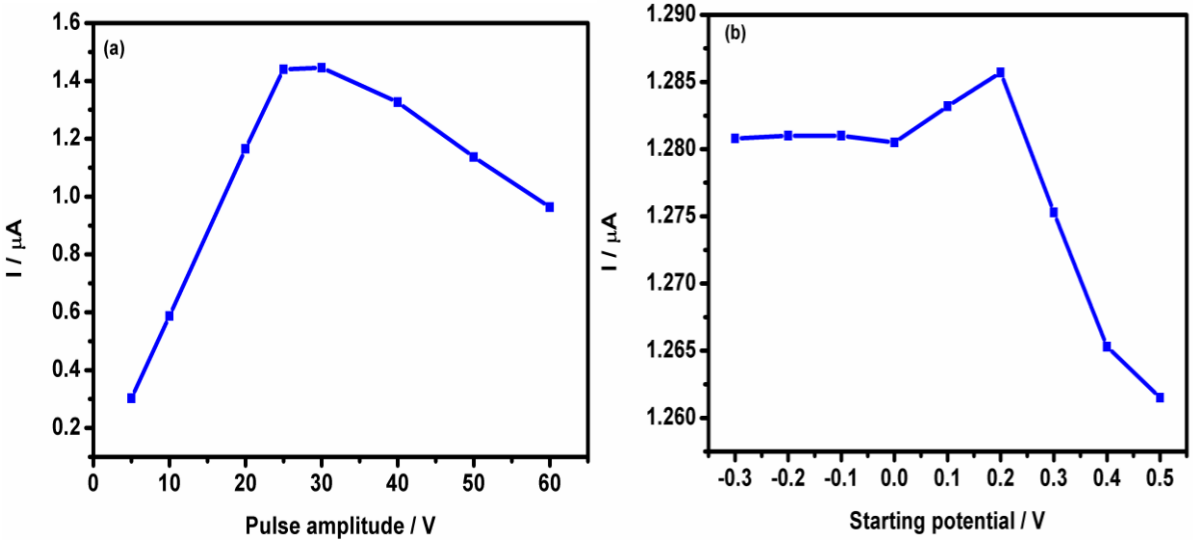


**Figure 5.5. (a) Optimization of pulse amplitude (b) Initial potential for 1.52 µM NVP on the MWCNT/Ag-Pt NPs 3:1/GCE at 20 mV $s^{-1}$.**

### 5.3.2.2 Effect of scan rate on electrooxidation of nevirapine

Cyclic voltammetry at different scan rates was used to elucidate the redox reaction mechanisms. The peaks shown at A, B and C are characteristics peaks of the bimetallic Ag-Pt 3:1 NPs as discussed in chapter 4. The peak at "NVP" corresponds to the electrooxidation of NVP. The variation of the scan rate was studied using 1.52 µM NVP in 0.01 M NaOH at MWCNT/Ag-Pt NPs 3:1/GCE, and the responses of the detector to the potential sweep rate were recorded at different sweep rates ranging from 5 to 100 mV $s^{-1}$ (Figure 5.6a).

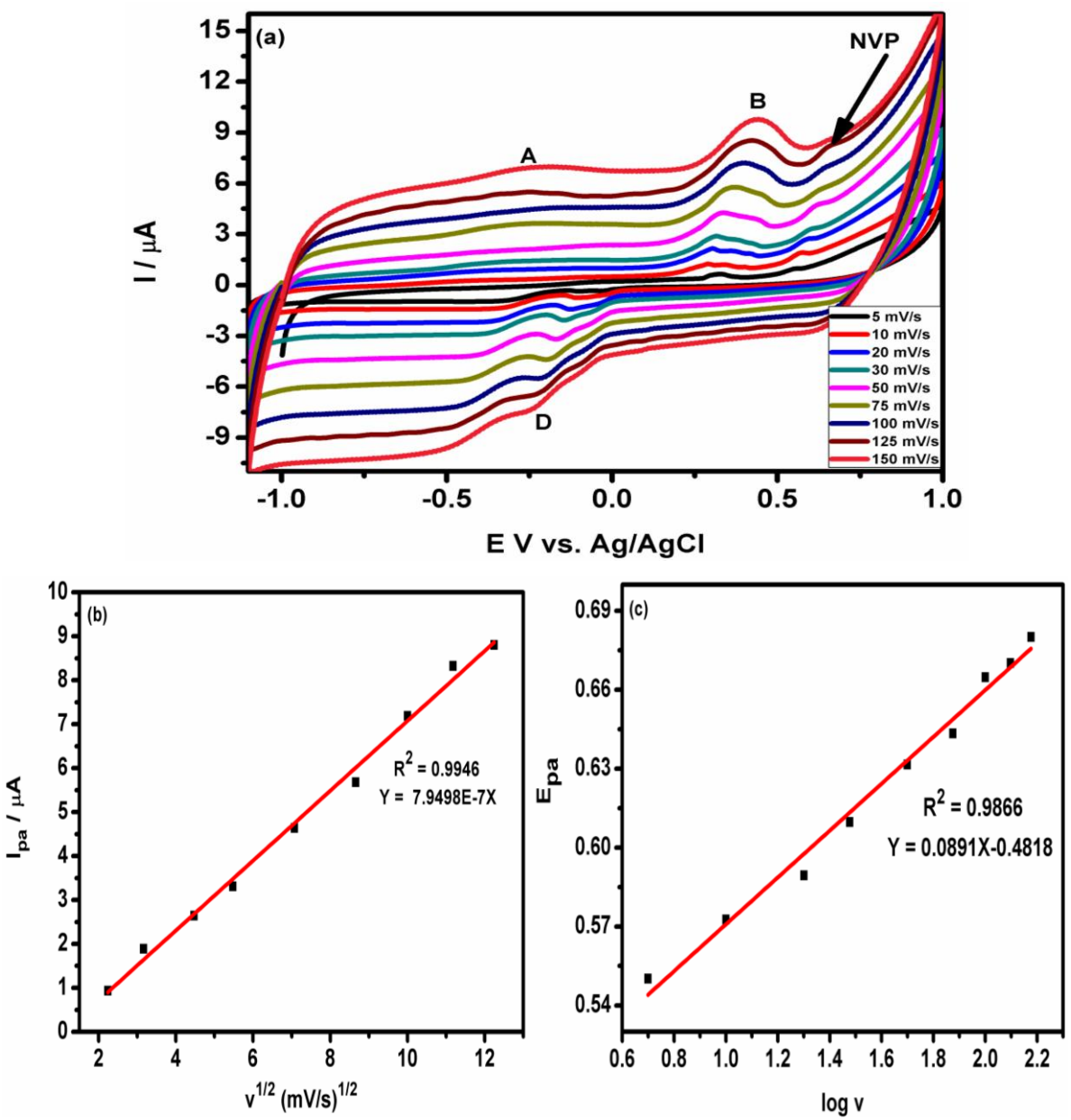


**Figure 5.6. (a) The influences of scan rates on the oxidation current. (b) Randles plot (c) Laviron plots for detection of 3.81 µM NVP on MWCNT/Ag-Pt 3:1 NPs/GCE in 0.01 M NaOH.**

The cyclic voltammetric results demonstrated that along with the increase of the scan rate, the oxidation peak currents of NVP increased gradually. The best scan rate for further experimental work was 20 mV $s^{-1}$, which was chosen based on best signal response. The peak current varied linearly with the square root of scan rate according to the linear regression equation: $I_{pa}$ (µA) = 7.95E-07$v^{1/2}$ and a correlation coefficient of 0.9946 (Figure 5.6b), indicating that the mass transfer and the electrochemical reaction of NVP is diffusion controlled as similarly noted (Teradal *et al.,* 2012; Shahrokhian *et al.,* 2015).

### 5.3.3 Determination of electron-transfer kinetic parameters

From the scan rates variation studies ranging from 5 to 150 mV $s^{-1}$, the relationship of the redox peak potentials with the scan rate was applied to calculate the electrochemical parameters using the Laviron's equation (1979) where for an irreversible electrode process, the oxidation peak potential ($E_{pa}$) is defined by the following equation,

$$E_{pa} = E^0 + \frac{2.303RT}{\alpha nF}\log(\frac{RTK_s}{\alpha nF}) + (\frac{2.303RT}{\alpha nF})\log v(mVs^{-1}) \quad \text{.....Equation 5.1}$$

Where α is the transfer coefficient, $k_s$ the standard heterogeneous rate constant of the reaction, n the number of electron transferred in the electrooxidation of NVP, v the scan rate, and $E^0$ is the formal redox potential, F is the Faraday constant, R as universal gas constant and T as absolute temperature. Thus the value of αn was calculated from the slope of $E_p$ versus log v. In this system, taking T = 298 K, R= 8.314 J $K^{-1}$ $mol^{-1}$, and F = 96480 C $mol^{-1}$.

Figure 5.6c reveals a positive shift in peak potential position ($E_{pa}$) with the log of scan rate (log v), further confirming that the electrooxidation process of NVP is irreversible. The linear regression equations of $E_{pa}$ versus log v could be expressed as $E_{pa}$ (mV) = 89.1log v (mV $s^{-1}$) + 481.4 with $R^2$ = 0.9866. The plot of $E_{pa}$ versus log v (Figure 5.6c) yields a straight line with a slope of 89.1. By using the following equation for irreversible electrochemical oxidation processes, according to the Laviron theory (Laviron, 1979), and considering number of electrons involved in the rate-determining step to be n = 2 based on the reaction mechanism proposed (Scheme 5.1), the charge transfer (α) was calculated to be 0.67. This indicates a better electrocatalytic mechanism for oxidation of NVP, and the electrode surface is fine and homogeneous. The value of αn was calculated to be 1.3.

Based on these results and as similarly reported (Antunes *et al.,* 2012; Zhang *et al.,* 2013; Shahrokhian *et al.,* 2015), two-electrons and two-protons are involved in the electrooxidation of NVP on the surface of the modified electrode. This was equally proposed in the reaction mechanism shown in Scheme 5.1. Further, based on Equation (5.1), the value of apparent heterogeneous rate constant $k_s$ was found to be 0.8835 $s^{-1}$. The positive value of $k_s$ indicates that the MWCNT/Ag-Pt NPs 3:1 showed good reversibility of the electron transfer process as similarly discussed (Wan *et al.,* 2011). The diffusion coefficient in this study was slightly below reported values for past similar studies done on other anti-HIV drugs like Zidovudine (Barone *et al.,* 2003) which was studied on a bare electrode surface.

**Table 5.2. Electrochemical parameters obtained from Laviron and Randles-Sevcik's plots for 3.81 µM NVP**

| Parameter | MWCNTs/Ag-Pt NPs 3:1/GCE |
|---|---|
| α | 0.31 |
| D ($10^{-10}$ $cm^2$ $s^{-1}$) | 5.2048 |
| $E^0$ | 0.560 |
| $K_s$ ($s^{-1}$) | 0.8835 |
| Charge transfer (α) | 0.67 |
| Randles plot ($R^2$) | 0.9946 |
| Laviron plot ($R^2$) | 0.9866 |

### 5.3.4 Calibration studies of NVP

Nevirapine standard was diluted to make various concentrations (0.76-4.57 µM) in 0.01 M NaOH solution and used as a target analyte. Differential pulse voltammetry measurements were carried out at room temperature in the potential range of 300 and 800 mV. The voltammograms representing the oxidation current versus concentration of NVP obtained using MWCNT/Ag-Pt NPs 3:1/GCE in 0.01 mol $L^{-1}$ NaOH is shown in Figure 5.7. The addition of NVP to the supporting electrolyte solution showed an increase in the anodic peak current. A linear relationship of $I_{pa}$ versus NVP concentration was established between of the oxidation peak current and NVP concentration in the range of 0.76 µM to 4.57 µM. The equation of the calibration curve was determined as $I_{pa}$ (µA) = 0.728C ($R^2$ = 0.9980). From these measurements, the best response with high sensitivity and good linearity was obtained.

Under the optimum conditions for NVP concentration range, the limit of detection (LOD) and limit of quantification (LOQ) values were calculated using the equation of LOD = 3 s / m, LOQ = 10 s / m, where s is the standard deviation of the blank signals (ten runs) and m is the slope of the calibration plot. According to results from this study, the modified MWCNT/Ag-Pt NPs 3:1/GC electrode gave a lower LOD and LOQ as shown in Table 5.3. These values are low compared to those previously reported in the literature (Table 5.4).

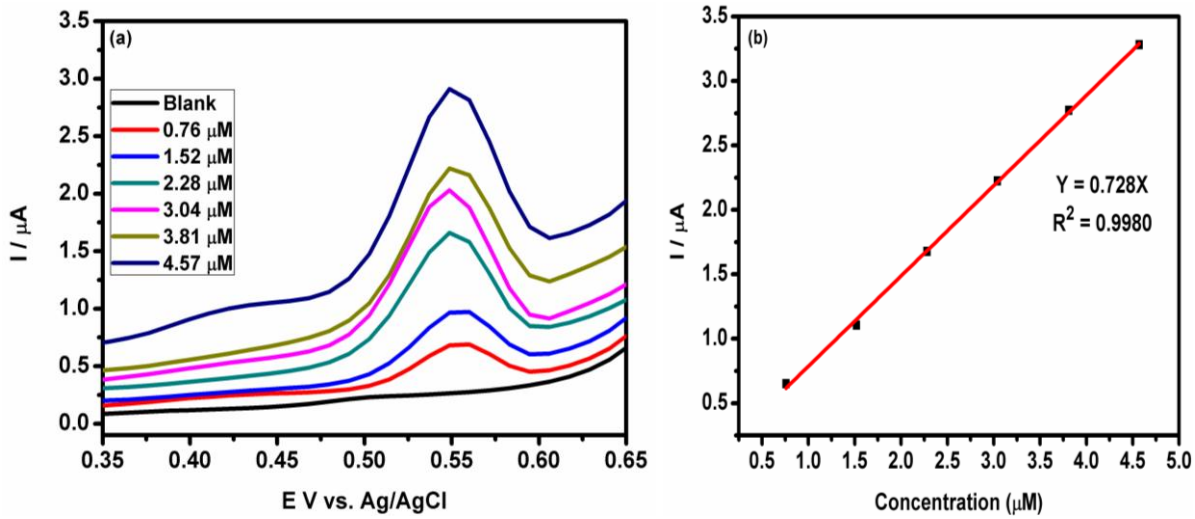


**Figure 5.7. (a) Variation of NVP concentrations (b) Calibration plots of NVP on MWCNT/Ag-Pt NPs 3:1/GCE in 0.01 M NaOH at 20 mV $s^{-1}$.**

**Table 5.3. Characteristics of NVP calibration plot using DPV at MWCNT/Ag-Pt NPs 3:1/GC electrode**

| Parameters | Nevirapine oxidation |
|---|---|
| Regression coefficient (n=5) | 0.9980 |
| Limit of detection (LOD) (mol $L^{-1}$) | 2.09 x $10^{-8}$ |
| Limit of quantification (LOQ) (mol $L^{-1}$) | 6.98 x $10^{-8}$ |
| Linear range (mol $L^{-1}$) | 7.6 × $10^{-7}$ - 4.6 × $10^{-6}$ |
| Sensitivity (μA $\mu M^{-1}$ $cm^{-2}$) | 10.25 |
| Peak potential (mV) vs. Ag/AgCl at 20 mV $s^{-1}$ | 555 ± 11 |

The low values of LOD and LOQ obtained confirmed the sensitivity of the proposed method and that the electrode exhibited good catalytic activity for the oxidation of NVP. In the literature, few electrochemical studies have been carried out on NVP using DPV technique as reported in this work. By considering the electrochemical oxidation of NVP at MWCNT/Ag-Pt NPs 3:1/GCE, an analytical method was developed using DPV for the first time.

**Table 5.4. Comparison of major characteristics of various methods for the determination of nevirapine**

| Electrochemical methods | | | | | |
|---|---|---|---|---|---|
| Method | Sensor | Electrolyte | Linear range (μM) | LOD (μM) | References |
| DPV | GCE/MWCNT/Ag-Pt NPs 3:1 | 0.01 M NaOH | 0.76-4.57 | 0.021 | This work |
| DPV | Au Electrode | 0.04 M BR buffer | 1.1-3.8 | - | Esteva *et al.,* 2014 |
| DPV | Ura/CPE | 0.1 M NaOH | 0.1-70.0 | 0.05 | Zhang *et al.,* 2013 |
| DPV | Bare GCE | PBS pH 10 | 5.0-350 | 1.026 | Teradal *et al.,* 2012 |
| AdSV | Hg film electrode | 2 mM NaOH | 0.04-0.5 | 0.003 | Castro *et al.,* 2011 |

| Non-electrochemical methods | | | |
|---|---|---|---|
| Method | Linear range (μM) | LOD (μM) | References |
| HPLC | 0.2-39.0 | 0.2 | Van Heeswijk *et al.,* 1998 |
| MALDI/TOF MS | 0.04-3.8 | 0.04 | Notari *et al.,* 2008 |
| LC-MS | 3.7-37.6 | 3.7 | Chi *et al.,* 2003 |
| MEKC | 9.3-930 | 6.0 | Sekar and Azhaguvel, 2008 |

Table 5.4 compares the electrochemical performance of the developed modified electrode in the present work with previously reported work for the determination of NVP. By comparison, the developed sensor in this study gave a lower LOD relative to the previous studies. This was lower than Teradal *et al.,* (2012), Zhang *et al.,* (2013) and Esteva *et al.,* (2014), but higher than that reported by Castro *et al.,* (2011).

### 5.3.5 Reproducibility and stability studies

The reproducibility of the MWCNT/Ag-Pt NPs 3:1/GC electrode response was determined by carrying out the electrode modification using the same fabrication procedure for the determination of 3.81 μM NVP solutions under DPV technique. The relative standard deviation (RSD) value of the modified electrode response to 3.81 μM nevirapine for six successive measurements on the same electrode was 4.3 %. The precision of the proposed method was obtained by measuring the peak currents of four replicate measurements in 3.81 μM NVP solutions using the same modified electrode. The resulting RSD value of 2.52 % indicated an acceptable precision for the proposed voltammetric method. Furthermore, the current response of MWCNT/Ag-Pt NPs 3:1/GCE to 3.81 μM nevirapine was run three times

with a RSD of 3.3 %, indicating good repeatability. The stability of MWCNT/Ag-Pt NPs 3:1/GCE was tested in the nevirapine solution intermittently. The oxidation current response to nevirapine was maintained at 86 % even after the electrode was stored dry at room temperature for 5 days.

### 5.3.6 Interference studies

Under optimized conditions, the influence of different interferants in the detection of nevirapine was investigated within the voltammetric response of 0.76 µM nevirapine in 0.01 M NaOH. The results showed that the current response of nevirapine was unaffected even in the presence of 5-fold concentration of sodium chloride (NaCl), calcium chloride ($CaCl_2$) and ascorbic acid (AA). In this study, the interferants were chosen based on their point sources such as food supplements ($CaCl_2$), liquid drips (NaCl) and vitamin supplements (AA), which are commonly within reach of HIV patients.

**Table 5.5. Effect of possible interfering compounds on NVP detection, percent interferants is in brackets**

| Interfering Compound | Mole ratio of Nevirapine: Interferant | | | |
|---|---|---|---|---|
| | NVP Alone | 1:1 | 1:5 | 5:1 |
| NaCl | 0.650 | 0.681(4.78) | 0.721(10.92) | 0.98(3.16) |
| $CaCl_2$ | 0.727 | 0.790(8.67) | 0.919(26.41) | 1.01(6.83) |
| Ascorbic acid (AA) | 0.731 | 0.828(13.27) | 0.923(26.13) | 1.07(9.60) |

Figure 5.8 shows the peak potential for the oxidation of NVP in the presence of NaCl, $CaCl_2$ and AA. From this observation (Figure 5.8), there is significantly little effect on the current response of NVP even in the presence of 10-fold excess of the interferants (Table 5.5). This revealed the practical applicability of the proposed electrode for the determination of NVP in the presence of several other compounds that may be present in clinical samples.

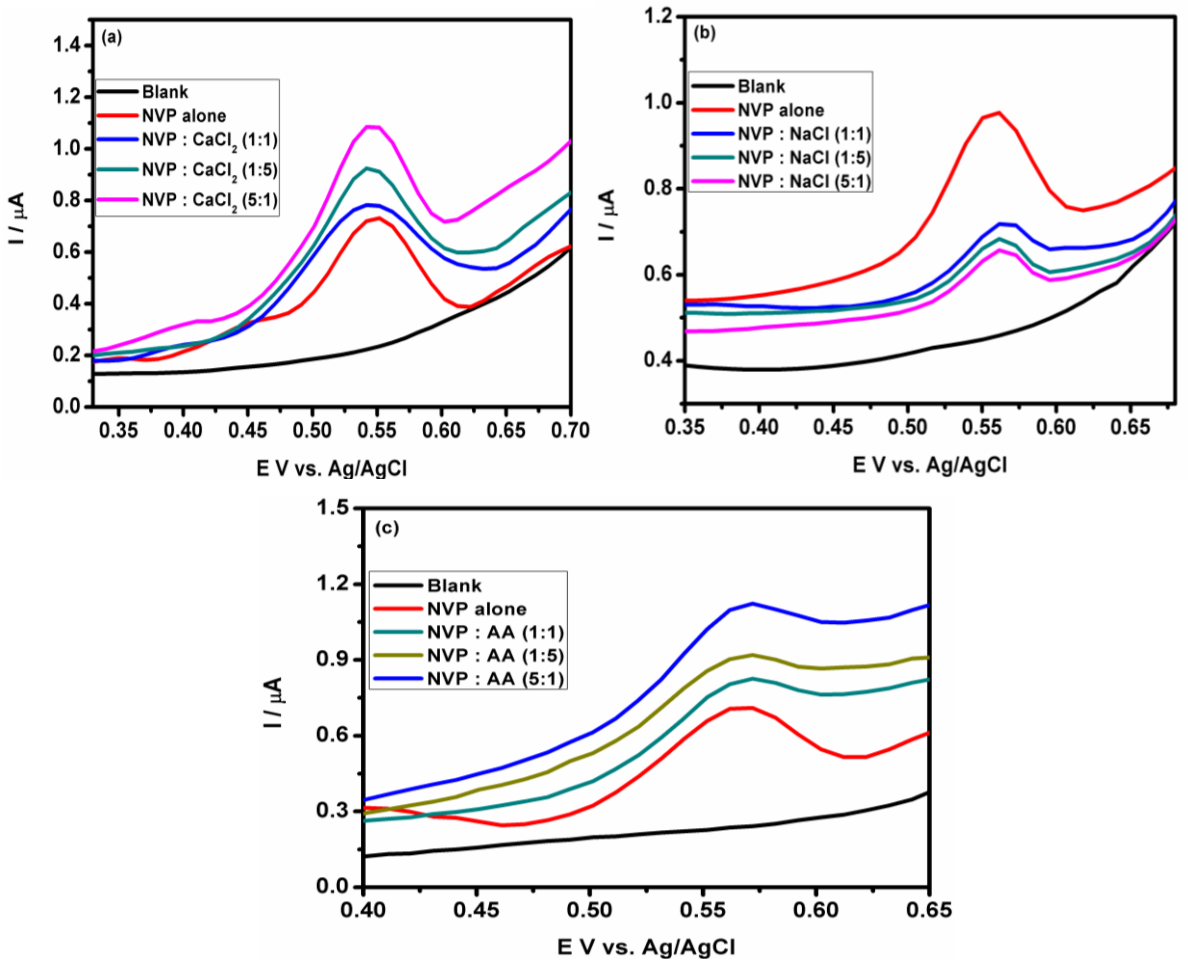


**Figure 5.8. Interference plots of AA, $CaCl_2$ and NaCl with 0.76 µM NVP at various interferants : NVP ratios.**

### 5.3.7 Real sample analysis

#### 5.3.7.1 Determination of NVP in milk and urine samples

In order to evaluate the accuracy of the developed procedure, the prepared MWCNT/Ag-Pt NPs 3:1/GCE was used for recovery tests in milk and human urine samples. Samples were spiked with different amounts of standard NVP solutions in the range of 0.76-1.52 µM. The proposed method was applied to the assay of NVP in spiked milk sample from a local shop. For this experiment, drug free milk samples were spiked with 0.76, 1.14 and 1.52 µM of NVP and differential pulse voltammograms were then recorded. The amount of NVP in the milk sample was calculated from the calibration plot. Similar experiments were conducted for drug free urine from a volunteer and the results of the analysis are summarized in Table 5.6. The percent recovery of NVP was determined by comparing the peak currents of the drug in urine and milk samples with those of pure NVP using the calibration curve. It can be observed that

the recovery range for nevirapine was between 90 % and 113 %. This shows that the proposed method is readily acceptable for analytical applications.

**Table 5.6. Results of analysis of NVP in spiked milk and human urine samples (n = 3)**

| | NVP µM | Recovery, µM | % Recovery | % RSD |
|---|---|---|---|---|
| milk samples | 0.76 | 0.86 | 112.97±0.4 | 3.89 |
| | 1.14 | 1.05 | 92.04±0.9 | 1.08 |
| | 1.52 | 1.37 | 90.23±0.8 | 1.16 |
| urine samples | | | | |
| | 0.76 | 0.82 | 108.89±2.3 | 1.95 |
| | 1.14 | 1.15 | 99.87±1.9 | 1.87 |
| | 1.52 | 1.45 | 96.05±2.9 | 3.04 |

### 5.3.7.2 Analysis of NVP in pharmaceutical tablets

The practical analytical application of the DPV method was further established by determining NVP concentrations in tablets. The NVP tablet was crushed and soaked in methanol for 24 hours. The suspension was filtered, the resulting solution was transferred to a 100 mL volumetric flask and the volume was completed with methanol. It contained 3.57 mg $mL^{-1}$ of NVP and the working solutions were prepared from this solution. Voltammograms of sample solutions were recorded as shown in Figure 5.9. The results obtained by means of the standard addition method showed that the content of NVP tablet was well estimated in the presence of nevirapine. Three standard additions were used of 2.5, 10 and 15 µL on 0.76 µM NVP equivalent to 1.14, 2.28 and 3.04 µM respectively.

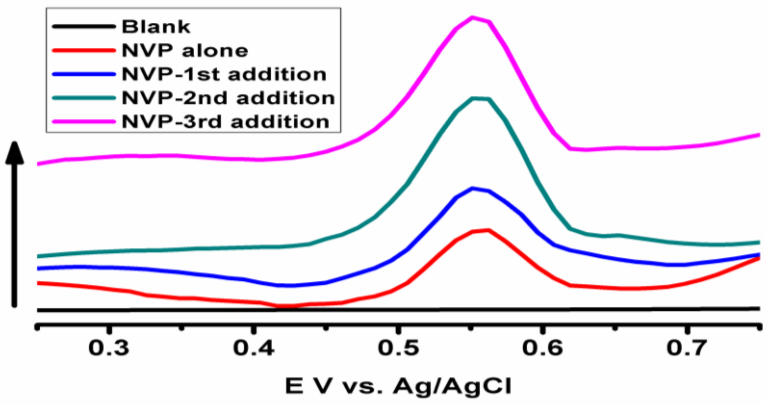


**Figure 5.9. DPV plots showing the standard additions of NVP tablet at 20 mV $s^{-1}$.**

**Table 5.7. Determination of NVP in pharmaceutical tablet (Aspen Nevirapine, 200 mg)**

| | Standard additions of NVP tablet to NVP | | |
|---|---|---|---|
| | NVP: 5 | NVP: 10 | NVP: 15 |
| Concentration (µM) | 1.26 | 2.12 | 2.80 |
| % Recovery | 109.2±2.7 | 92.8±1.1 | 93.1±0.9 |
| % RSD | 4.07 | 1.43 | 1.38 |

The low RSD values highlighted the reproducibility of the results (Table 5.7). Recovery studies were carried out using a standard addition method. Known quantities of pure NVP were mixed with defined amounts of pre-analyzed formulations; then the mixtures were analyzed as before. The total amount of the drug was then determined, and the amount of drug added was calculated by the difference. The high percentage of recovery indicates that the commonly encountered excipients in the formulation did not interfere with the proposed method.

## 5.4 Conclusion

A sensitive sensor based on MWCNT/Ag-Pt NPs 3:1/GCE for the determination of nevirapine was developed. The sensor improved on the electron transfer, enhanced the oxidation peak current of nevirapine, and decreased the oxidation overpotential relative to other detection platforms in this study, indicating efficient catalytic activity in the detection of nevirapine. Under the optimum conditions of 0.01 M NaOH and 20 mV $s^{-1}$, the MWCNT/Ag-Pt NPs 3:1/GC electrode exhibited a variety of good electrochemical characteristics including low detection limit, high sensitivity, and favourable reproducibility besides simple modification. The present strategy provided a novel insight into the sensitive determination of nevirapine using only a modified electrode. These results indicate that the proposed sensor based on MWCNT/Ag-Pt NPs 3:1/GC electrode has a wide potential for analytical application mainly in pharmaceutical drug monitoring.

## 5.5 References

Amiri, M., Shahrokhian, S., Marken, F. 2007. Ultrathin carbon nanoparticle composite film electrodes: distinguishing dopamine and ascorbate. *Electroanalysis,* 19: 1032-1038.

Antunes, A.M.M., Novais, D.A., Ferreira da Silva, J.L., Santos, P.P., Oliveira, M.C., Beland, F.A., Marques, M.M. 2011. Synthesis and oxidation of 2-hydroxynevirapine, a metabolite of the HIV reverse transcriptase inhibitor nevirapine. *Org. Biomol. Chem.,* 9: 7822-7835.

Antunes, A.M.M., Sidarus, M., Novais, D.A., Harjivan, S.G., Santos, P.P., Ferreira da Silva, J.L., Beland, F.A., Marques, M.M. 2012. Oxidation of 2-Hydroxynevirapine, a phenolic metabolite of the anti-HIV drug nevirapine: evidence for an unusual pyridine ring contraction. *Molecules*, 17: 2616-2627.

Barone, G.C., Halsall, H.B., and Heineman, W.R. 1991. Electrochemistry of azidothymidine, *Analytica Chimica Acta*, 248(2): 399-407, 1991.

Bielinska, A., Eichman, J., Lee, I., Baker, J. and Balogh, L. 2002. Imaging {Au0-PAMAM} gold-dendrimer nanocomposites in cells. *J. Nanopart. Res.*, 4(5): 395-403.

Binks, B.P., Cui, Z.G., Fletcher, P.D.I. 2006. Optical microscope absorbance imaging of carbon black nanoparticle films at solid and liquid surfaces. *Langmuir*, 22(4): 1664-1670.

Breuer, O. and Sundararaj, U. 2004. Big returns from small fibers: a review of polymer/carbon nanotube composites. *Polym. Composites*, 25(6): 630-645.

Castro, A.A., Aucelio, R.Q., Rey, N.A., Miguel, E.M., Farias, P.A.M. 2011. Determination of the antiretroviral drug nevirapine in diluted alkaline electrolyte by adsorptive stripping voltammetry at the mercury film electrode. *Comb. Chem. High Throughput Screen.,* 14: 22-27.

Chen, W., Lu, Z. and Li, C.M. 2008. Sensitive human interleukin 5 impedimetric sensor based on polypyrrole-pyrrolepropylic acid-gold nanocomposite. *Anal. Chem.*, 80(22): 8485-8492.

Chi, J., Jayewardene, A.L., Stone, J.A., Aweeka, F.T. 2003. An LC-MS-MS method for the determination of nevirapine, a non-nucleoside reverse transcriptase inhibitor, in human plasma. *J. Pharm. Biomed. Anal.,* 31: 953-959.

Choi, H.C., Shim, M., Bangsaruntip, S. and Dai, H. 2002. Spontaneous reduction of metal ions on the sidewalls of carbon nanotubes. *J. Am. Chem. Soc.*, 124(31): 9058-9059.

Datta, K.K.R., Eswaramoorthy, M. and Rao, C.N.R. 2007. Water-solubilized aminoclay-metal nanoparticle composites and their novel properties. *J. Mater. Chem*., 17(7): 613-615.

De Oliveira M.P.R., Lermo, A., Campoy, S., Yamanaka, H., Barbé, J., Alegret, S. and Pividori, M.I. 2009. Double-tagging polymerase chain reaction with a thiolated primer and

electrochemical genosensing based on gold nanocomposite sensor for food safety. *Anal. Chem.*, 81(4): 1332-1339.

Dogan-Topal, B., Sibel, S.A., Uslu, B. 2010. The analytical applications of square wave voltammetry on pharmaceutical analysis. *The Open Chemical and Biomedical Methods Journal,* 3: 56-73.

Esteva Guas, A.M., Balbin Tamayo, A.I., Piña Leite-vidal, J.J. 2014. Determination of nevirapine in the presence of cucurbit (7) uril with a gold electrode. *J. Electrochem. Sci. Eng.,* 4(1): 37-44.

Ghalkhani, M., Shahrokhian, S., Ghorbani-Bidkorbeh, F. 2009. Voltammetric studies of sumatriptan on the surface of pyrolyticgraphite electrode modified with multi-walled carbon nanotubes decorated with silver nanoparticles. *Talanta*, 80: 31-38.

Guo, D.J. and Li, H.L. 2004. High dispersion and electrocatalytic properties of Pt nanoparticles on SWCNT bundles. *J. Electroanal. Chem.,* 573: 197-202.

He, Z., Chen, J., Liu, D., Zhou, H. and Kuang, Y. 2004. Electrodeposition of Pt-Ru nanoparticles on carbon nanotubes and their electrocatalytic properties for methanol electrooxidation. *Diamond Relat. Mater.,* 13: 1764-1770.

Heli, H., Zarghan, M., Jabbari, A., Parsaei, A., Moosavi-Movahedi, A.A. 2010. Electrooxidation of dextromethorphan on a carbon nanotube-carbon microparticle-ionic liquid composite: applied to determination in pharmaceutical forms. *J. Solid State Electrochem*., 14: 787-795.

Ho, J.A., Lin, Y.C., Wang, L.S., Hwang, K.C., Chou, P.T. 2009. Carbon nanoparticle-enhanced immunoelectrochemical detection for protein tumor marker with cadmium sulfide biotracers. *Anal. Chem.*, 81(4): 1340-1346.

Hrapovic, S., Majid, E., Liu, Y., Male, K. and Luong, J.H.T. 2006. Metallic nanoparticle-carbon nanotube composites for electrochemical determination of explosive nitroaromatic compounds. *Anal. Chem.,* 78: 5504-5512.

Huang, Y., Miao, Y.E., Ji, S., Tjiu, W.W., Liu, T. 2014. Electrospun carbon nanofibers decorated with Ag-Pt bimetallic nanoparticles for selective detection of dopamine. *ACS Appl. Mater. Interfaces,* 6**:** 12449-12456.

Ispasoiu, R.G., Balogh, L., Varnavski, O.P. and Tomalia, D.A. 2000. Large optical limiting from novel metal-dendrimer nanocomposite materials. *J. Am. Chem. Soc.*, 122(44): 11005-11006.

Jacobs, C.B., Peairs, M.J., Venton, B.J. 2010. Carbon nanotube based electrochemical sensors for biomolecules. *Anal. Chim. Acta*, 662: 105-127.

Kim, B. and Sigmund, W. 2004. Functionalized multiwall carbon nanotube/gold nanoparticle composites. *Langmuir*, 20(19): 8239-8242.

Laviron, E. 1979. General expression of the linear potential sweep voltammogram in the case of diffusionless electrochemical systems. *J. Electroanal. Chem.,* 101: 19-28.

Lee, J., Yang, J., Ko, H., Oh, S., Kang, J., Son, J., Lee, K., Lee, S., Yoon, H., Suh, J., Huh, Y. and Haam, S. 2008. Multifunctional magnetic gold nanocomposites: human epithelial cancer detection via magnetic resonance imaging and localized synchronous therapy. *Adv. Funct. Mater.*, 18(2): 258-264.

Li, J., Lin, X. 2007. Electrocatalytic reduction of nitrite at polypyrrole nanowires-platinum nanocluster modified glassy carbon electrode. *Microchem. J.,* 87: 41-46.

Li, W., Kuai, L., Qin, Q., Geng, B. 2013. Ag-Au bimetallic nanostructures: co-reduction synthesis and their component-dependent performance for enzyme-free $H_2O_2$ sensing. *J. Mater. Chem. A*, 1: 7111-7117.

Liu, S., Zhang, C., Yuan, L., Bao, J., Tu, W., Han, M., Dai, Z. 2013. Component-controlled synthesis of small-sized Pd-Ag bimetallic alloy nanocrystals and their application in a non-enzymatic glucose biosensor. *Part. Part. Syst. Charact.,* 30(6): 549-556.

Mishra, Y.K., Mohapatra, S., Avasthi, D.K., Kabiraj, D., Lalla, N.P., Pivin, J.C., Sharma, H., Kar, R. and Singh, N. 2007. Gold-silica nanocomposites for the detection of human ovarian cancer cells: a preliminary study. *Nanotechnology*, 18(34): 345606.

Mohan, S., Okumu, F., Oluwafemi, O., Matoetoe, M. and Arotiba, O. 2016. Electrochemical behaviour of silver nanoparticle-MWCNTs hybrid nanostructures synthesized via a simple method. *Int. J. Electrochem. Sci.,* 11: 745-753.

Notari, S., Mancone, C., Alonzi, T., Tripodi, M., Narciso, P., Ascenzi, P. 2008. Determination of abacavir, amprenavir, didanosine, efavirenz, nevirapine, and stavudine concentration in human plasma by MALDI-TOF/TOF. *J. Chromatogr. B*, 863: 249-257.

Qu, S.L., Song, Y.L., Du, C.M., Wang, Y.X., Gao, Y.C., Liu, S.T., Li, Y.L. and Zhu, D.B. 2001. Nonlinear optical properties in three novel nanocomposites with gold nanoparticles. *Opt. Commun.*, 196(1-6): 317-323.

Raghuveer, M.S., Agrawal, S., Bishop, N. and Ramanath, G. 2006. Microwave-assisted single-step functionalization and *in situ* derivatization of carbon nanotubes with gold nanoparticles. *Chem. Mater.*, 18(6): 1390-1393.

Satishkumar, B.C., Vogl, E.M., Govindaraj, A. and Rao, C.N.R. 1996. Rapid communication: The decoration of carbon nanotubes by metal nanoparticles. *J. Phys. D Appl. Phys.*, 29: 3173-3176.

Sekar, R., Azhaguvel, S. 2008. MEKC determination of antiretroviral reverse transcriptase inhibitors lamivudine, stavudine, and nevirapine in pharmaceutical formulations. C*hromatographia*, 67: 389-398.

Shahmiri, M.R., Bahari, A., Karimi, H.M., Hosseinzadeh, R., Mirnia, N. 2013. Ethynylferrocene-NiO/MWCNT nanocomposite modified carbon paste electrode as a novel voltammetric sensor for simultaneous determination of glutathione and acetaminophen. *Sens. Actuators B*, 177: 70-77.

Shahrokhian, S., Kohansal, R., Ghalkhani, M. and Amini, M.K. 2015. Electrodeposition of copper oxide nanoparticles on precasted carbon nanoparticles film for electrochemical investigation of anti-hiv drug nevirapine. *Electroanalysis*, 27: 1989-1997.

Shahrokian, S., Ghalkhani, M., Adeli M., Amini, M.K. 2009. Multiwalled carbon nanotubes with immobilised cobalt nanoparticle for modification of glassy carbon electrode: application to sensitive voltammetric determination of thioridazine. *Biosens. Bioelectron.,* 24: 3235-3241.

Shimada, T., Ookubo, K., Komuro, N., Shimizu, T. and Uehara, N. 2007. Blue-to-red chromatic sensor composed of gold nanoparticles conjugated with thermoresponsive copolymer for Thiol sensing. *Langmuir*, 23(22): 11225-11232.

Sreeja, V., Sasikumar, R., Alagarsamy, M., Manisankar, P. 2011. Multiwall carbon nanotube modified electrochemical sensor for reactive black 5. *Am. J. Anal. Chem.,* 2: 814-819.

Teradal, N.L., Prashanth, S.N., Seetharamappa, J. 2012. Electrochemical studies of nevirapine, an anti-HIV drug, and its assay in tablets and biological samples. *J. Electrochem. Sci. Eng.,* 2: 67-75.

Van Heeswijk, R.P.G., Hoetelmans, R.M.W., Meenhorst, P.L., Mulder, J.W., Beijnen, J.H. 1998. Rapid determination of nevirapine in human plasma by ion-pair reversed phase high-performance liquid chromatography with ultraviolet detection. *J. Chromatogr.* B, 713: 395-399.

Wan, L., Song, Y., Zhu, H., Wang, Y., Wang, L. 2011. Electron transfer of Co-immobilized cytochrome c and horseradish peroxidise in chitosan0graphene oxide modified electrode. *Int. J. Electrochem. Sci.,* 6: 4700-4713.

Wildgoose, G.G., Banks, C.E. and Compton, R.G. 2006. Metal nanoparticles and related materials supported on carbon nanotubes: methods and applications. *Small,* 2(2): 182-193.

Yan, J., Liu, S., Zhang, Z., He, G., Zhou, P., Liang, H., Tian, L., Zhou, X., Jiang, H. 2013. Simultaneous electrochemical detection of ascorbic acid, dopamine and uric acid based on graphene anchored with Pd-Pt nanoparticles. *Colloids Surf. B,* 111: 392-397.

Zhang, F., Li, L., Luo, L., Ding, Y. Liu, X. 2013. Electrochemical oxidation and determination of antiretroviral drug nevirapine based on uracil-modified carbon paste electrode. *J. Appl. Electrochem*., 43: 263-269.

Zhang, M., Su, L. and Mao, L. 2006a. Surfactant functionalization of carbon nanotubes (CNTs) for layer-by-layer assembling of CNT multi-layer films and fabrication of gold nanoparticle/CNT nanohybrid. *Carbon*, 44(2): 276-283.

Zhang, R.Y. and Wang, X.M. 2007. One step synthesis of multiwalled carbon nanotube/gold nanocomposites for enhancing electrochemical response. *Chem. Mater.*, 19(28): 976-978.

Zhang, R.Y., Hummelgard, M. and Olin, H. 2009b. Simple and efficient gold nanoparticles deposition on carbon nanotubes with controllable particle sizes. *Mater. Sci. Eng. B*, 158(1-3): 48-52.

Zhang, R.Y., Hummelgård, M. and Olin, H. 2010c. Simple synthesis of clay-gold nanocomposites with tunable color. *Langmuir*, 26: 5823-5828.

Zijlstra, P., Chon, J.W. and Gu, M. 2007. Effect of heat accumulation on the dynamic range of a gold nanorod doped polymer nanocomposite for optical laser writing and patterning. *Opt. Express*, 15(19): 12151-12160.

# CHAPTER SIX

# CONCLUSION AND RECOMMENDATION

## 6.1 Conclusion

This chapter deals with the conclusions based on the results in this study and makes further recommendations towards detection of NVP. Synthesis, kinetics and spectroscopic characterization of bimetallic Ag-Pt NPs was reported in this work. Bimetallic Ag-Pt nanoparticles were successfully prepared by the reduction of $H_2PtCl_6.6H_2O$ and $AgNO_3$ with sodium citrate. During Ag-Pt NPs formation, rate-determining step was linked to the Pt NPs formation with a fast rate of formation in Ag NPs. The presence of a central Ag metal NP in the core shell structure of our bimetallic Ag-Pt NPs presented an interesting spectroscopic phenomenon, which controlled the particle sizes in the various molar ratios. Spectral characterization explained the unique structures such as the Ag metal's sensitivity to the presence of Pt NPs resulting to the shelling effect observed in all BM NPs ratios. This was also possible due to an induced electron transfer between Ag and Pt NPs. The synthesized nanoparticles gave spectroscopic information typical of their metallic nature. The formation of chemical composition-dependent core shell of Ag-Pt NP was confirmed by TEM. From the band gap results, there was a variation in values for the synthesized nanoparticles. This was attributed predominantly to the particle size and or inter-atomic size variation. General trend of low electrochemical band gaps with relatively high optical band gaps was observed. Studies of XRD showed the formation of face centred cubic crystal structure in the synthesized nanoparticles with confirmation of the intact bimetallic arrangement in the various ratios.

Nanomaterials Modified GCE electrodes showed good electrochemical properties for potential application as sensors. A close analysis of the voltammograms of the metal NPs showed higher electron transfer coefficient, surface coverages and apparent heterogenous rate constants in the BM NPs relative to monometallic NPs. This was an indication that the BM NPs obtained in this study were relatively more conducting or electroactive than their monometallic NP counterparts based on the current densities. However, their signal instability, disqualified them as sensor. To improve signal stability, bimetallic Ag-Pt NPs 3:1 and multi walled carbon nanotube (MWCNT) were combined to form nanocomposite platform as an electrochemical sensor (MWCNT/Ag-Pt 3:1/GCE). This provided conduction centers that facilitated electron transfer between the analyte and the electrode surface. The voltammetric studies showed that the application of MWCNT/Ag-Pt 3:1/GCE significantly increased the sensitivity of the determination of NVP. From the optimization of the

voltammetric method, the use of DPV for the oxidation of the NVP provided the most sensitive signals. Further optimization studies showed that the scan rate, starting potential and the pulse amplitude affected the voltammetric responses. The sensor exhibited a strong electroactivity towards the oxidation of NVP. A significantly low detection limit of about 2.1 x $10^{-8}$ M and high sensitivity was achieved. The detection limit was much lower than those obtained using chromatographic techniques and was within the concentration range of ARVs in various clinical samples. Therefore, this method provides sufficient sensitivity for the determination of NVP without any pre-concentration step. This makes the method better compared to the spectroscopic techniques reported in literature. This work opens an entirely new approach in the detection of NVP by the use of bimetallic NPs platform.

The applicability of developed DPV method was tested and proved through the analysis of NVP in real samples. Conditions for electrochemical analysis of NVP in the presence of typical natural interferants such as ascorbic acid, sodium chloride and calcium chloride were evaluated and results showed minimal interferences on NVP detection. The electrochemical sensor is therefore sufficient in providing high sensitivity for determination of NVP in real samples at residue levels. The high sensitivity of the sensor was due to the nanostructured MWCNT/Ag-Pt NPs used for the modification of the GCE surface. The nanofilms provided a suitable micro-environment and acted as a mediator enhancing the heterogeneous direct electron transfer with the electrode surface. The high stability of the MWCNT/Ag-Pt NPs film was due to the electrostatic attachment provided by the hydrogen bonding in the interaction of MWCNTs and bimetallic Ag-Pt NPs 3:1. The sensor also demonstrated its simplicity, ease of construction, rapidity and sensitivity compared to the conventional analytical techniques corroborating its effective ability in the monitoring of the ARVs at clinical levels on a regular basis. In summary, bimetallic NPs are excellent electrode materials for electroanalysis, and there is still much room for the scientific research and application of bimetallic Ag-Pt NPs based theory and materials. These bimetallic nanomaterials could play an enormous role in achieving efficiency in various analyte detections. Therefore, the work in BM Ag-Pt nanomaterials has far-reaching significance. These results contribute to enriching the knowledge that refers to the electrochemical method of analysis of pharmaceutical drugs.

## 6.2 Future work and recommendations

Further studies of consideration include the following aspects;

- Morphology studies on the thin film structure and surface topography using atomic force microscopy (AFM) to understand the arrangement of atoms within and on the surface of the particles.

- Electrochemical impedance studies (EIS) to determine the charge transfer resistance ($R_{ct}$) and capacitive quality of the electrode/electrolyte interface.

- Kinetics work could be carried out within the reaction time to find out when the core shells are formed. This could be preliminarily carried out with UV-vis spectroscopy, coupled with TEM analysis.

- Further investigation on the effect of the nanofilms concentration on the voltammetric responses of the NVP detections is equally needed.

- Use of scanning electrochemical microscopy (SEM) to measure and optimize areas of reactivity related to surface morphology. To better understand the NPs catalytic performance, and tailor selectivity by controlling the spread of reactive sites on the surface. This will help correlate the catalytic properties of nanoparticles with their structure and atomic level make-up and to further understand the differences in the CV response of modified BM NPs electrodes.

## APPENDICES

**Appendix A:** EDX spectrum for Ag NPs

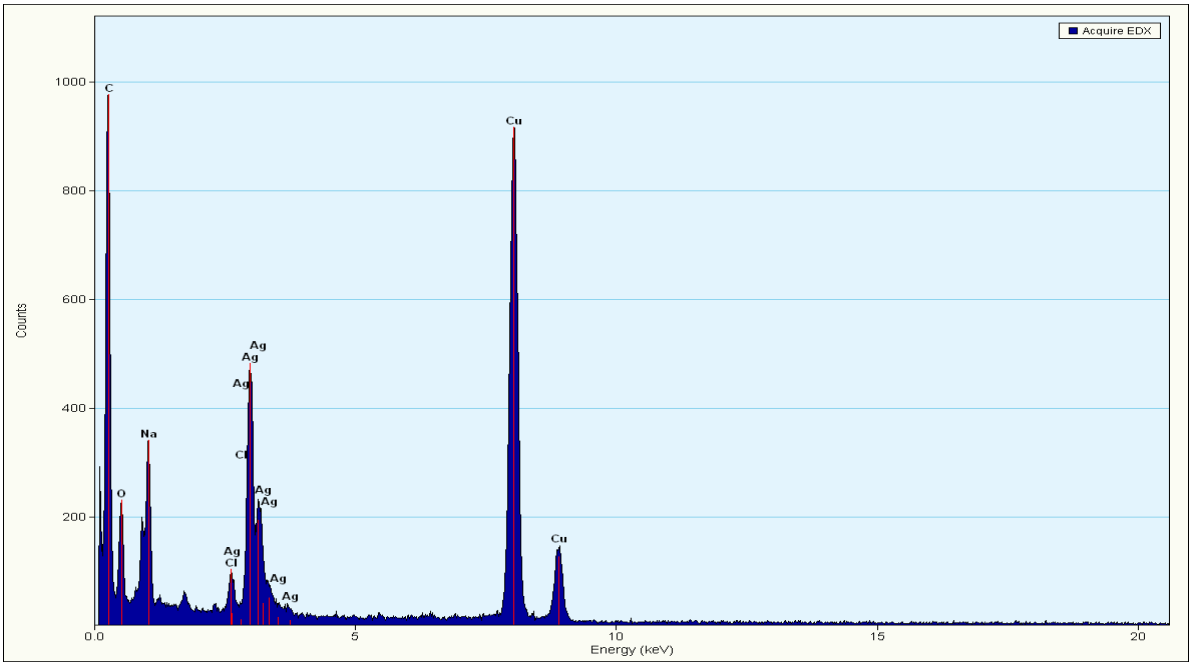


**Appendix B:** EDX spectrum for Pt NPs

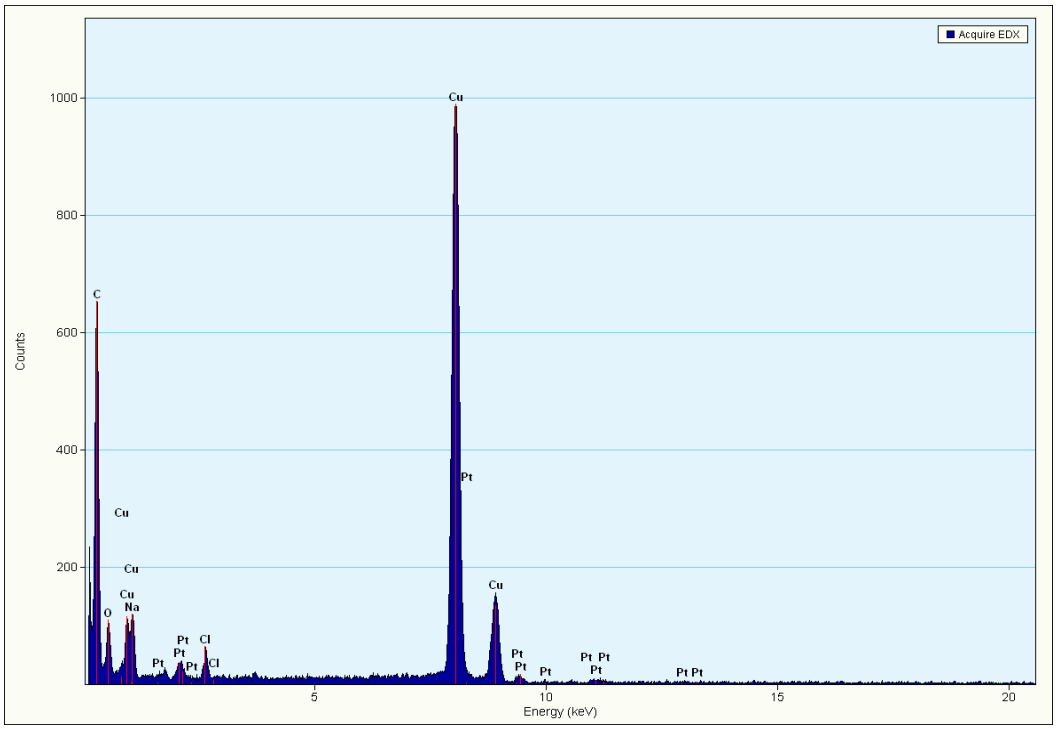

**Appendix C:** EDX spectrum for Ag-Pt NPs 1:1

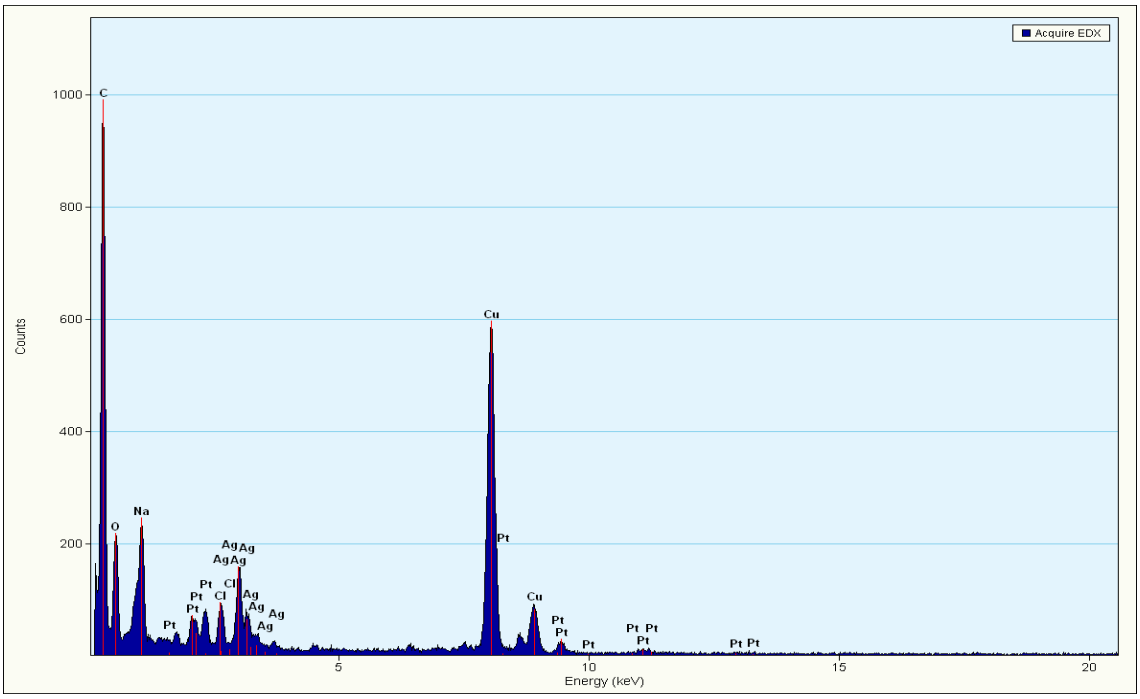


**Appendix D:** EDX spectrum for Ag-Pt NPs 1:3

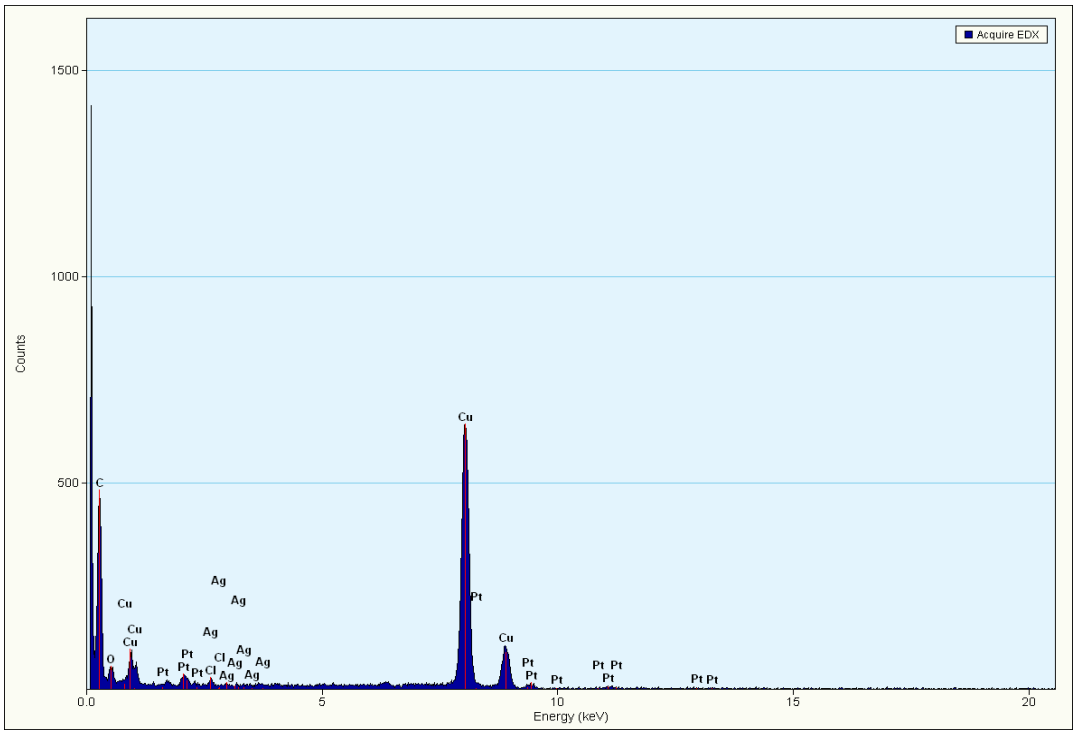

**Appendix E:** EDX spectrum for Ag-Pt NPs 3:1

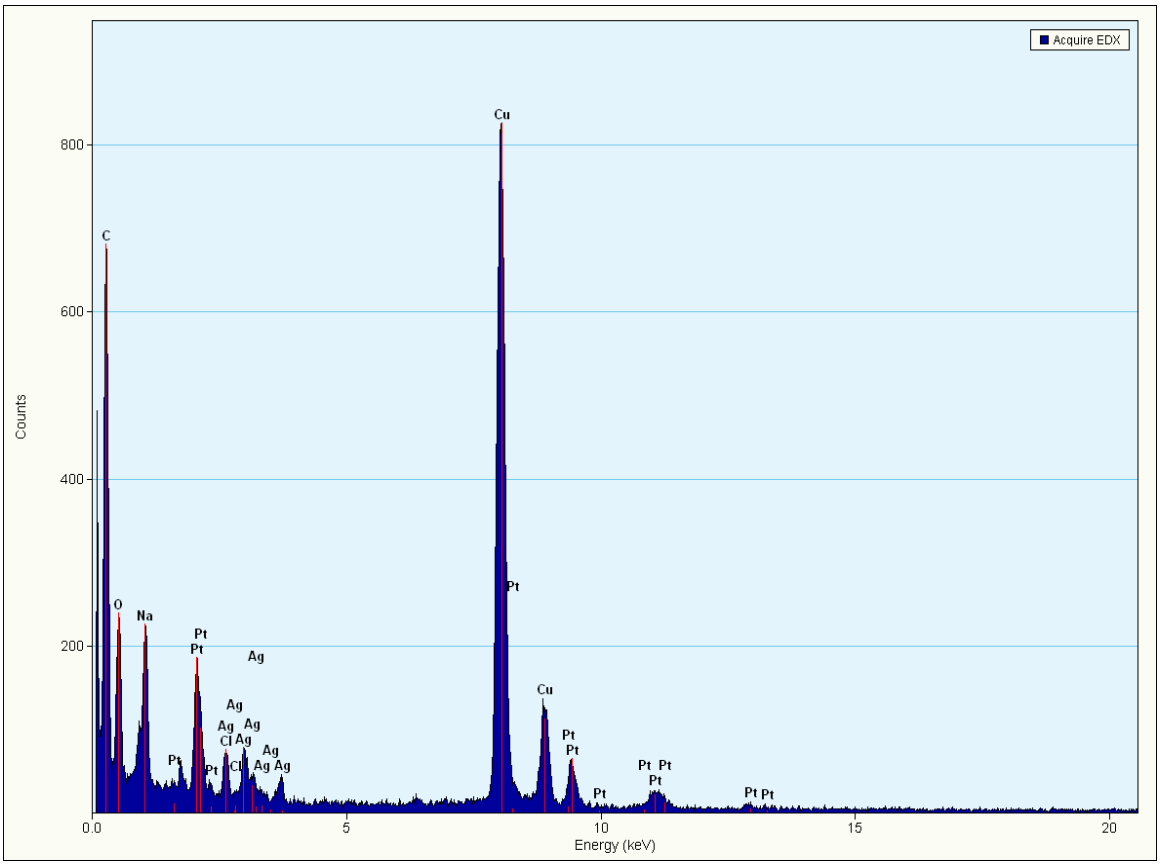

**Appendix F:** Quantification results for Ag-Pt NPs 1:1

| Element | Weight % | Atomic % | Uncert. % | Detector Correction | k-Factor |
|---|---|---|---|---|---|
| C(K) | 74.15 | 88.88 | 0.57 | 0.26 | 3.940 |
| O(K) | 6.67 | 6.00 | 0.13 | 0.49 | 1.974 |
| Na(K) | 4.61 | 2.89 | 0.08 | 0.81 | 1.171 |
| Cl(K) | 1.95 | 0.79 | 0.05 | 0.95 | 1.063 |
| Ag(L) | 8.39 | 1.12 | 0.13 | 0.95 | 2.617 |
| Pt(L) | 4.20 | 0.31 | 0.12 | 0.75 | 5.547 |

**Appendix G:** Quantification results for Ag-Pt NPs 1:3

| Element | Weight % | Atomic % | Uncert. % | Correction | k-Factor |
|---|---|---|---|---|---|
| C(K) | 94.92 | 98.30 | 1.11 | 0.26 | 3.940 |
| O(K) | 1.70 | 1.32 | 0.13 | 0.49 | 1.974 |
| Cl(K) | 0.50 | 0.17 | 0.04 | 0.95 | 1.063 |
| Ag(L) | 0.30 | 0.03 | 0.06 | 0.95 | 2.617 |
| Pt(L) | 2.56 | 0.16 | 0.20 | 0.75 | 5.547 |

**Appendix H:** Quantification results for Ag-Pt NPs 3:1

| Element | Weight % | Atomic % | Uncert. % | Detector Correction | k-Factor |
|---|---|---|---|---|---|
| C(K) | 61.27 | 83.21 | 0.64 | 0.26 | 3.940 |
| O(K) | 9.15 | 9.33 | 0.17 | 0.49 | 1.974 |
| Na(K) | 6.22 | 4.41 | 0.10 | 0.81 | 1.171 |
| Cl(K) | 1.83 | 0.84 | 0.05 | 0.95 | 1.063 |
| Ag(L) | 5.79 | 0.87 | 0.12 | 0.95 | 2.617 |
| Pt(L) | 15.70 | 1.31 | 0.29 | 0.75 | 5.547 |